Absolute sea level maps in the Kuroshio extension derived from drifter and satellite altimetry data

Nikolai A. Maximenko

International Pacific Research Center[1], SOEST, University of Hawaii

and

P. P. Shirshov Institute of Oceanology, Russian Academy of Sciences,

Moscow, Russia

and

Pearn P. Niiler

Scripps Institution of Oceanography

March 2002

IPRC Technical Notes No. 3

---

[1] The International Pacific Research Center is sponsored in part by the Frontier Research System for Global Change.

Sea level maps are computed from satellite altimetry and drifter data as described in detail by Niiler et al. (2002). The direct velocity data are derived from 657 drifters that were deployed in or drifted to the Northwestern Pacific (NWP: 20-50^{0}N, 120-180^{0}E) in the period 25 June 1989 to 31 May 2001. Most drifters were comprised of a spherical surface float with a holey sock drogue tethered at 15m depth (e.g. Niiler, 2001). The ARGOS location data were processed into six hourly positions and velocity estimates by kriging (Hansen and Poulain, 1996) and is a data set maintained by the Drifter Data Center at the Atlantic Oceanographic and Meteorological Laboratory of National Ocean and Atmospheric Administration. During each six-hour segment, the NCEP/NCAR reanalysis six-hourly surface wind vector was interpolated to the drifter location. These wind data were used to correct the six-hour drifter velocity for a wind slip for drifters with drogues and, for drifters which had lost their drogues, an additional bias correction was added according to the methodology described by Niiler (2001) and Pazan and Niiler (2001). These six-hour interpolated and wind-corrected position and velocity data are available by request from: STYL@ucsd.edu. Further smoothing of the drifter position vector and the velocity vector over two inertial periods was done by a newly developed 'curvature compensation' technique (Niiler et al., 2002). A total of 337 years (with approximately one third of this number coming from undrogued drifters) comprise the data set of direct velocity observations at 15m depth. The data distribution in time within ten-degree boxes in Figure 1 shows that about twice as much data were available in the Kuroshio Extension (KE: 25-42^{0}N; 142-180^{0}E) region in 1991-1995 than in the rest of the time period. All trajectories of drogued drifters are shown in Figure 2. Colors used for different groups of buoys indicate that only about 3% of the drifters crossed the Kuroshio front, either into the East China Sea or between the Subtropical and Subpolar regions.

The NWP map of 1-degree drifter ensemble averaged velocity $\langle \mathbf{V}_D \rangle$, shown on Figure 3, is drawn on two velocity scales because a single scale would emphasize the KE jet while the recirculation regions, having much smaller velocities, would not be visible. The Kuroshio appears as a narrow current in excess of 30 cm/sec that follows the continental margin of the East China Sea and passes into the deep NWP over the Izu Ridge south and east of Honshu. In the KE region, two prominent meanders appear directly east of the Izu Ridge, with a third meander, or deflection of about 300 km to the north, on the eastern side of the Shatsky Rise.

Three anticyclonic recirculation regions are evident to the south and east of the Kuroshio jet. The southernmost with the velocities exceeding 50 cm/s is centered approximately at (26.5^0N, 130.5^0E) over the continental rise that surrounds the Daito Island. This pattern has not been recognized in the literature before. Further to the northeast is the recirculation region centered at 31^0N, 137^0E generally south of Honshu that has been observed by current meter arrays along the ASUKA line (Imawaki et al., 2001). It is possible that the Daito circulation is its southern, intensified limb as both are in the same topographically constrained basin, but from present surface current data this connection cannot be clearly ascertained. The easternmost dome lies to the east of the Izu Ridge and west of the Shatsky Rise, north of 31^0N and south of the KE jet. The deep flow of this Kuroshio Extension Recirculation (KER) has been observed with current meter arrays along 152^0E (Schmitz et al., 1982). KER is blocked to the east by the western portion of the Shatsky Rise. Its surface elevation time variability can be seen in the satellite altimeter data (Qiu, 1995). Whether a fourth recirculation region present east of the Shatsky rise is only suggested by the data.

The sea level anomaly field provided by AVISO (CNES, France) (Ducet et al., 2000; AVISO Handbook, 1996) is on a two-dimensional 0.25-degree grid, every ten days. The correlation time scale for the AVISO mapping of satellite observations is 15 days and its correlation space

scale over the NWP changes from 240 km at 20^0N to 140 km at 50^0N. In the KE region, the AVISO data were adjusted to a zero time mean at each location over the satellite data record length from October 22, 1992 to December 29, 2000 (with a gap from November 26, 1993 to April 10, 1995 when due to the failure of ERS sensors only data from TOPEX/Poseidon were mapped).

Following Ralph and Niiler (1999), a geostrophic drifter velocity component $\mathbf{V}_{DG}$ was computed from drifter data by subtracting an Ekman current according to the formula, in complex notation:

$$\mathbf{V}_E = (U_E + iV_E) = 7.0 \times 10^{-5} (\sec^{-1/2})(f)^{-1/2} W \exp\{i(\Theta_W - 54^0)\}, \quad (1)$$

The magnitudes of the Ekman currents are typically much smaller than the eddy currents, but because these have large spatial scales on the time mean, they contribute in a significant way to the sea level slopes across the KE regions.

Mean correlation between contemporaneous drifter ($\mathbf{V}^K{}_{DG}'$) and AVISO ($\mathbf{V}^K{}_S'$) geostrophic velocities is about 0.8 in the KE (numbers in Figure 1). The ratio of the rms geostrophic drifter and satellite velocities,

$$R = \mathrm{rms}(\mathbf{V}^K{}_{DG}')/\mathrm{rms}(\mathbf{V}^K{}_S'), \quad (2)$$

shown in Figures 4a,b reveals (Figure 4c) that R is both smaller and larger than unity, with a tendency of the drifter observations to be larger in all regions except in the KER where the satellite derived velocities are larger. Because of the relative large correlation scales used in the AVISO maps it would be expected that the rms($\mathbf{V}^K{}_S'$) should be always smaller than rms($\mathbf{V}^K{}_{DG}'$), and R

greater than one (Ohlmann et al., 2001). If there were a tendency for a predominant population of cyclonic eddies south of the KE jet, then the centrifugal force would increase the geostrophic current estimated from sea level. In general, this potential deficiency is dynamically based and is quantified below with computation of the eddy Rossby number or the validity of the geostrophic approximation in the computation. It is found that nonlinear terms in the momentum balance within the KE jet as well as the region to the south can change the geostrophic approximation from which the AVISO currents were computed by as much as 25% (Figure 5a). Figure 5b illustrates the predominance of cyclonic/anticyclonic eddies south/north of the KE axis.

As suggested above, the drifter observations provide a mean velocity that may be biased toward observations that have non-uniform sampling intervals at a location. A practical scheme is now adopted for converting the AVISO velocities to levels of the eddy energy that agree with the drifter data and, at the same time, obtaining a less biased mean velocity from the combined data sets. This conversion is robust because of the 0.80 level of correlation of the AVISO data to drifter observations.

Consider that the uniformly sampled time series of velocity is given at times t_i and 0.25-degree grid centers $\mathbf{x}$ by:

$$\mathbf{V}_G(t_i;\mathbf{x}) = A(\mathbf{x})\cdot\mathbf{V}_S'(t_i;\mathbf{x}) + \mathbf{V}_C(\mathbf{x}), \qquad (3)$$

where A is the local "adjustment" of amplitude of the AVISO velocity and $\mathbf{V}_C$ is the "unbiased" mean velocity such that $\langle\langle \mathbf{V}_S' \rangle\rangle = 0$, where $\langle\langle \ldots \rangle\rangle$ is the uniformly sampled time average over the AVISO observation period.

A and $\mathbf{V}_C$ are computed then by minimizing at the center of each 0.25-degree spatial grid the value of $\{\{(\mathbf{V}_G - \mathbf{V}_{DG})^2\}\}$, where $\{\{\ldots\}\}$ designates time-average over contemporaneous drifter and satellite data and spatial smoothing with the mapping function used in AVISO (Ducet et al., 2000) but its spatial coherence scale reduced by 0.5. After applying this minimization the desired expressions are:

$$\mathbf{V}_C = \{\{\mathbf{V}_{DG}\}\} - A\cdot\{\{\mathbf{V}_S'\}\} \tag{4.1}$$

and

$$A = (\{\{\mathbf{V}_{DG}\cdot\mathbf{V}_S'\}\} - \{\{\mathbf{V}_{DG}\}\}\cdot\{\{\mathbf{V}_S'\}\}/(\{\{\mathbf{V}_S'\cdot\mathbf{V}_S'\}\} - \{\{\mathbf{V}_S'\}\}\cdot\{\{\mathbf{V}_S'\}\}). \tag{4.2}$$

Note that $\{\{V_S'\}\}$ does not vanish, and thus it corrects the bias that the drifter data might have in establishing an "unbiased" mean.

The map of $\mathbf{V}_C$, the unbiased estimate of the mean geostrophic velocity in Figure 6, appears, at first glance, very much like the map of $\langle\mathbf{V}_D\rangle$ in Figure 3, first, because the Ekman currents are much smaller (not shown) than the geostrophic currents over most of the KE region and, second, the drifter data density was relatively well distributed in the vicinity of the strong current region of the KE jet in time over the sampling period of AVISO data. In Figure 6, more spatially coherent current systems now appear both north and south of the KE jet. In the area north of 38^0N the two meanders, or Oyashio Intrusions, that lay west of the organization region of the Oyashio front at 155^0E are now more clearly evident as is the Oyashio frontal current (Kawai, 1972). To the south, the topography of the Shatsky Rise appears to steer $\mathbf{V}_C$, more to the south than was evident in $\langle\mathbf{V}_D\rangle$. Most importantly, there now appears a large-scale southward geostrophic flow nearly

everywhere east of 153^0E. This southward flow, an unbiased nine-year mean, has significant consequences for the large spatial scale momentum balance of the KE region.

The mean sea level is now determined from the upper ocean momentum balance that includes the Coriolis force based on the unbiased geostrophic mean velocity and eddy momentum convergence determined from the statistics of AVISO variable currents. A complementary calculation is also made from the drifter mean velocity and eddy statistics. The time mean, horizontal momentum equations near the surface, written in the Bernoulli form are:

$$-\nabla B = (f+\langle\langle z_G \rangle\rangle)\mathbf{k}x\langle\langle \mathbf{V}_G \rangle\rangle + \mathbf{k}x\langle\langle A^2 z' \mathbf{V}_S' \rangle\rangle + \langle\langle z_G \rangle\rangle \mathbf{k}x\langle\langle \mathbf{V}_E \rangle\rangle, \quad (5)$$

where the Bernoulli function is

$$B = B_O + gh + \langle\langle \mathbf{V}_G \rangle\rangle \cdot \langle\langle \mathbf{V}_G \rangle\rangle/2 + \langle\langle A^2 \mathbf{V}_S' \cdot \mathbf{V}_S' \rangle\rangle/2, \quad (6)$$

B_O is a constant and the Ekman velocity $\mathbf{V}_E$ is defined by (1). In (5) the relative vorticity terms are computed from the unbiased mean geostrophic velocity $\mathbf{V}_C$ and from quasi-geostrophic definitions

$$\mathbf{k}xf\mathbf{V}_G' = -Ag\nabla h' \text{ and } z' = (g/f)\cdot A\nabla^2 h', \quad (7)$$

The maps of the mean sea level in the KE region are plotted for solutions of (5-6) in Figure 7a**.** Figure 7b shows mean sea level computed using drifter-mean velocities and geostrophic form of equations (5-6), and Figure 7c shows the difference between Figures 7a and 7b. Both figures are graphed relative to a zero value at (25^0N, 142^0E). Clearly visible in both panels is the KE jet across

which is a sea level decrease to the north by 110 cm from 32^0N to 38^0N at 142^0E. At 145^0E and 160^0E part of the KE bifurcates northward forming a number of quasi-zonal jets. Sea level difference further decreases east of 155^0E where southern part of the KE turns to the south closing the recirculation cell seen at 32^0N, 142-153^0E. Another decrease of 50 cm occurs across the Oyashio front at the approximate latitudes of 38-42^0N. One jet flows along 40^0N through 165^0E and then turns more to the north following the position of the subarctic front. Another jet seen at 40.5-42^0N, 143-147^0E turns north immediately and follows the Oyashio water mass front. In Figure 7a, the KER appears as a relative high of 15 cm south of the KE jet and west of 157^0E, or the western margin of the Shatsky Rise. East of 150^0E begins the southward deflection of the subtropical gyre. In Figure 7a are also drawn $\mathbf{V}_C$ on two amplitude scales, and there is a broad southward geostrophic velocity south of 31^0N and east of 153^0E that produces a 25-45cm sea level decrease from 142^0E to 180^0E. The geostrophic velocity does not follow exactly along the sea level contours because there are other relatively small momentum convergences in (5) other than the Coriolis force.

Rms uncertainties in the computed mean sea level shown in Figure 7a due to a non-zero convergence of the right-hand terms in (5) are estimated to be equal to 2.4 cm and those due to errors in velocities $\mathbf{V}_G$ are about 4.5 cm.

The climatological steric sea surface height relative to 2000m of Qu et al. (2001) is subtracted from the absolute sea level, and pressure gradients larger than the uncertainty of defining the absolute sea level are found at 2000m depth (Figure 8). The KE jet with its three meanders, Oyashio jet and the Subarctic frontal jet are all evident at 2000m. The net dynamic height change across these systems at 145^0E is 75 dynamic cm. KER occupies a larger area at 2000m depth than at the surface and extends to 170^0E, west of which no persistent geostrophic southward flow is evident as there was in the absolute sea level. There appears a 20cm relative high north of the KE

jet and an implied anticyclonic geostrophic circulation around this high. Thus the dynamic height difference between the relative highs on either side of the KE jet is 10cm, or above the net uncertainty of 4.8cm in the methodology of deriving this map. The computation of steric height obtained from quality controlled hydrographic data in the WHOI/Hydrobase (McDonald et al., 2001) was also plotted (not shown) relative to the sea level of Figure 7a and the patterns of the relative highs north and south of the KE jet appear to stand out from the eddy noise. Whether the pattern of pressure at 2000m is consistent with the pattern of 4000m depth current meter observations (Niiler et al., 1985; Joyce and Schmitz, 1988) requires more hydrographic observations than in the world hydrographic data bases today.

It is now possible to construct the absolute sea level map of each ten-day period in the KE region, using the absolute mean sea level from Figure 7a and the AVISO sea level anomaly. These maps for October 22, 1992 through August 6, 2001 shown in Figure 9 also display a number of 40-day long drifter tracks. The movement of the drifters around the various mesoscale features of KE region that would be implied by geostrophic flow is quite remarkable but expected because of the high level of correlation that was computed between drifter and AVISO geostrophic currents. The Ekman current was a much smaller value in this location than the KE jet and its eddies. A sequence of such maps in Figure 9 shows the tremendous complexity of the absolute sea level in the region so that the three semi-permanent meanders are not readily visible. Isolated high sea level regions (warm rings) are found to the north of the KE jet and the isolated low sea level regions (cold rings) are found to the south, both being formed out of the large amplitude meanders of the KE jet. While isolated eddies of different direction of rotation can be identified on either side of the KE jet, the structure of the pressure anomaly at 2000m depth implies recirculation regions of the same sign. If

eddies indeed drive the KE recirculation regions, as has been implied by observations south of the Gulf Stream (Hogg, 1983) they do so in a different fashion to the north of the KE system.

In summary, the drifter observations display a strong and coherent Kuroshio Current that flows from the northern coast of Taiwan to the Emperor Seamounts. The influence of bottom topography, whether at the continental rise along the East China Sea or in the KE region, is marked in the shape of its path. The two-dimensional eddy currents from the AVISO satellite altimeter analyses were highly coherent at 0.80 with the drifter observations and these were adjusted to drifter amplitude levels. The principal axis of eddy stress ellipse tends to be in the direction of the meandering mean velocity. An evaluation of the eddy Rossby number and the quasi-geostrophic vorticity suggests that significant non-geostrophic, or cyclostrophic, effects occur in the eddy momentum balance south of the KE jet. The AVISO two-dimensional analysis was instrumental in correcting the biases of the mean circulation from drifters because of their non-uniform sampling of a decadal change that occurred in the KE region. An absolute sea level map was constructed from the unbiased mean and eddy momentum convergences in the near surface momentum balance equation.

This study demonstrates the synergy between the *in situ* and remote sensing of the oceans that is needed to produce new estimates of ocean circulation on basin-wide scales. The drifter data, though highly accurate, are sparse. The satellite altimeter data, though voluminous, cannot be assumed to be in geostrophic balance in high eddy energy regions and it requires a spatially non-uniform smoothing function to be specified by *in situ* observations. It is the ocean circulation that establishes the sea level gradients, principally through the Coriolis force of the geostrophic current. Eddy-induced sea level variations due the Bernoulli effect in the mid-latitudes are smaller than 5cm. The ocean circulation and its eddy fields are not homogeneous, demonstrating a wide range of

amplitude, space and time scales. The lessons learned in merging the *in situ* and satellite data in the KE basin with simple methods applied in this study will probably have to be re-learned many times over before a global circulation pattern can be synthesized. For example, AVISO MSLA shows low correspondence with drifter velocities in the region directly south Honshu, where along the ASUKA line, Uchida et al. (1998) obtained 96% correlation between drifter velocities and geostrophic currents estimated from a single TOPEX/Poseidon track line. The present AVISO mapping technique recognizes no boundary conditions at the coast, small temporal and spatial scales in a sub-region or high errors due to poor regional tidal models. The development of a global circulation synthesis requires more powerful tools than introduced here that can perhaps be brought about by the application of basin-scale, eddy-resolving ocean circulation models.

This notes and associated digital files can be obtained on request from nikolai@soest.hawaii.edu or downloaded from http://www.soest.hawaii.edu/~nikolai/KE-SSH/KE-SSH.html.

Acknowledgements

This research was partly sponsored at the International Pacific Research Center by the Frontier Research System for Global Change. At the Scripps Institution of Oceanography it was sponsored by the NOAA Office of Global Programs through the Joint Institute of Marine Observations and the National Aeronautical and Space Administration with a grant NAG5-8351. The authors acknowledge Bo Qiu and Lynne Talley for the insights they provided about the variability of KE region and Tangdong Qu for graciously lending us his numerical data on the

relative dynamic topography of the KE region. The assistance of Sharon Lukas in the data preparation is gratefully acknowledged.

References

Archiving, Validation, and Interpretation of Satellite Oceanographic Data (AVISO), *AVISO Handbook for Merged TOPEX/Poseidon products*, 3rd ed., Toulouse, France, 1996.

Ducet, N., P.-Y. LeTaon, and G. Reverdin, Global high-resolution mapping of ocean circulation from TOPEX/Poseidon and ERS-1 and –2, *J. Geophys. Res*., **105**, 19,477-19,498, 2000.

Hansen, D. V., and P.-M. Poulain, Quality control and interpolations of WOCE-TOGA drifter data, *J. Atmos. Ocean. Technol.*, **13**, 900-909, 1996.

Hogg, N.G., A note on the deep circulation of the western North Atlantic: its nature and causes, *Deep-Sea Res*., 30, 945-961**.**

Imawaki, S., H. Uchida, H. Ichikawa, M. Fukasawa, S. Umatani, and ASUKA Group, Satellite altimeter monitoring the Kuroshio transport south of Japan, *Geophys. Res. Lett*. (submitted, 2001).

Joyce, T. M, and W. J. Schmitz, Zonal velocity structure and transport in the Kuroshio Extension, *J. Phys. Oceanogr*., **18**, 1484-1494, 1988.

Kawai, H., Hydrography of the Kuroshio Extension, In: *KUROSHIO: Physical aspects of the Japan Current*, Eds. H. Stommel and K. Yoshida, University of Washington Press, Seattle, 1972.

McDonald, A. M., T. Suga, and R. G. Curry, An isopycnally averaged North Pacific Climatology, *J. Atmos. Ocean. Technol.*, **18**, 394-420, 2001.

Niiler, P., The World Ocean Surface Circulation. In: *Ocean Circulation and Climate-Observing and Modeling the Global Ocean*, Eds. J. Church, G. Siedler, and J. Gould, Academic Press, London, 2001.

Niiler, P. P., N. A. Maximenko, G. G. Panteleev, T. Yamagata, and D. B. Olson, Near-surface Dynamical Structure of the Kuroshio Extension, *J. Geophys. Res*., 2002 (submitted).

Niiler, P. P., W. J. Schmitz, and D.-K. Lee, Geostrophic volume transport in the high eddy-energy areas o the Kuroshio Extension and Gulf Stream, *J. Phys. Oceanogr*, **15**, 825-843, 1985.

Ohlmann, J. C., P. P. Niiler, C. A. Fox, and R. R. Leben, Eddy energy and shelf interactions in the Gulf of Mexico, *J. Geophys. Res*., **106**, 2,605-2,620, 2001.

Pazan, S., and P. P. Niiler, Recovery of near surface velocity from undrogued drifters, *J. Atmos. Ocean. Tech*., **18**, 476-489, 2001.

Qiu, B., Variability and energetics of the Kuroshio Extension and its recirculation gyre from the first two-year TOPEX data, *J. Phys. Oceanogr.*, **25**, 1827-1842, 1995.

Qu, T., H. Mitsudera, and B. Qiu, A climatological view of the Kuroshio/Oyashio system east of Japan, *J. Phys. Oceanogr.*, **31**, 2575-2589, 2001.

Ralph, E. A., and P. P. Niiler, Wind driven currents in the tropical Pacific, *J. Phys., Oceanog.*, **29**, 2121-2129, 1999.

Schmitz, W. J., P. P. Niiler, R. L. Bernstein, and W. R. Holland, Recent long-term moored instrument observations in the western North Pacific, *J. Geophys. Res*., **87**, 9425-9440, 1982.

Uchida, H., S. Imawaki, and J.-H. Hu, Comparison of Kuroshio surface velocities derived from satellite altimeter and drifting buoy data, *J. Oceanogr*., **54**,115-122, 1998.

Figure captions

Figure 1. Number of data days per year provided by drogued (filled bars) and undrogued drifters in 10^0E x 10^0N bins. Numbers are the correlations between drifter and geostrophic AVISO velocities.

Figure 2. Trajectories of drogued drifters that were deployed north of 35^0N (black), entered Tsushima Strait (blue) and others (red). Solid colors are used for the trajectories, whose behavior is different from one of the other drifters in the same groups. Blue, red and black boxes show the areas discussed in text.

Figure 3. 1-degree average drifter velocities $<\mathbf{V}_D>$. Large velocity vectors (> 10 cm/s) are red and re-scaled. Vectors, whose length is smaller than standard error (computed using 15 day decorrelation time), are light red and blue. Light green contour interval of bottom topography is 250 m. Vector (50 cm/s) and ellipses (50 cm/s radius) scales are shown in the upper left corners of the panels.

Figure 4. Rms eddy velocities computed from drifters *(a)* and AVISO altimetry *(b)* and their ratio *(c)*.

Figure 5. Distribution of eddy Rossby number *(a)*

$\mathrm{Sqrt}\{(<<z>>/f)^2 + [<<z'^2>>(<<\mathbf{V}_G>>)^2 + <<(z'\mathbf{V}_G')'.(z'\mathbf{V}_G')'>>]/(f^2<<\mathbf{V}_G'.\mathbf{V}_G'>>)\}$

and $F = <<z'^3>>/(<<z'^2>>)^{3/2}$ *(b)*.

Figure 6. $\mathbf{V}_C$ as computed from formula (4). Grey color is for the vectors smaller than 10 cm/s. 50 cm/s scales are shown in the box.

Figure 7. Mean sea level computed *(a)* from full equation (5) using AVISO data calibrated by (3) and *(b)* from geostrophic balance of mean drifter velocities and difference *(c)* between *(a)*

and *(b).* Contour interval is 5 cm. Vectors are $\mathbf{V}_C$ *(a)* and $<\mathbf{V}_{DG}>$ *(b),* both scaled as in Figure 6.

Figure 8. Pressure anomaly distribution at 2000 m depth computed using mean sea level (Fig.11a) and dynamic height (Qu et al., 2001). Contour interval is 5 cm.

Figure 9. Ten-day maps of absolute sea level computed from AVISO MSLA data referenced to absolute mean sea level of Figure 7a for October 22, 1992 - August 6, 2001. Contour interval is 10 cm. White markers show six-hourly positions of drogued (large dots) and undrogued (small dots) during 20-day time period centered at a date of map. Titles show dates of maps, julian days and satellites used for AVISO/MSLA mapping. Numbers on colorscale are cm.

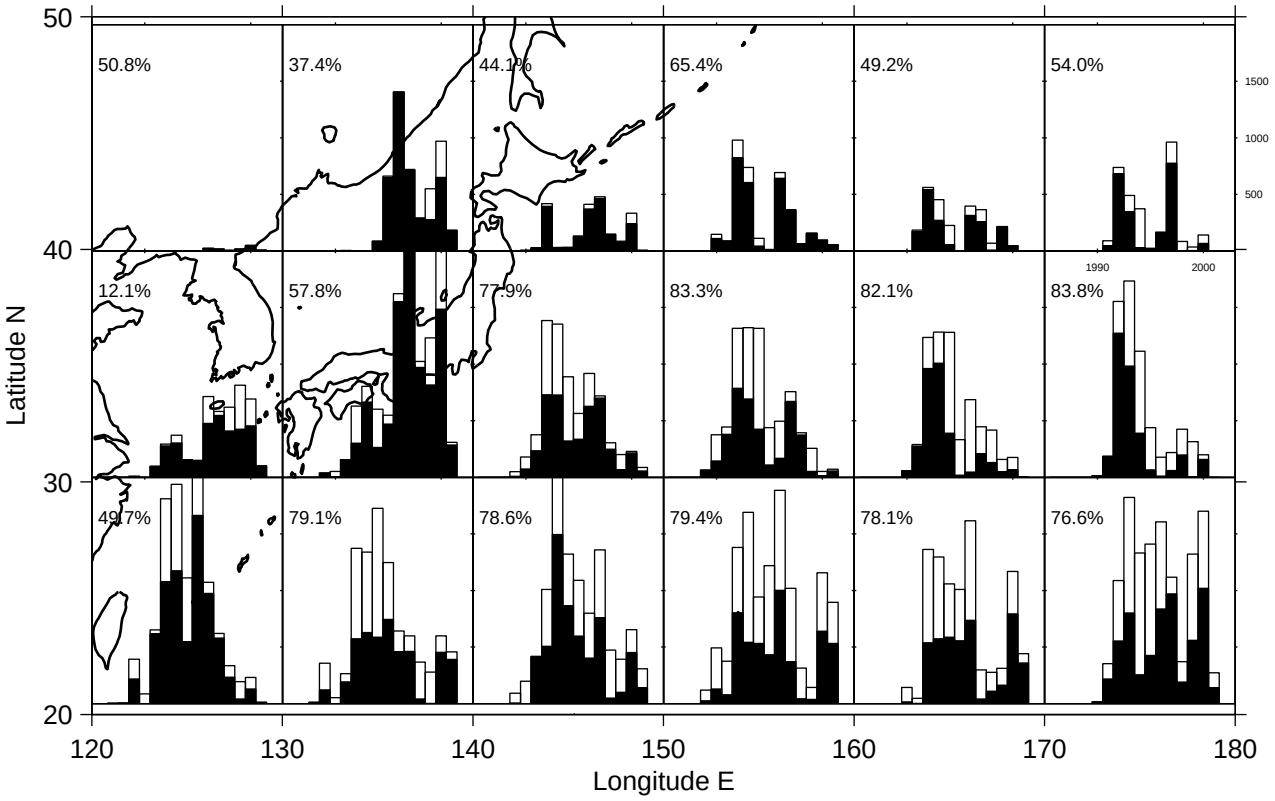

50.8%
37.4%
44.1%
65.4%
49.2%
54.0%
12.1%
57.8%
77.9%
83.3%
82.1%
83.8%
49.7%
79.1%
78.6%
79.4%
78.1%
76.6%
1500
1000
500
1990
2000
50
40
30
20
120
130
140
150
160
170
180
Latitude N
Longitude E

Fig.1

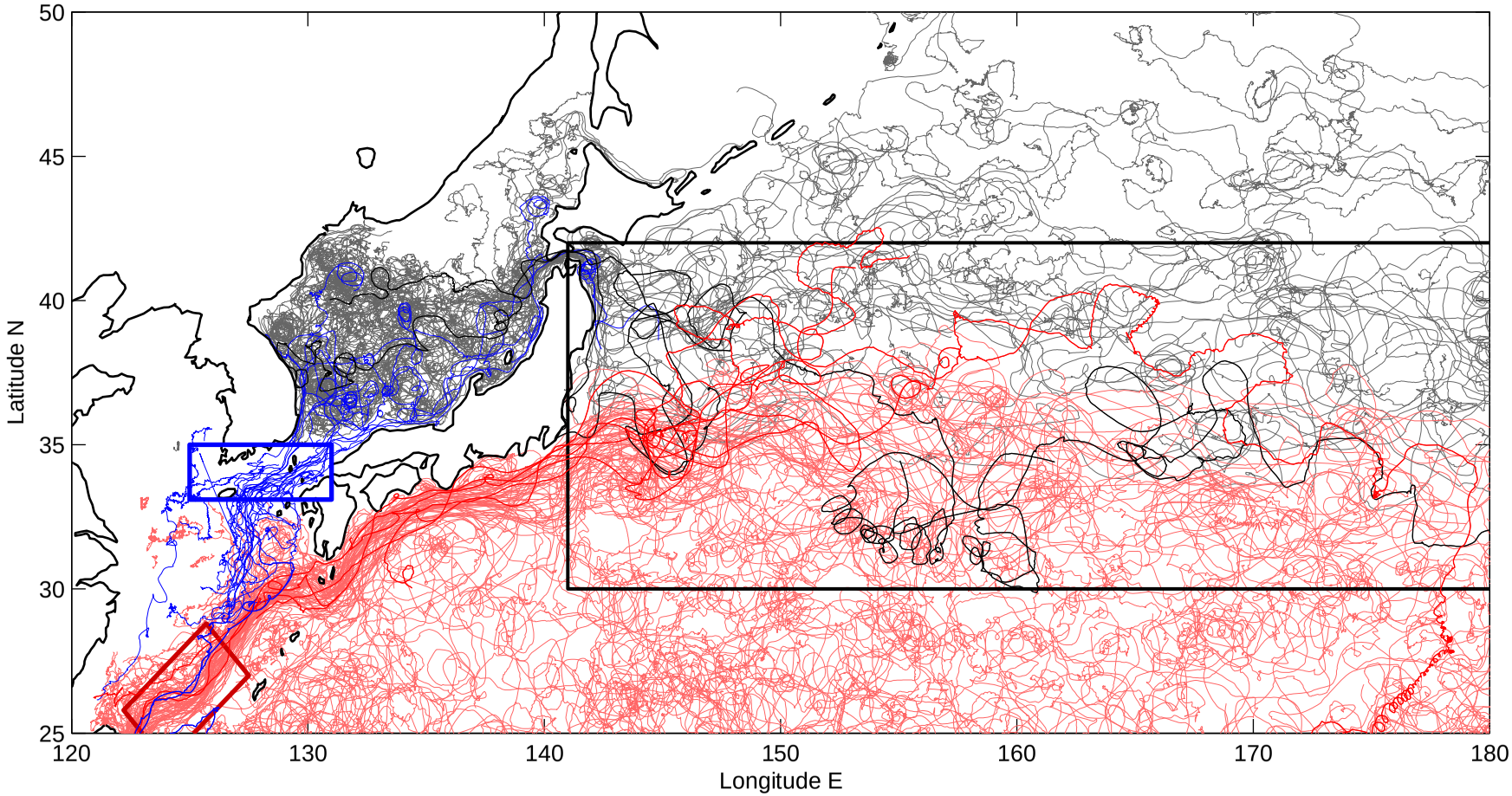

50
45
40
35
30
25
Latitude N
120
130
140
150
160
170
180
Longitude E

Fig.2

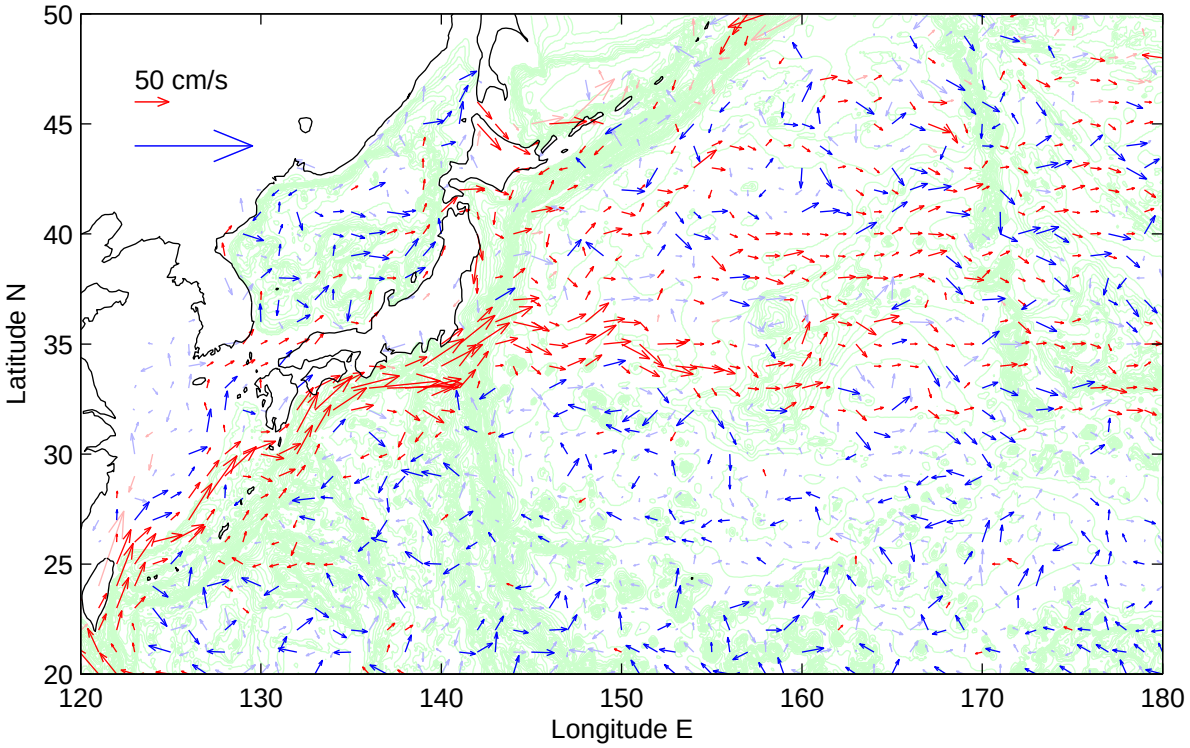

50 cm/s
Latitude N
Longitude E
50
45
40
35
30
25
20
120
130
140
150
160
170
180

Fig.3

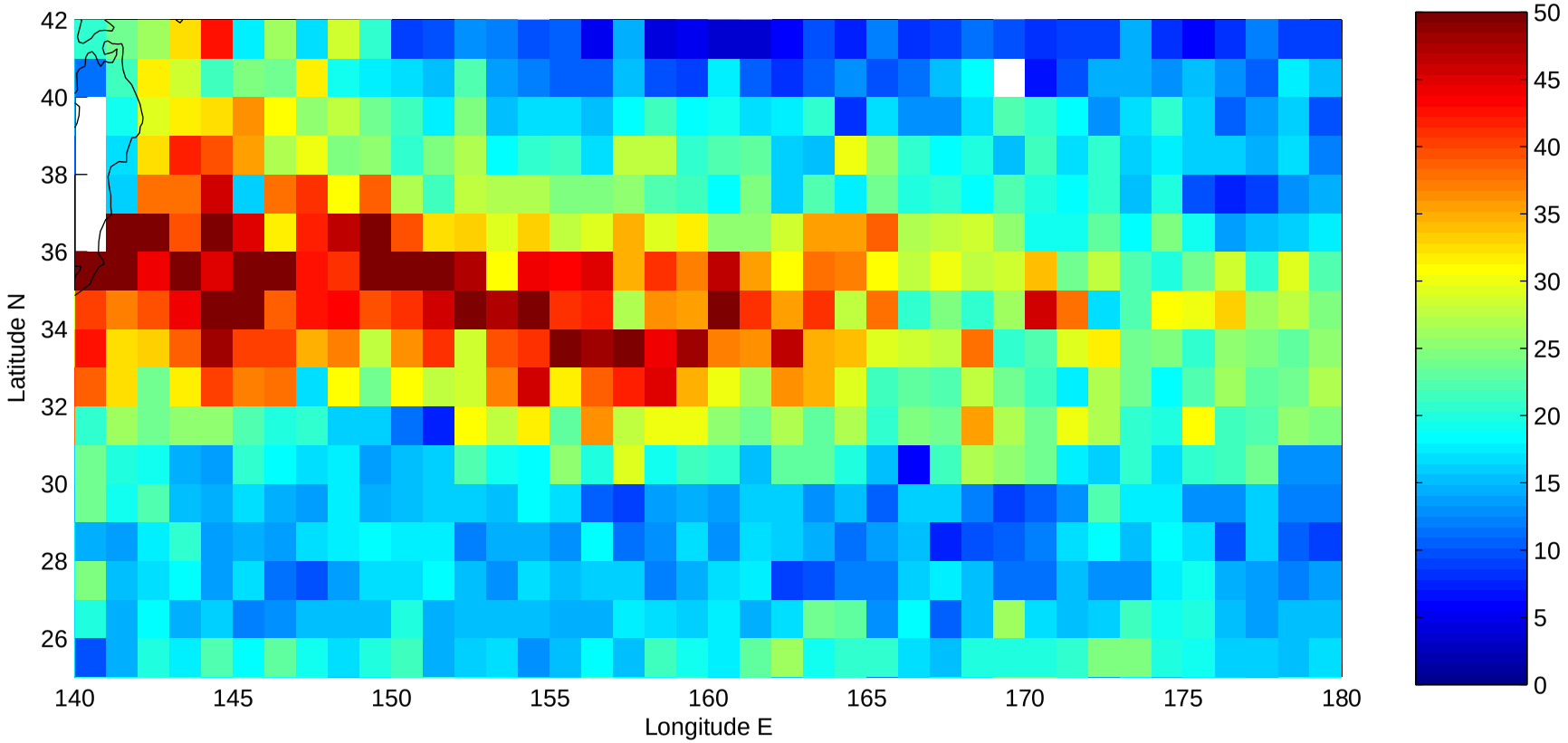

Latitude N
42
40
38
36
34
32
30
28
26
140
145
150
155
160
165
170
175
180
Longitude E
50
45
40
35
30
25
20
15
10
5
0

Fig.4a

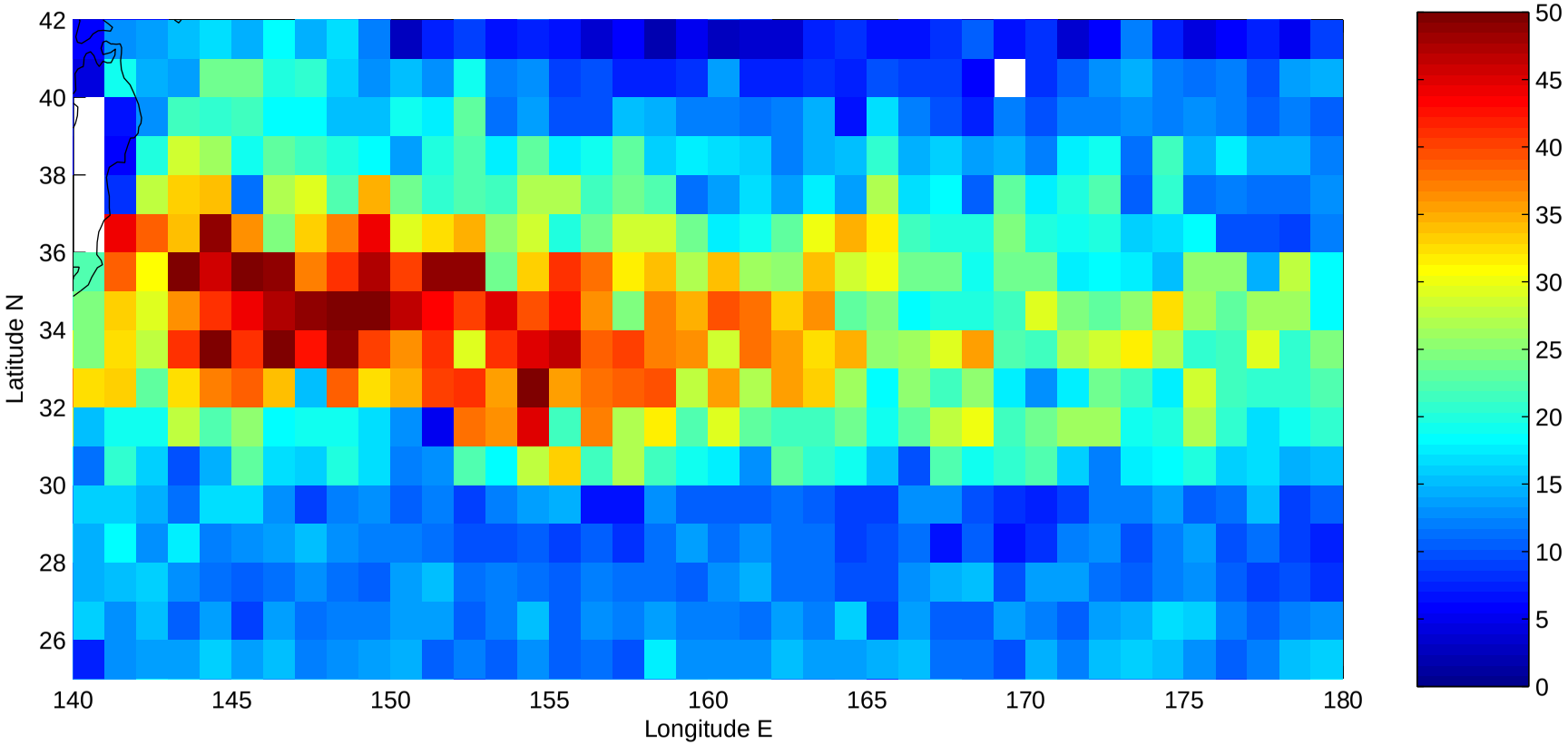

Latitude N
42
40
38
36
34
32
30
28
26
140
145
150
155
160
165
170
175
180
Longitude E
50
45
40
35
30
25
20
15
10
5
0

Fig.4b

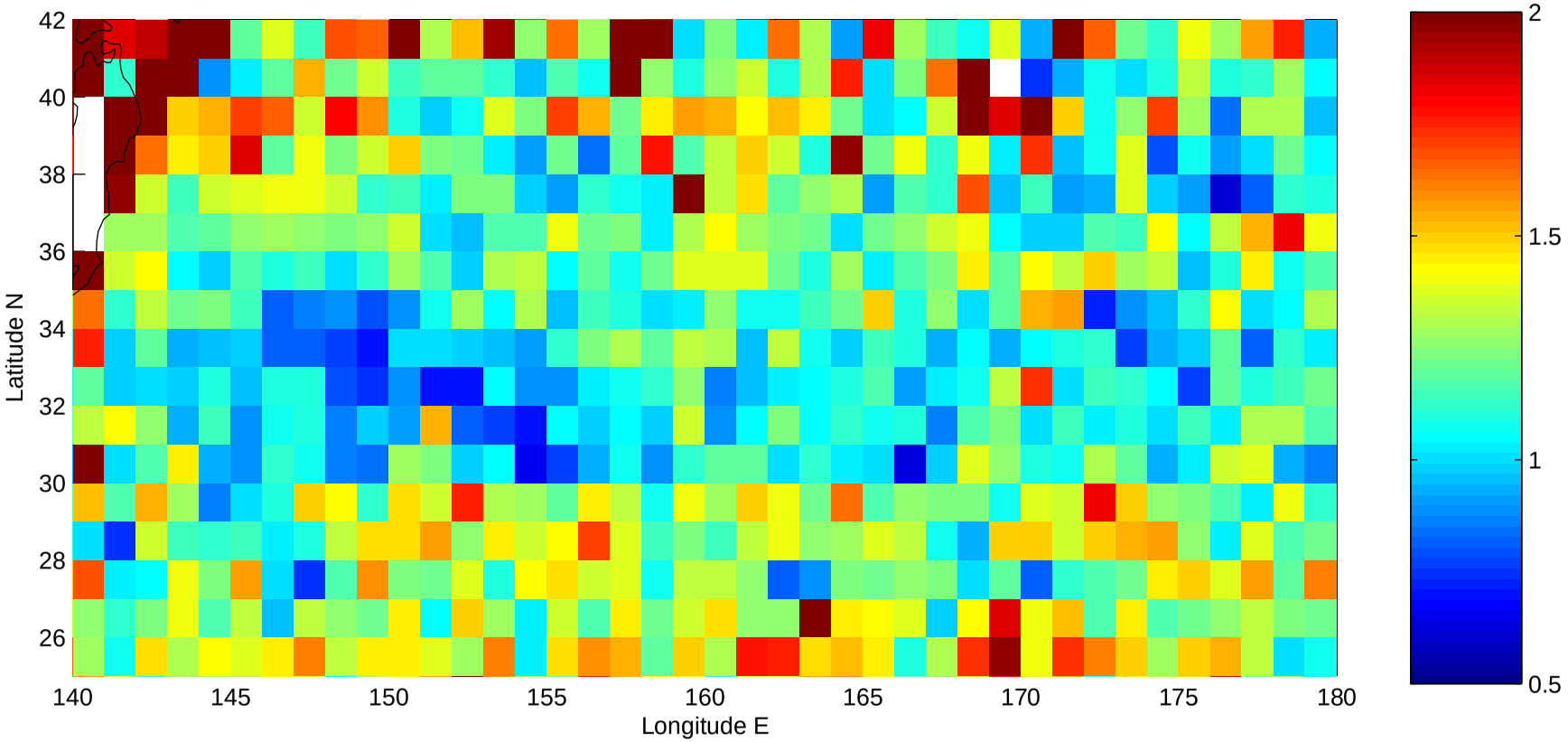

42
40
38
36
34
32
30
28
26
Latitude N
140
145
150
155
160
165
170
175
180
Longitude E
2
1.5
1
0.5

Fig.4c

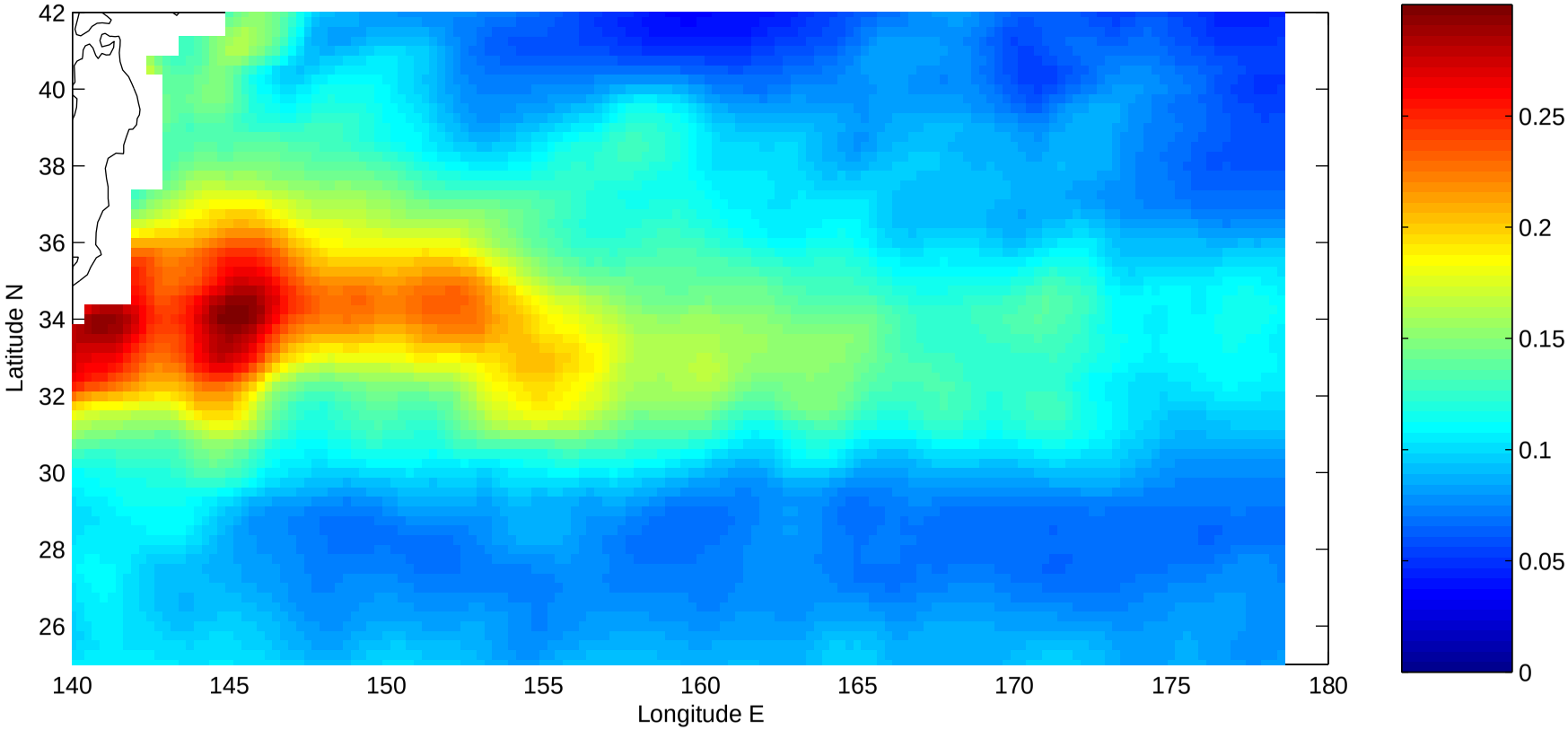

42
40
38
36
34
32
30
28
26
Latitude N
140
145
150
155
160
165
170
175
180
Longitude E
0.25
0.2
0.15
0.1
0.05
0

Fig.5a

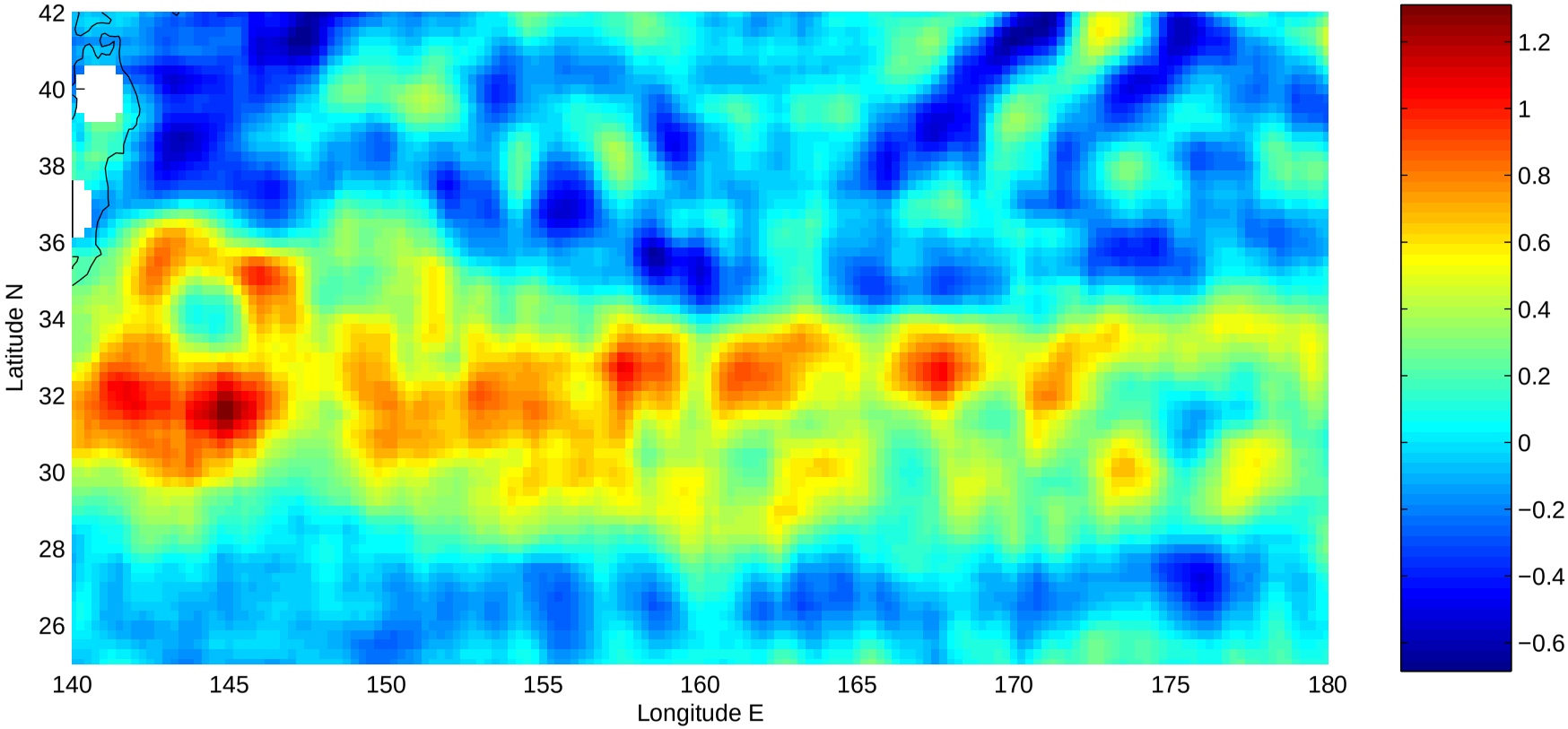

Latitude N
42
40
38
36
34
32
30
28
26
140
145
150
155
160
165
170
175
180
Longitude E
1.2
1
0.8
0.6
0.4
0.2
0
−0.2
−0.4
−0.6

Fig.5b

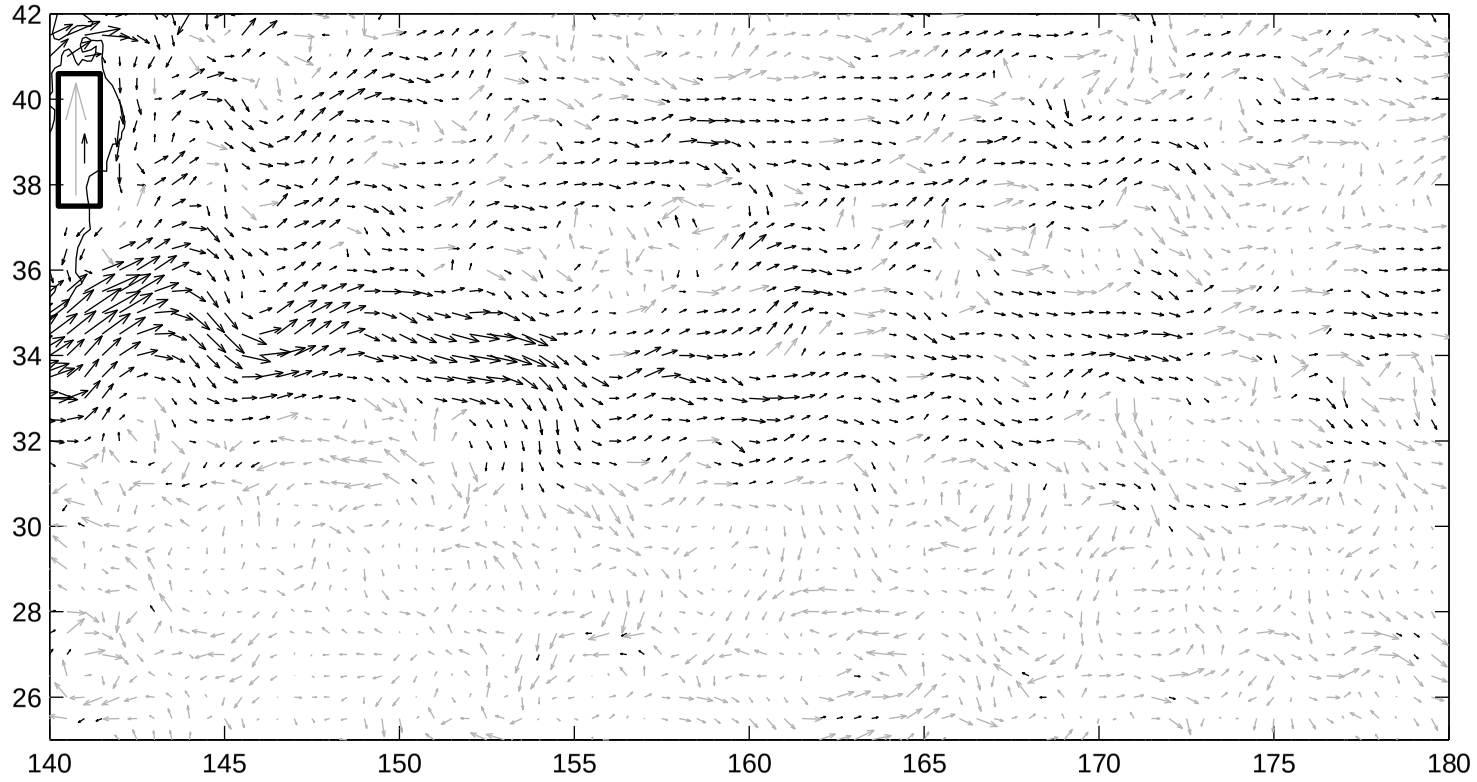


Fig.6

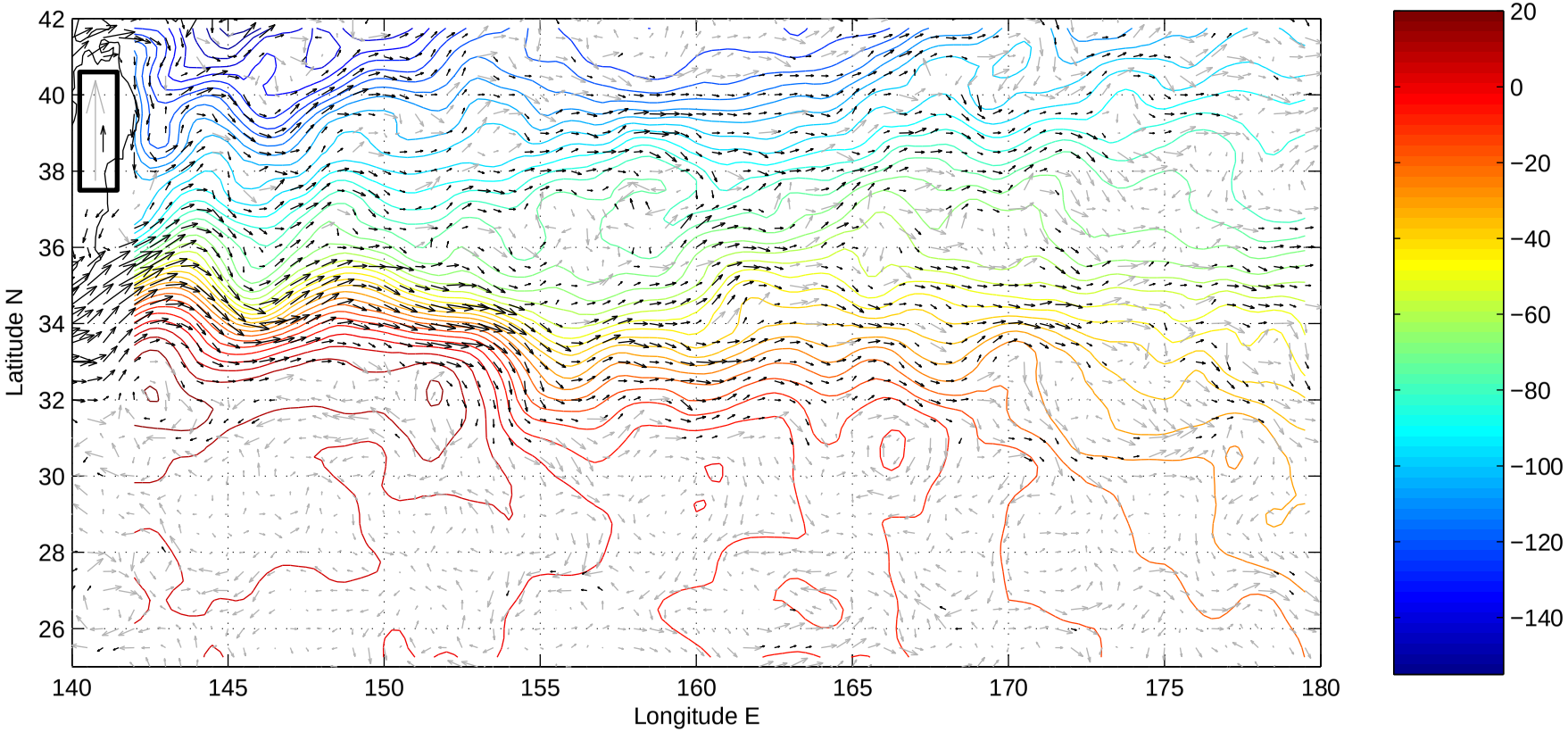

Latitude N
42
40
38
36
34
32
30
28
26
140
145
150
155
160
165
170
175
180
Longitude E
20
0
−20
−40
−60
−80
−100
−120
−140

Fig.7a

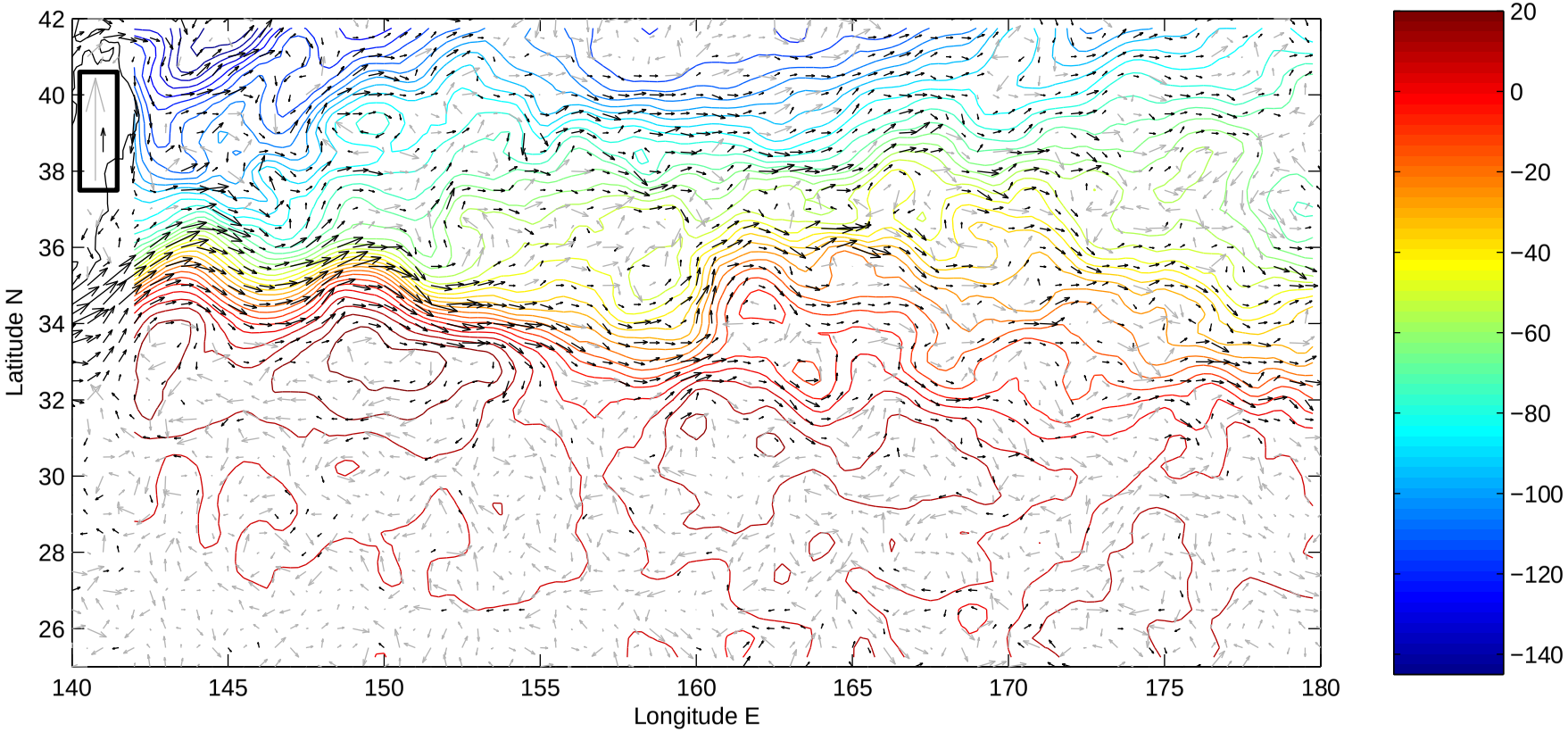

Latitude N
42
40
38
36
34
32
30
28
26
140
145
150
155
160
165
170
175
180
Longitude E
20
0
−20
−40
−60
−80
−100
−120
−140

Fig.7b

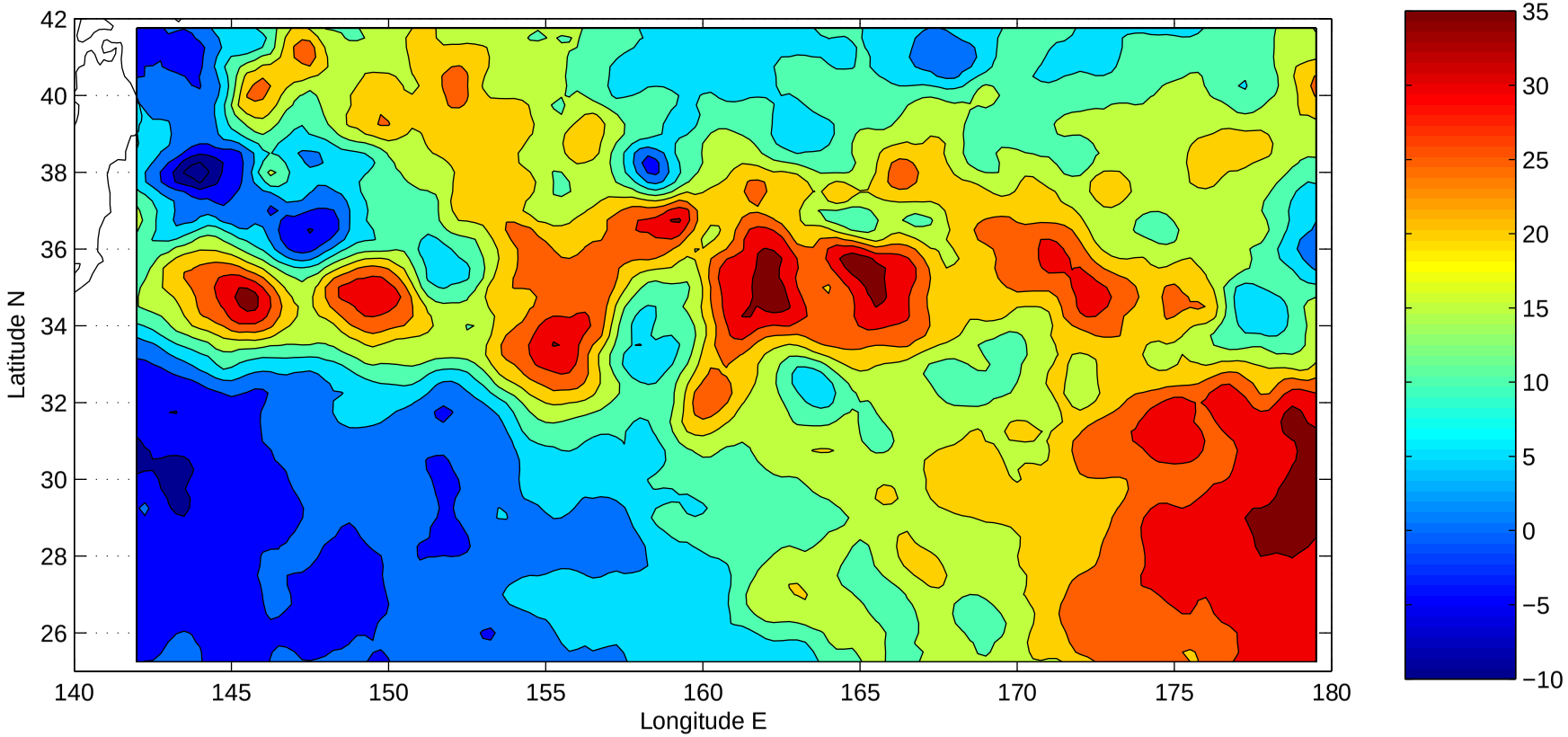

Latitude N
42
40
38
36
34
32
30
28
26
140
145
150
155
160
165
170
175
180
Longitude E
35
30
25
20
15
10
5
0
−5
−10

Fig.7c

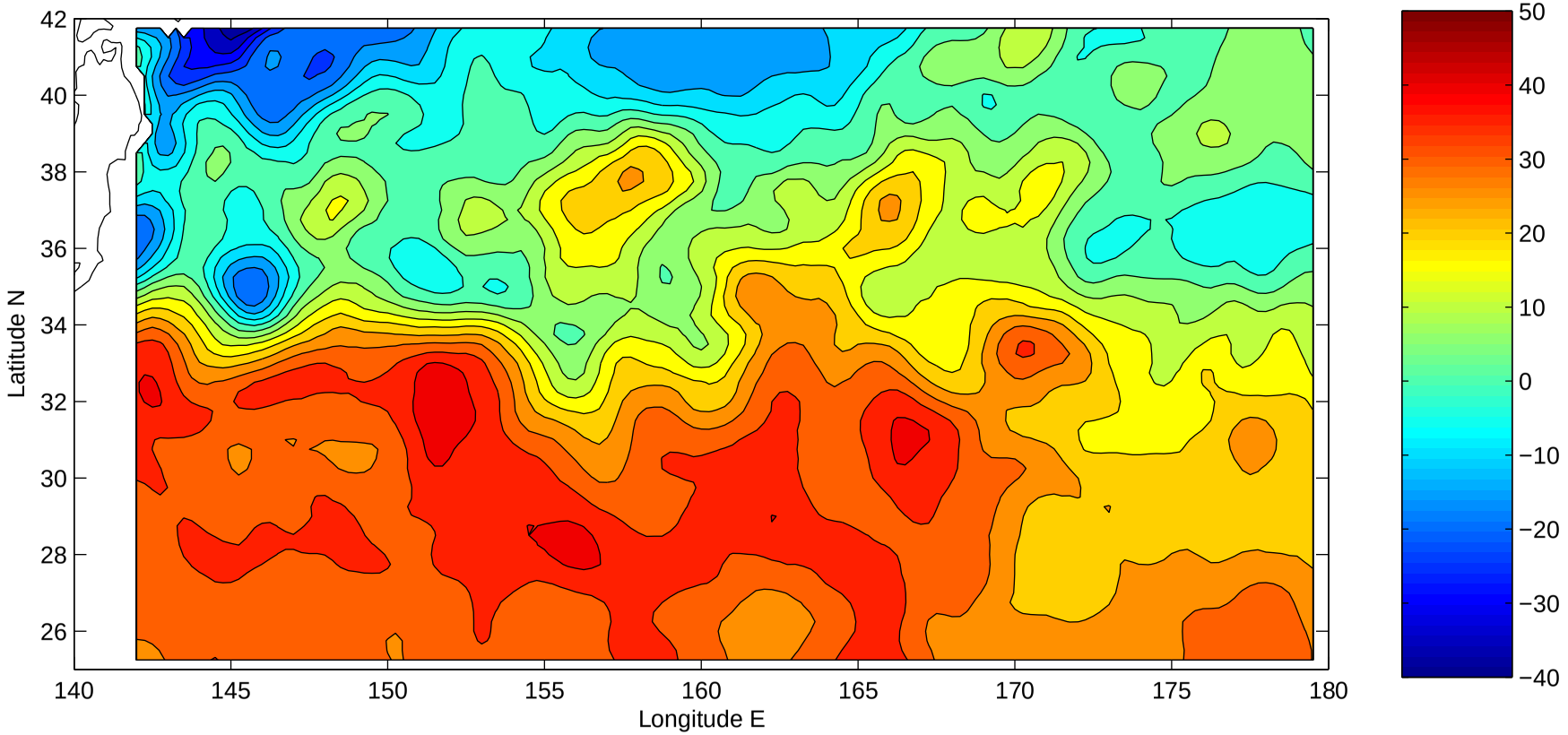

Latitude N
42
40
38
36
34
32
30
28
26
140
145
150
155
160
165
170
175
180
Longitude E
50
40
30
20
10
0
−10
−20
−30
−40

Fig.8

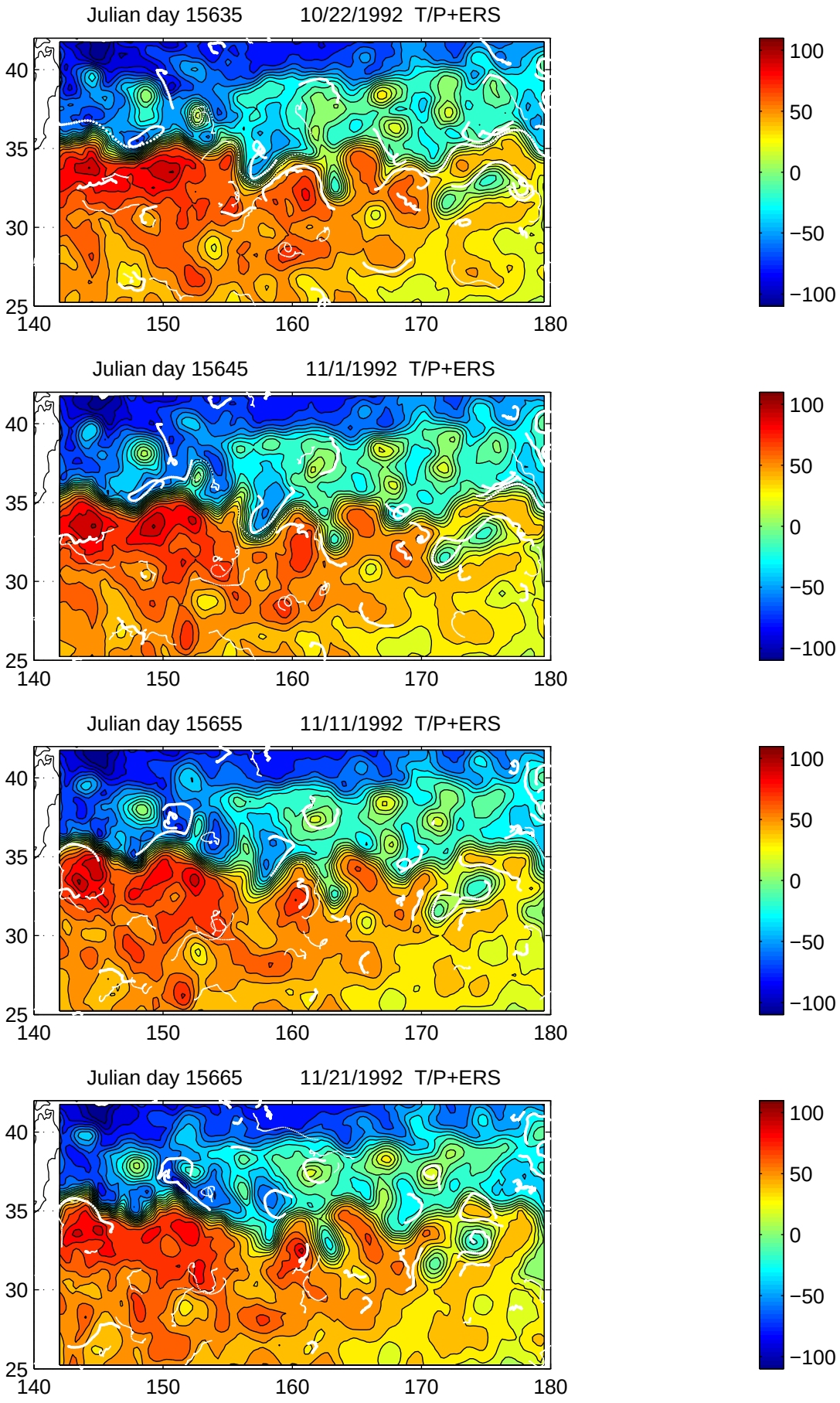

Julian day 15635 10/22/1992 T/P+ERS
Julian day 15645 11/1/1992 T/P+ERS
Julian day 15655 11/11/1992 T/P+ERS
Julian day 15665 11/21/1992 T/P+ERS
40
35
30
25
140
150
160
170
180
100
50
0
−50
−100

Fig.9−1

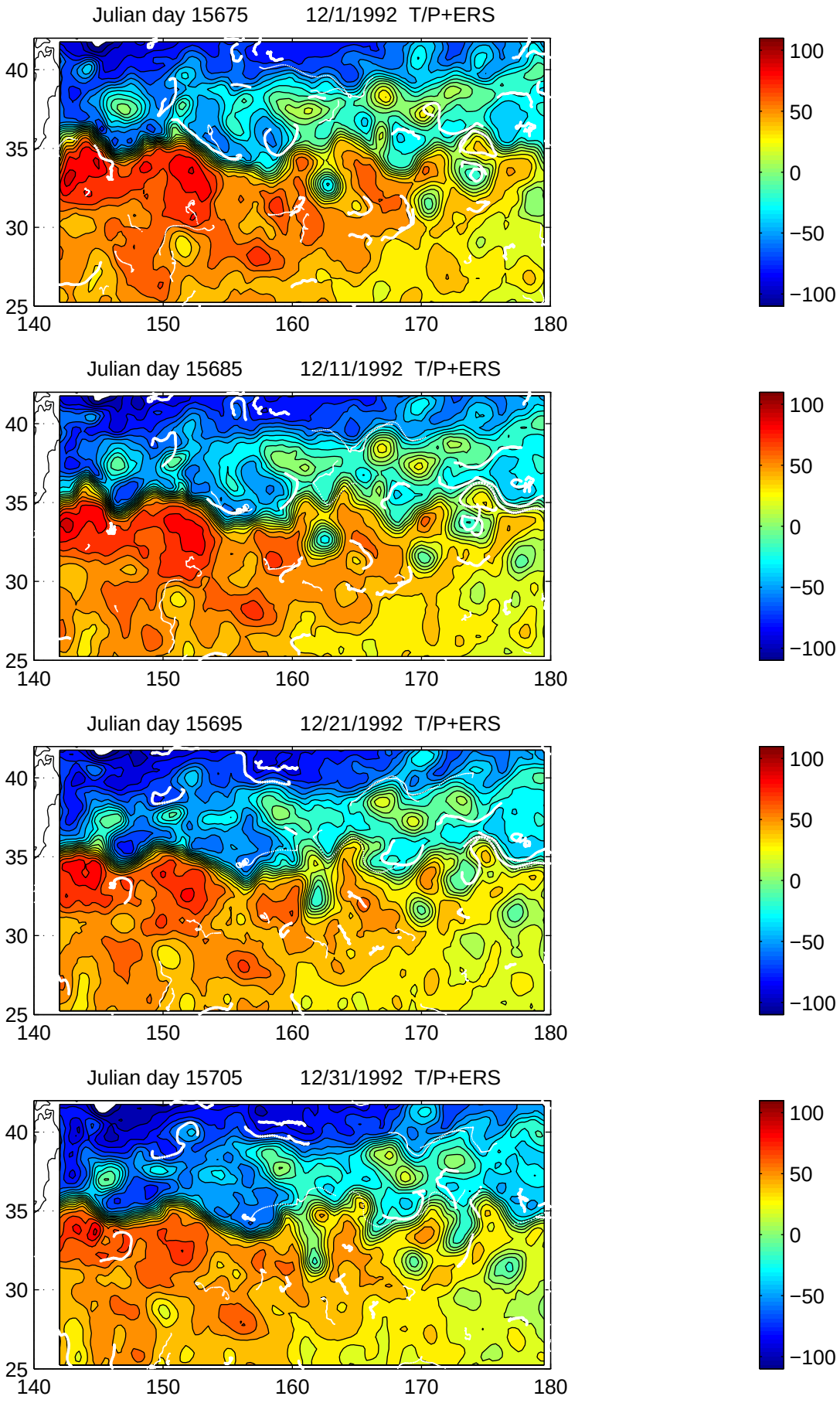

Julian day 15675 12/1/1992 T/P+ERS
Julian day 15685 12/11/1992 T/P+ERS
Julian day 15695 12/21/1992 T/P+ERS
Julian day 15705 12/31/1992 T/P+ERS
40
35
30
25
140
150
160
170
180
100
50
0
−50
−100

Fig.9−2

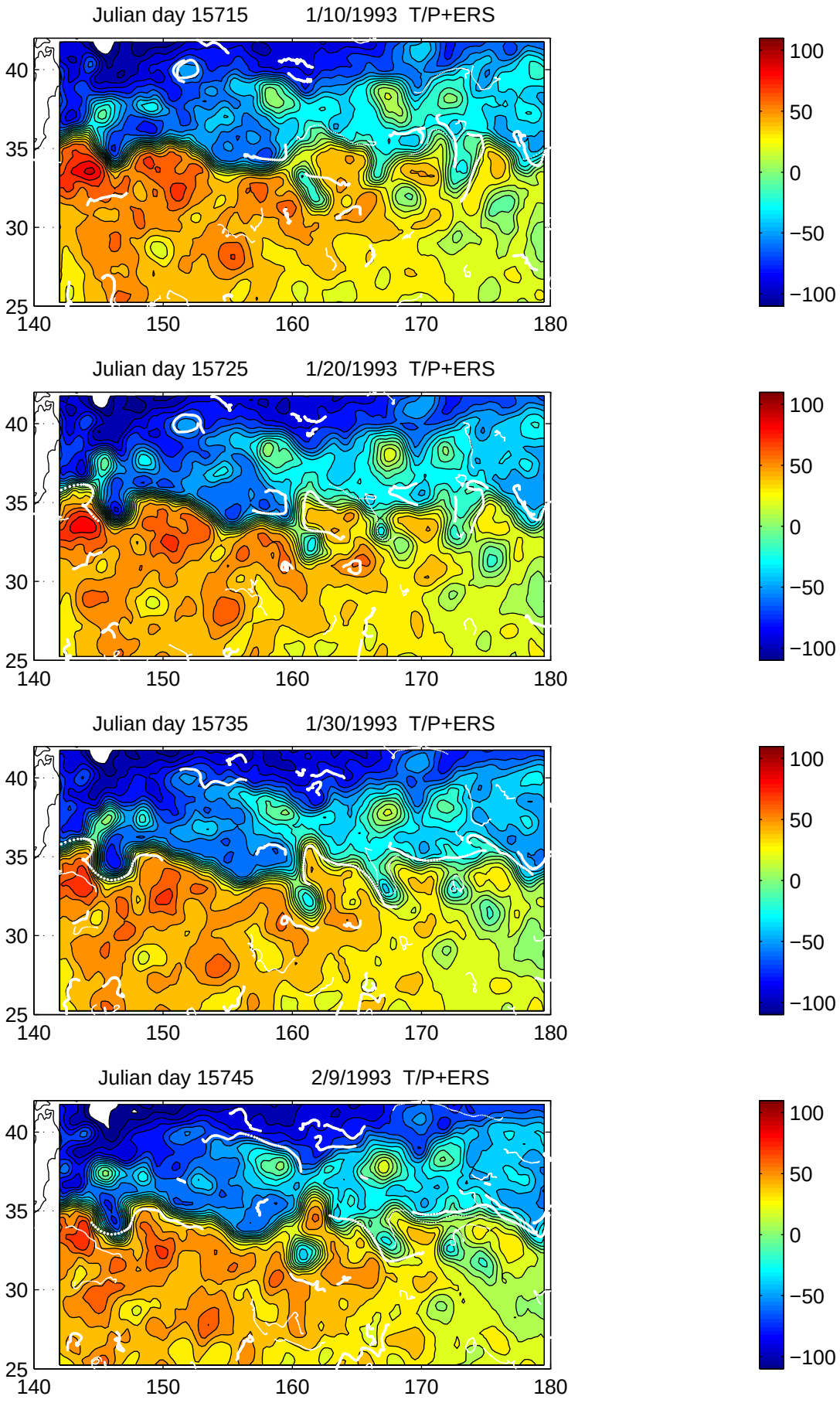

Julian day 15715 1/10/1993 T/P+ERS
Julian day 15725 1/20/1993 T/P+ERS
Julian day 15735 1/30/1993 T/P+ERS
Julian day 15745 2/9/1993 T/P+ERS
40
35
30
25
140
150
160
170
180
100
50
0
−50
−100

Fig.9−3

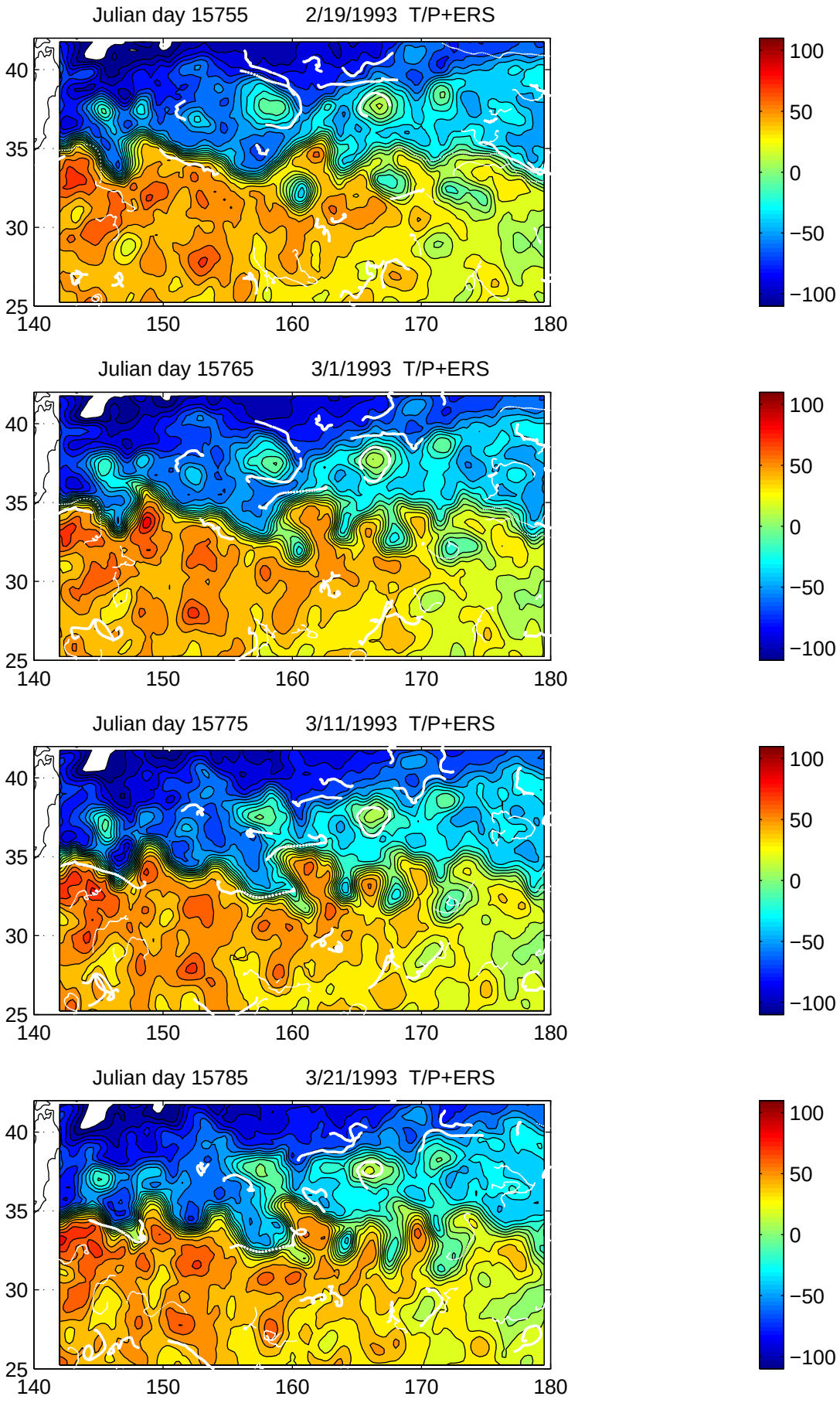

Julian day 15755 2/19/1993 T/P+ERS
Julian day 15765 3/1/1993 T/P+ERS
Julian day 15775 3/11/1993 T/P+ERS
Julian day 15785 3/21/1993 T/P+ERS
40
35
30
25
140
150
160
170
180
100
50
0
−50
−100

Fig.9−4

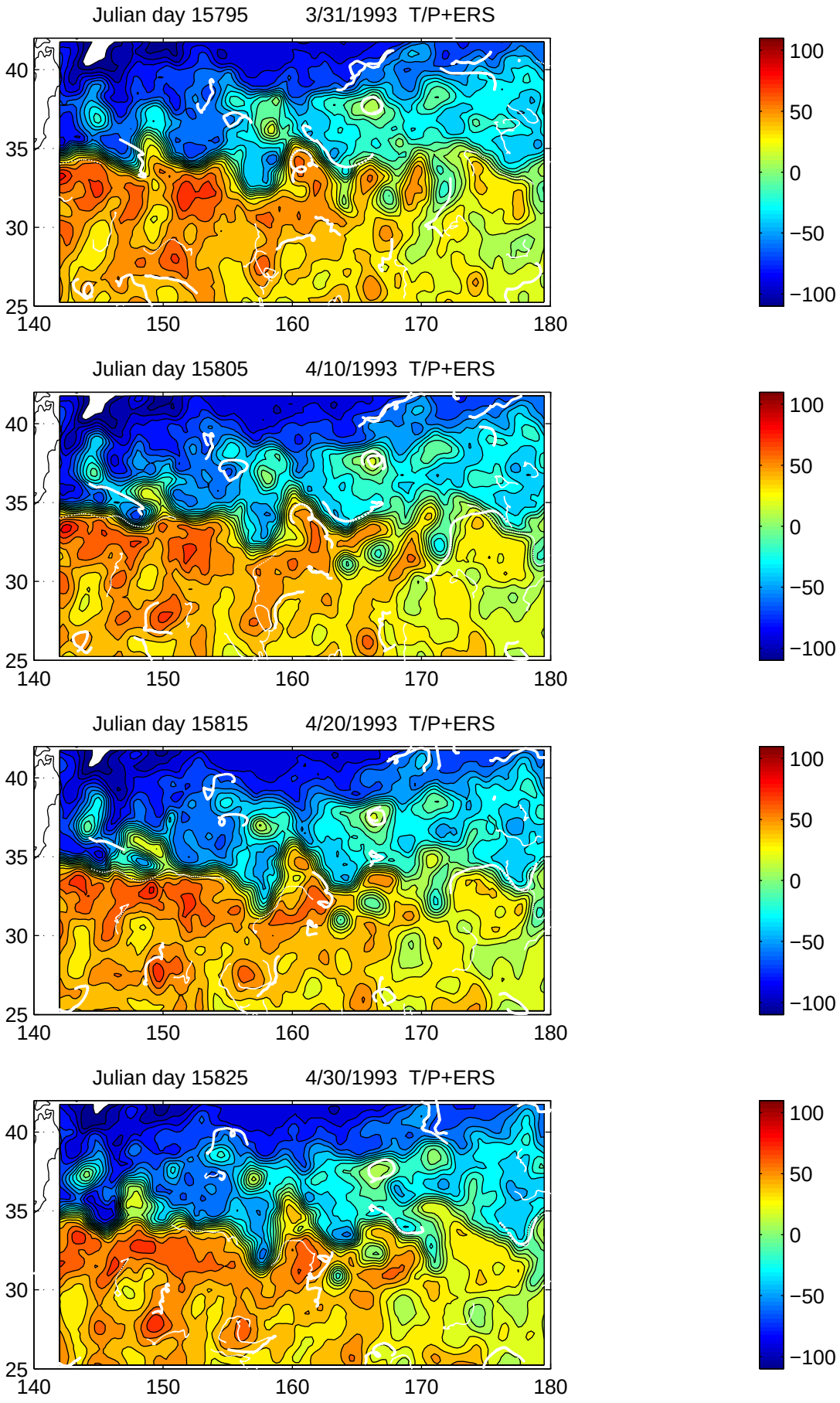

Julian day 15795 3/31/1993 T/P+ERS
Julian day 15805 4/10/1993 T/P+ERS
Julian day 15815 4/20/1993 T/P+ERS
Julian day 15825 4/30/1993 T/P+ERS
40
35
30
25
140
150
160
170
180
100
50
0
−50
−100

Fig.9−5

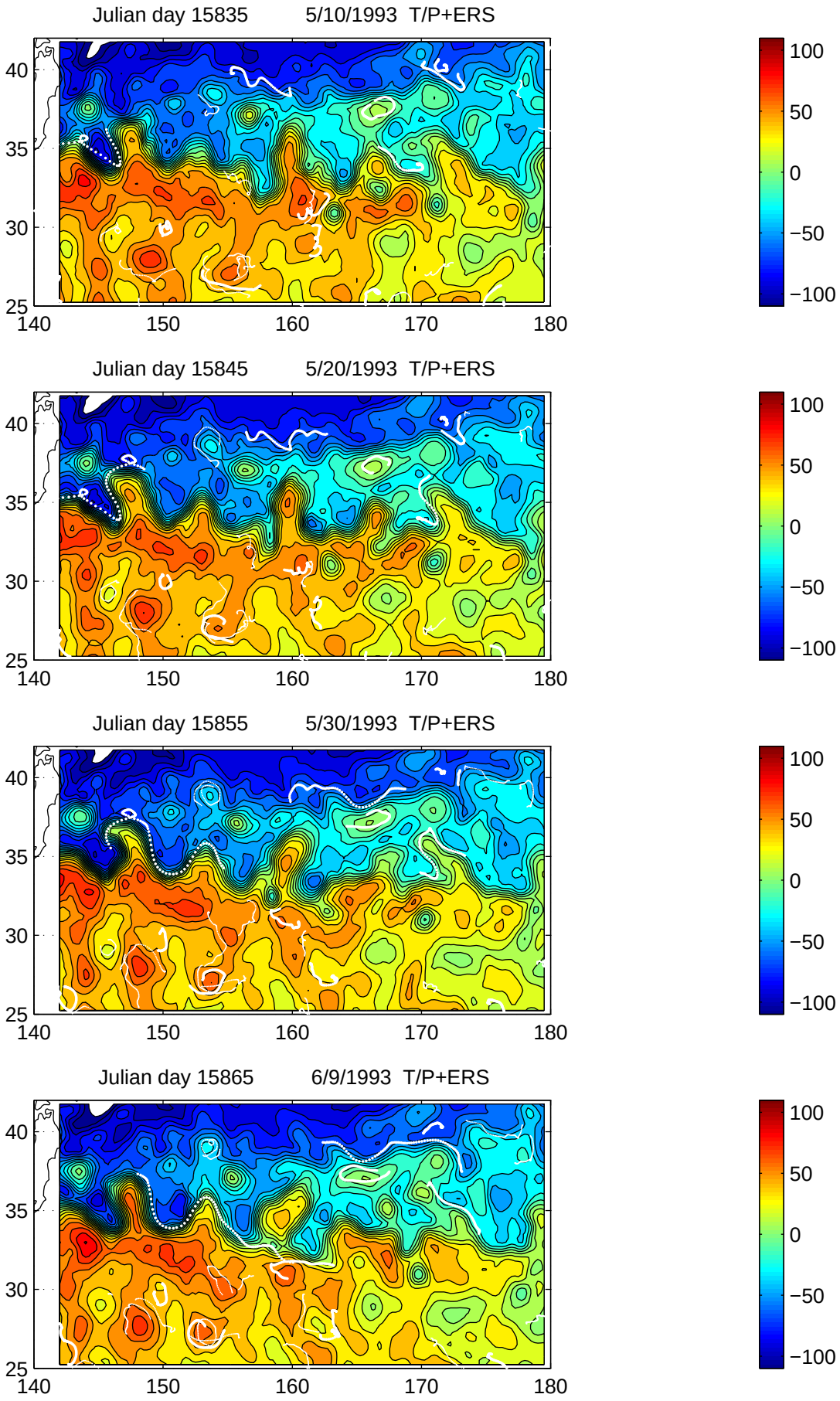

Julian day 15835 5/10/1993 T/P+ERS
Julian day 15845 5/20/1993 T/P+ERS
Julian day 15855 5/30/1993 T/P+ERS
Julian day 15865 6/9/1993 T/P+ERS
40
35
30
25
140
150
160
170
180
100
50
0
−50
−100

Fig.9−6

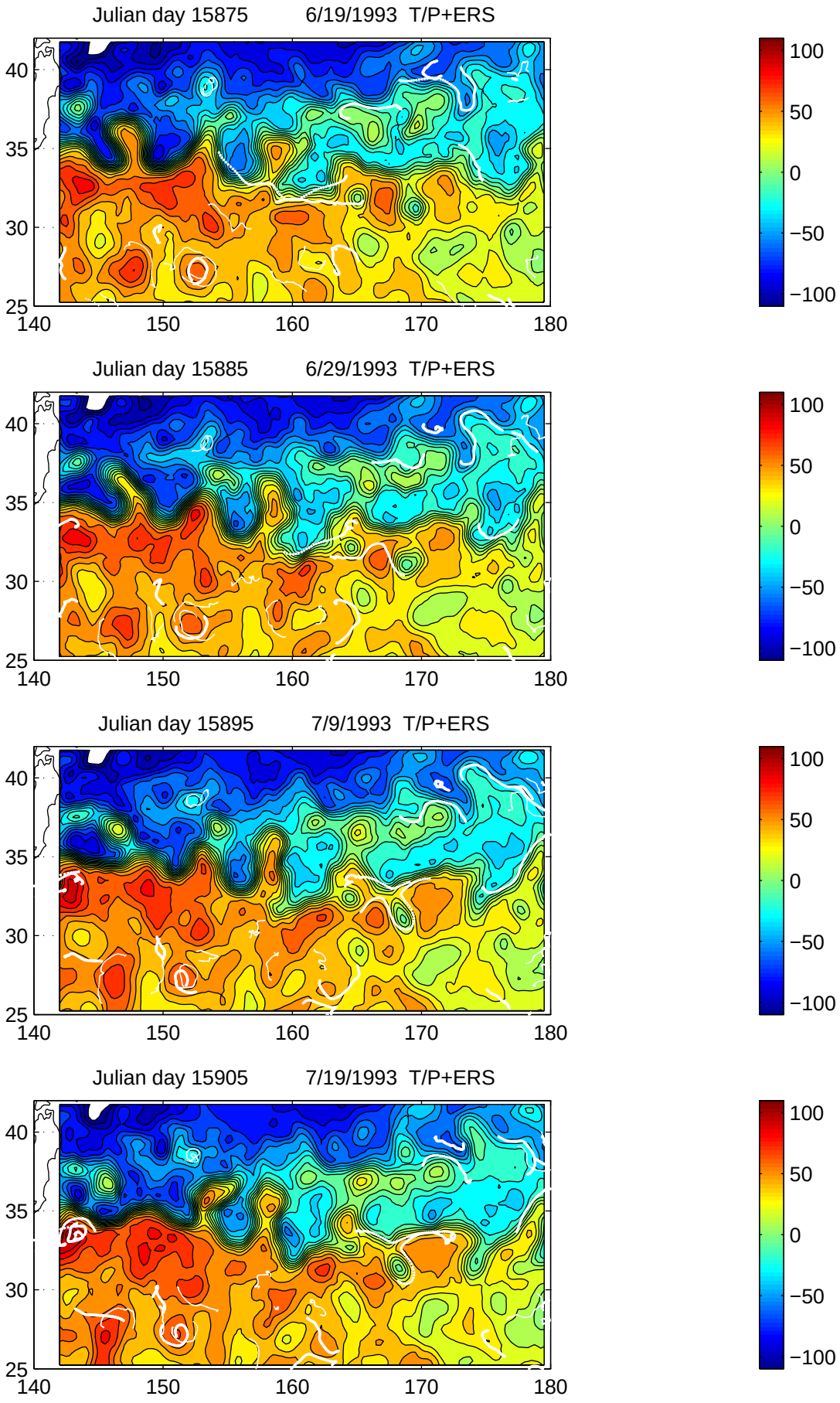

Julian day 15875 6/19/1993 T/P+ERS
Julian day 15885 6/29/1993 T/P+ERS
Julian day 15895 7/9/1993 T/P+ERS
Julian day 15905 7/19/1993 T/P+ERS
40
35
30
25
140
150
160
170
180
100
50
0
−50
−100

Fig.9−7

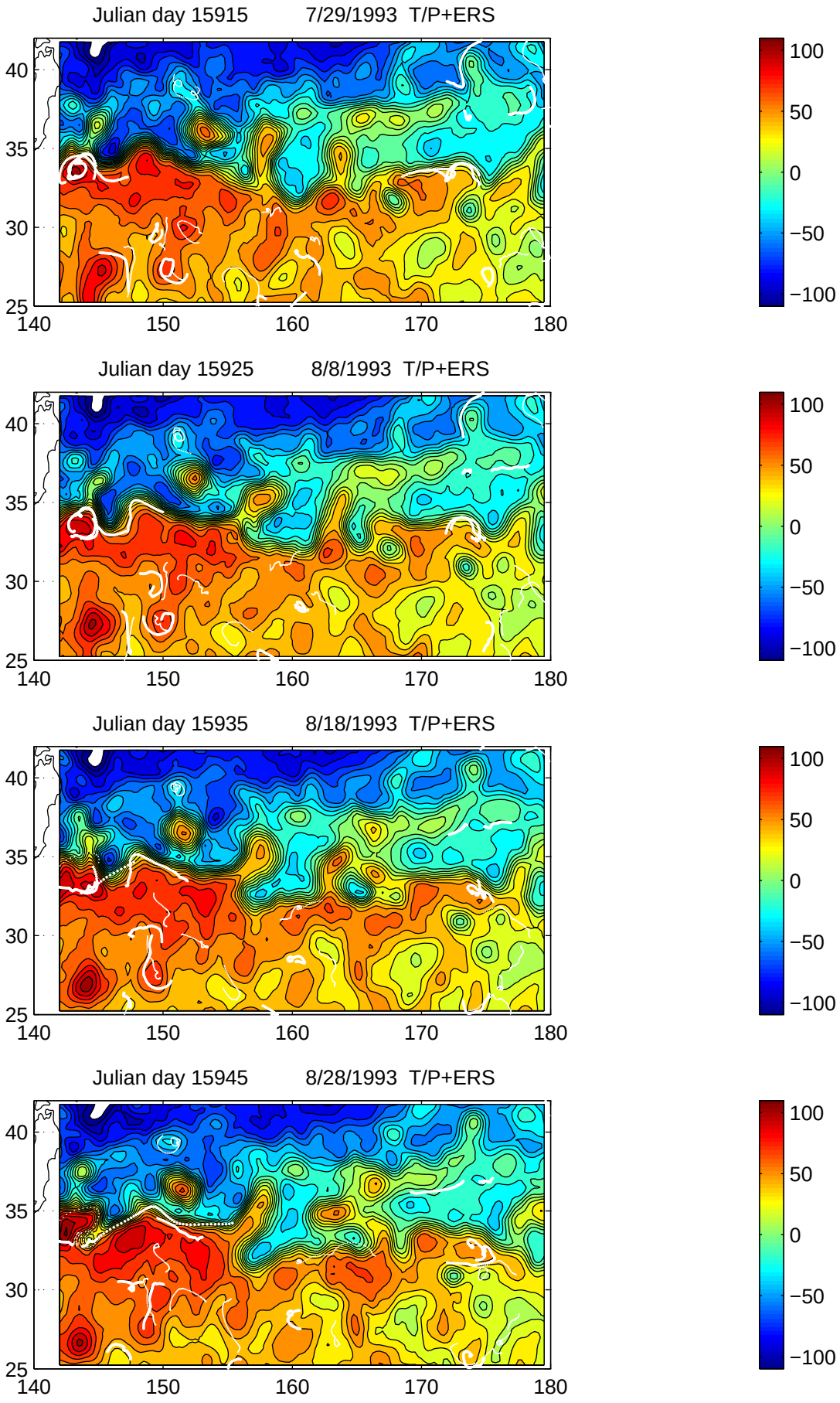

Julian day 15915 7/29/1993 T/P+ERS
Julian day 15925 8/8/1993 T/P+ERS
Julian day 15935 8/18/1993 T/P+ERS
Julian day 15945 8/28/1993 T/P+ERS
40
35
30
25
140
150
160
170
180
100
50
0
−50
−100

Fig.9−8

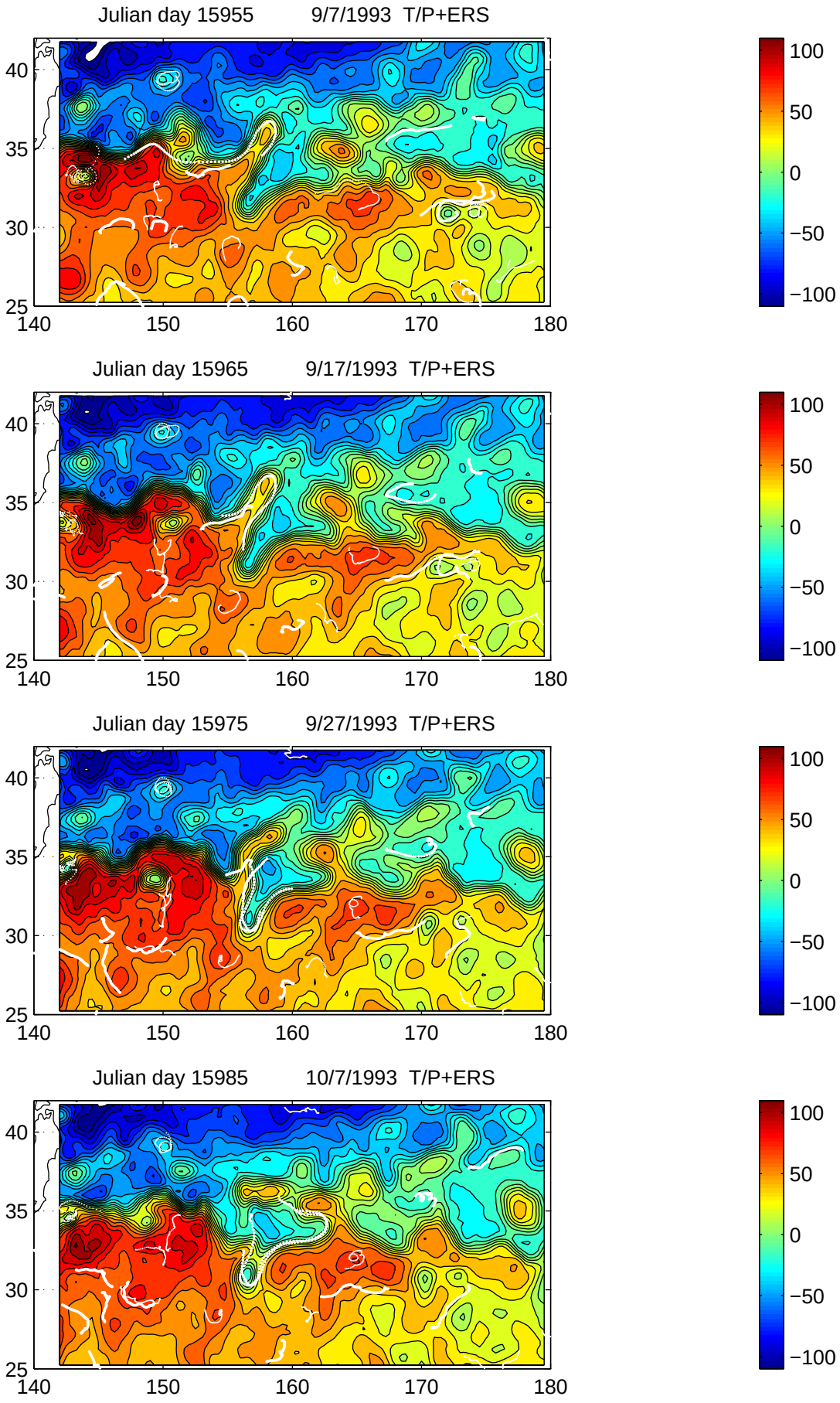

Julian day 15955 9/7/1993 T/P+ERS
Julian day 15965 9/17/1993 T/P+ERS
Julian day 15975 9/27/1993 T/P+ERS
Julian day 15985 10/7/1993 T/P+ERS
40
35
30
25
140
150
160
170
180
100
50
0
−50
−100

Fig.9−9

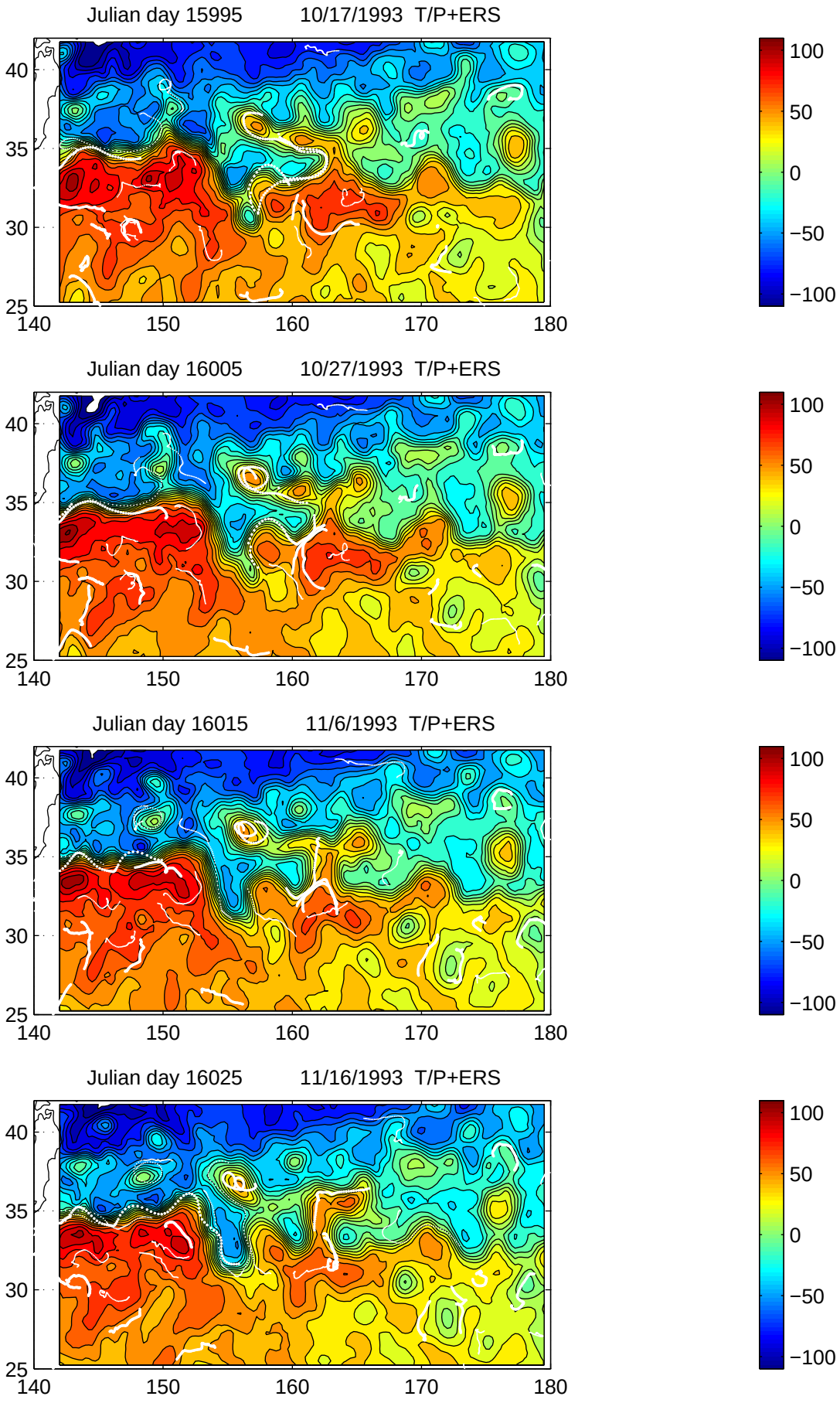

Julian day 15995 10/17/1993 T/P+ERS
Julian day 16005 10/27/1993 T/P+ERS
Julian day 16015 11/6/1993 T/P+ERS
Julian day 16025 11/16/1993 T/P+ERS
40
35
30
25
140
150
160
170
180
100
50
0
−50
−100

Fig.9−10

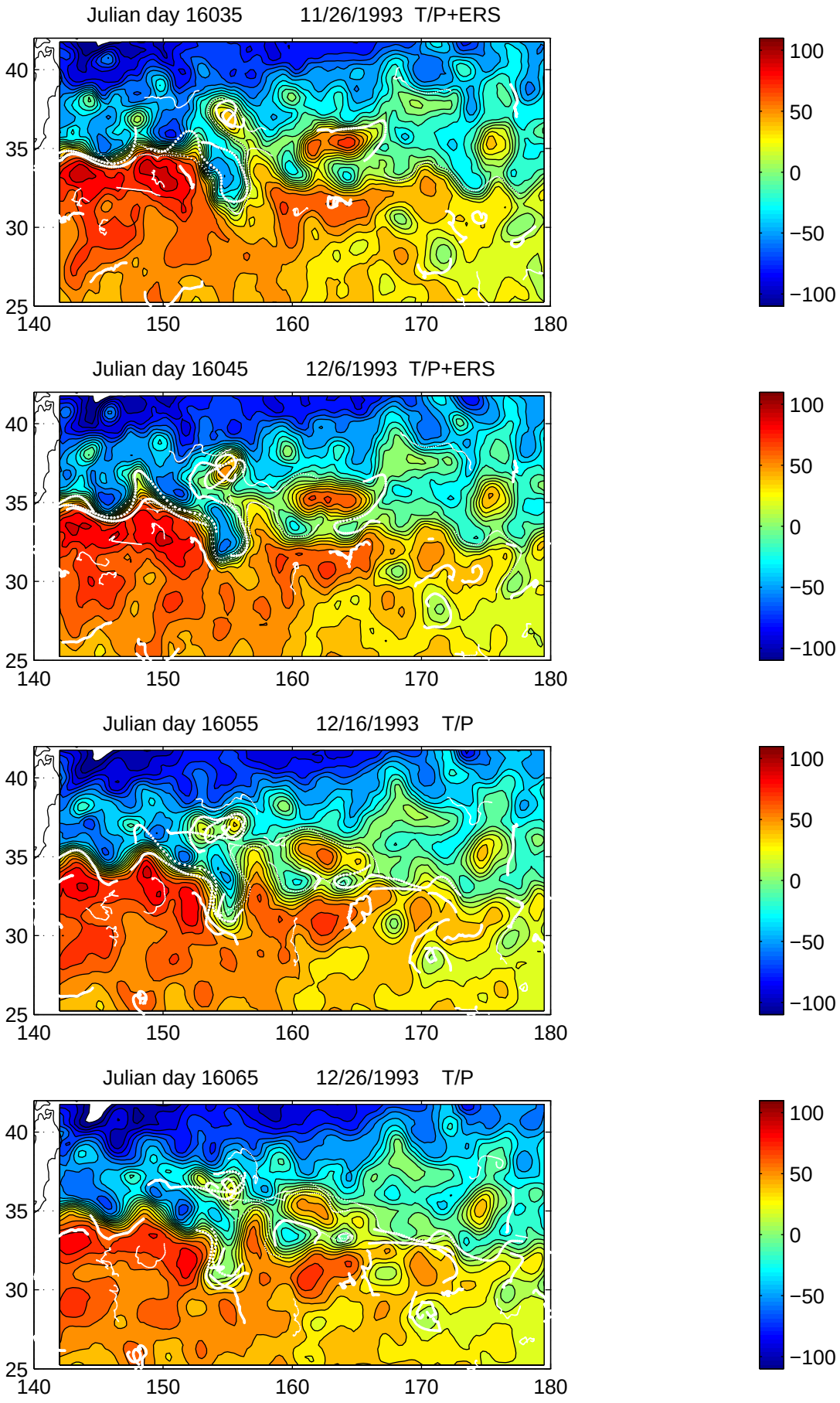

Julian day 16035 11/26/1993 T/P+ERS
Julian day 16045 12/6/1993 T/P+ERS
Julian day 16055 12/16/1993 T/P
Julian day 16065 12/26/1993 T/P
40
35
30
25
140
150
160
170
180
100
50
0
−50
−100

Fig.9−11

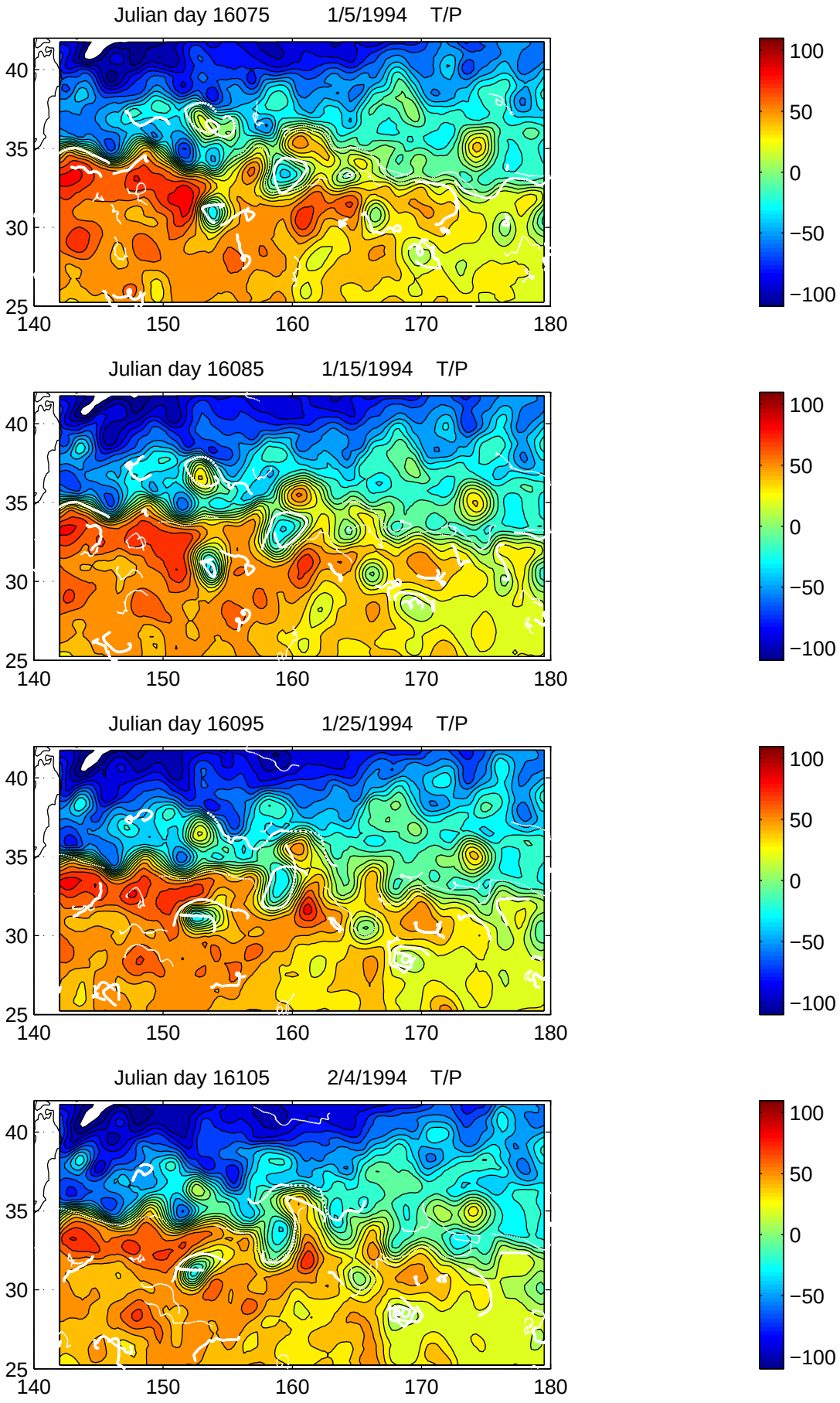

Julian day 16075 1/5/1994 T/P
Julian day 16085 1/15/1994 T/P
Julian day 16095 1/25/1994 T/P
Julian day 16105 2/4/1994 T/P
40
35
30
25
140
150
160
170
180
100
50
0
−50
−100

Fig.9−12

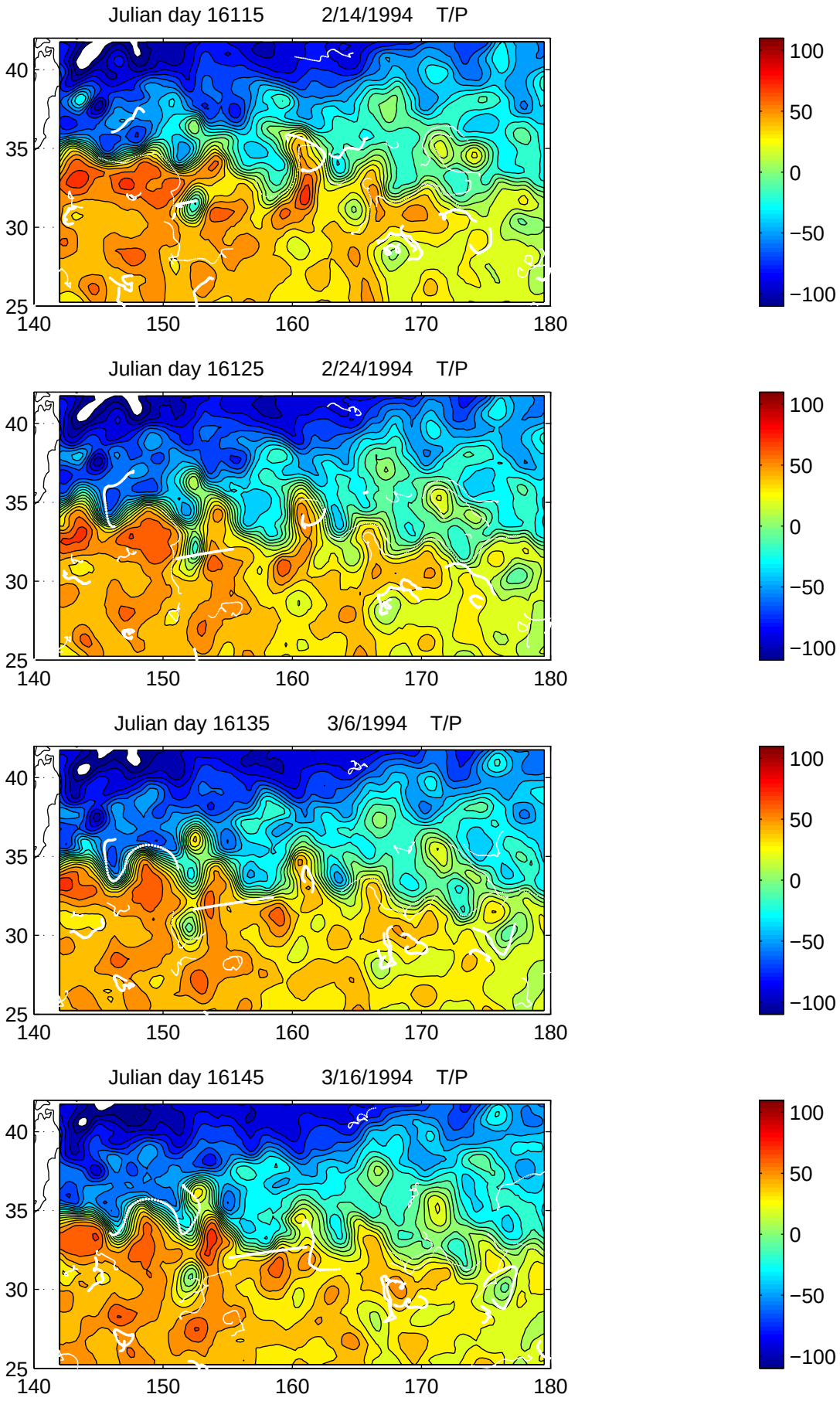

Julian day 16115 2/14/1994 T/P
Julian day 16125 2/24/1994 T/P
Julian day 16135 3/6/1994 T/P
Julian day 16145 3/16/1994 T/P
40
35
30
25
140
150
160
170
180
100
50
0
−50
−100

Fig.9−13

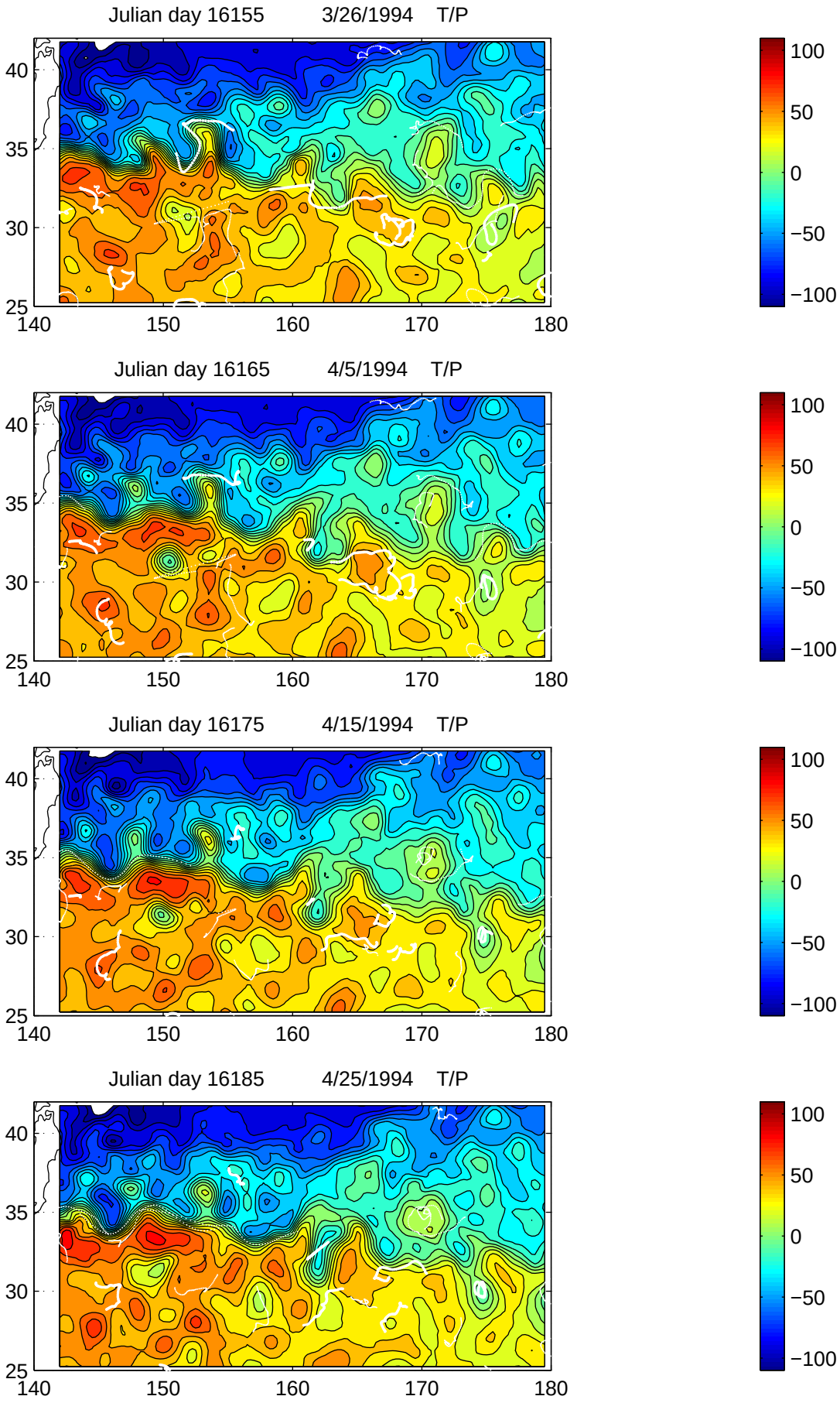

Julian day 16155 3/26/1994 T/P
Julian day 16165 4/5/1994 T/P
Julian day 16175 4/15/1994 T/P
Julian day 16185 4/25/1994 T/P
40
35
30
25
140
150
160
170
180
100
50
0
−50
−100

Fig.9−14

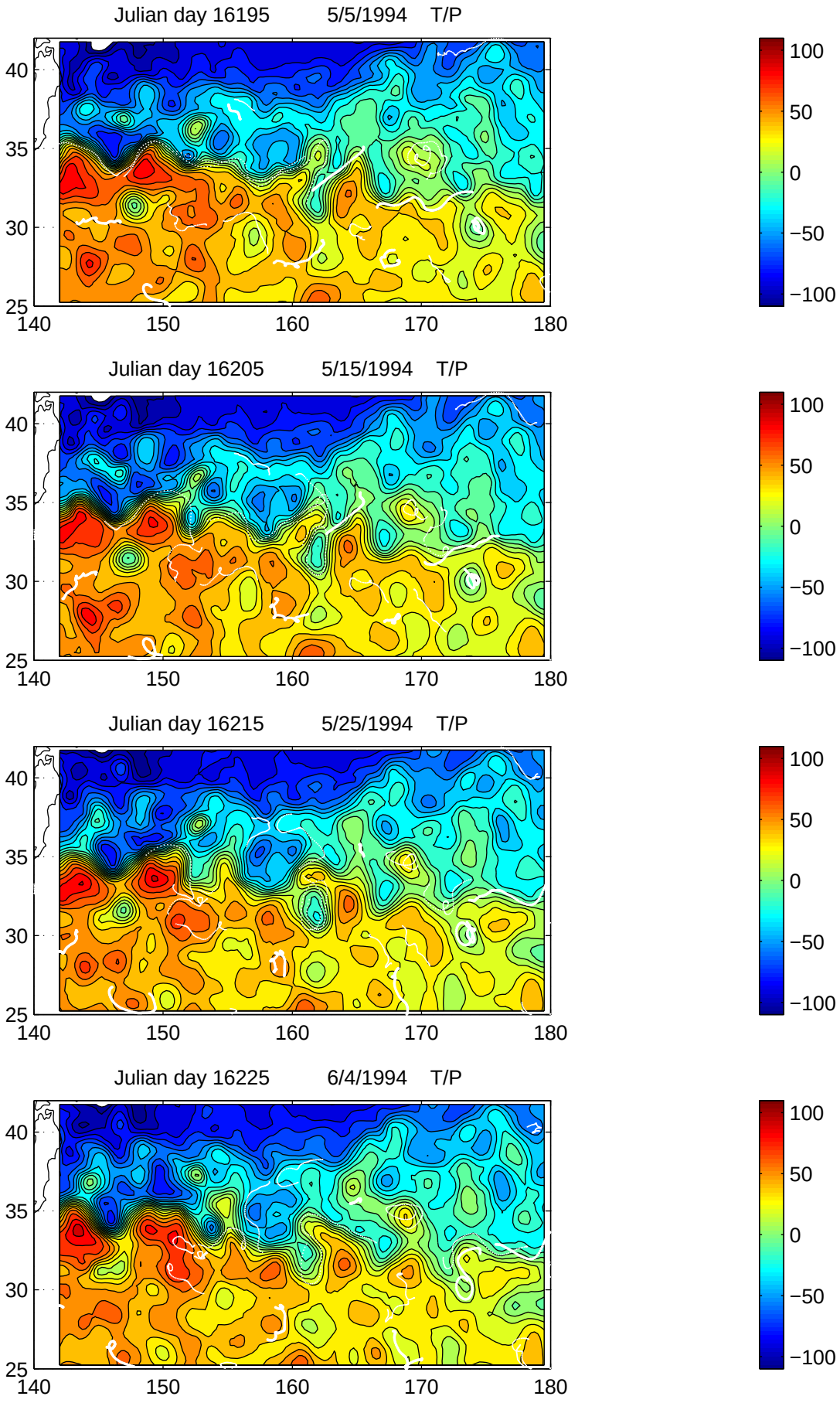

Julian day 16195 5/5/1994 T/P
Julian day 16205 5/15/1994 T/P
Julian day 16215 5/25/1994 T/P
Julian day 16225 6/4/1994 T/P
40
35
30
25
140
150
160
170
180
100
50
0
−50
−100

Fig.9−15

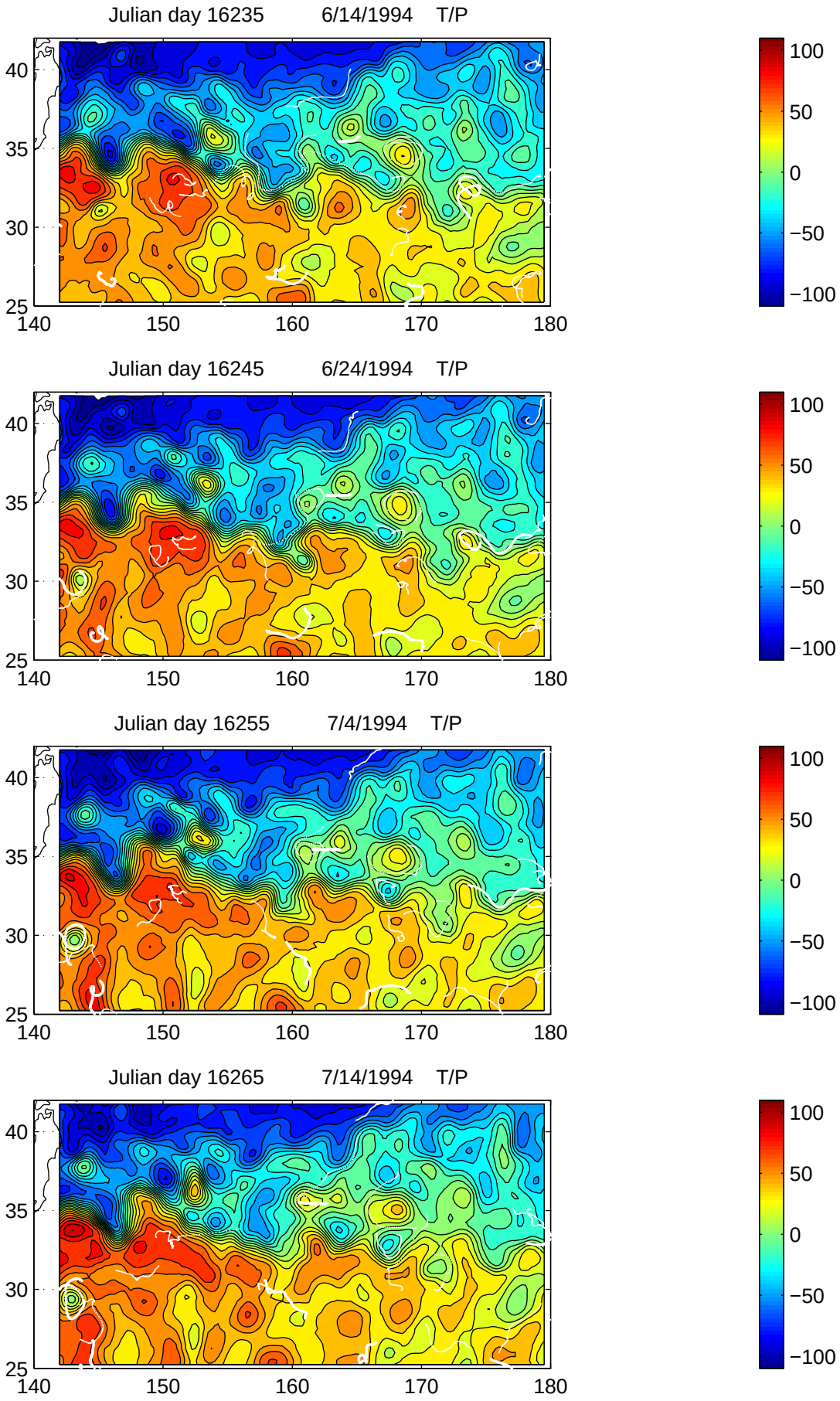

Julian day 16235 6/14/1994 T/P
Julian day 16245 6/24/1994 T/P
Julian day 16255 7/4/1994 T/P
Julian day 16265 7/14/1994 T/P
40
35
30
25
140
150
160
170
180
100
50
0
−50
−100

Fig.9−16

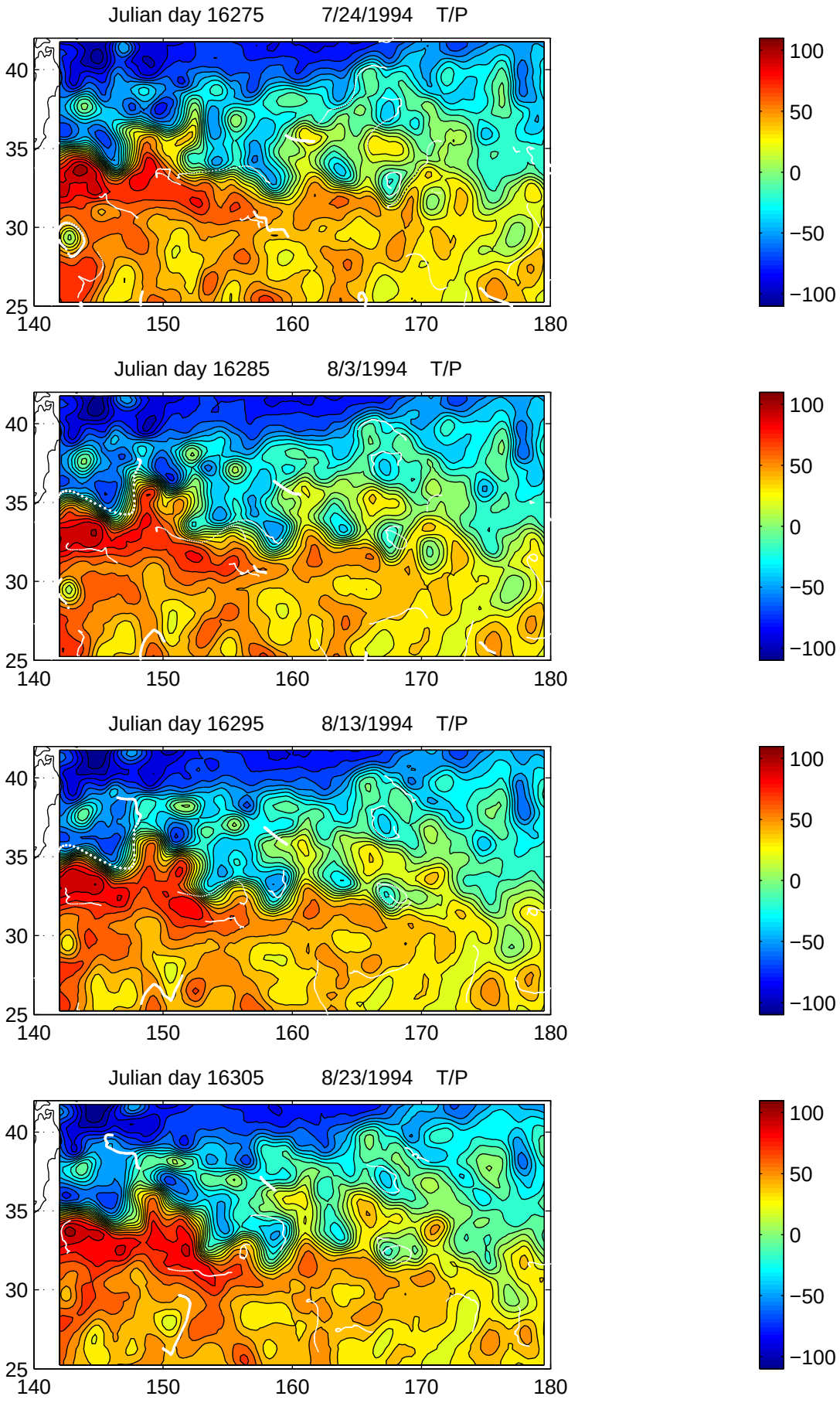

Julian day 16275 7/24/1994 T/P
Julian day 16285 8/3/1994 T/P
Julian day 16295 8/13/1994 T/P
Julian day 16305 8/23/1994 T/P
40
35
30
25
140
150
160
170
180
100
50
0
−50
−100

Fig.9−17

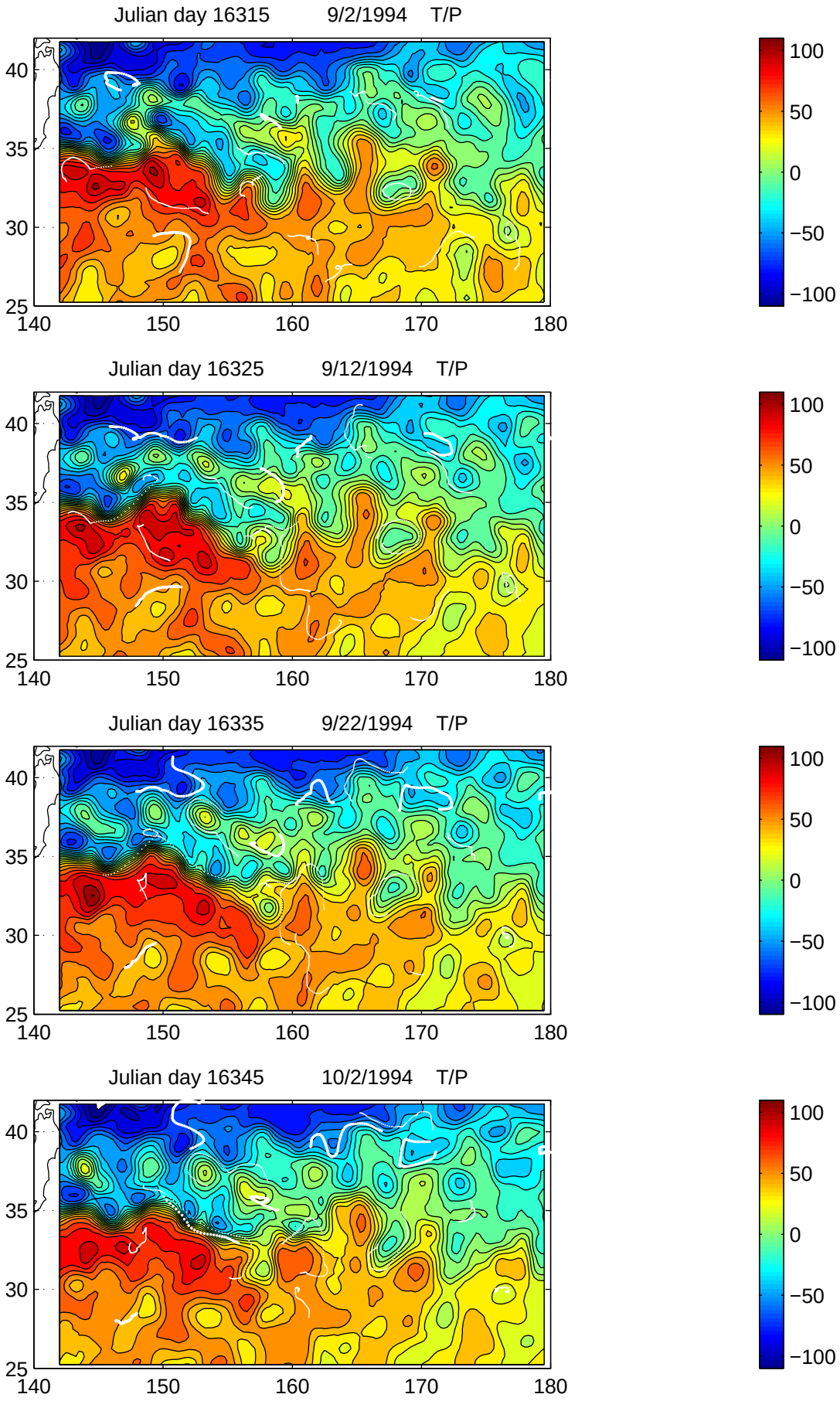

Julian day 16315 9/2/1994 T/P
Julian day 16325 9/12/1994 T/P
Julian day 16335 9/22/1994 T/P
Julian day 16345 10/2/1994 T/P
40
35
30
25
140
150
160
170
180
100
50
0
−50
−100

Fig.9−18

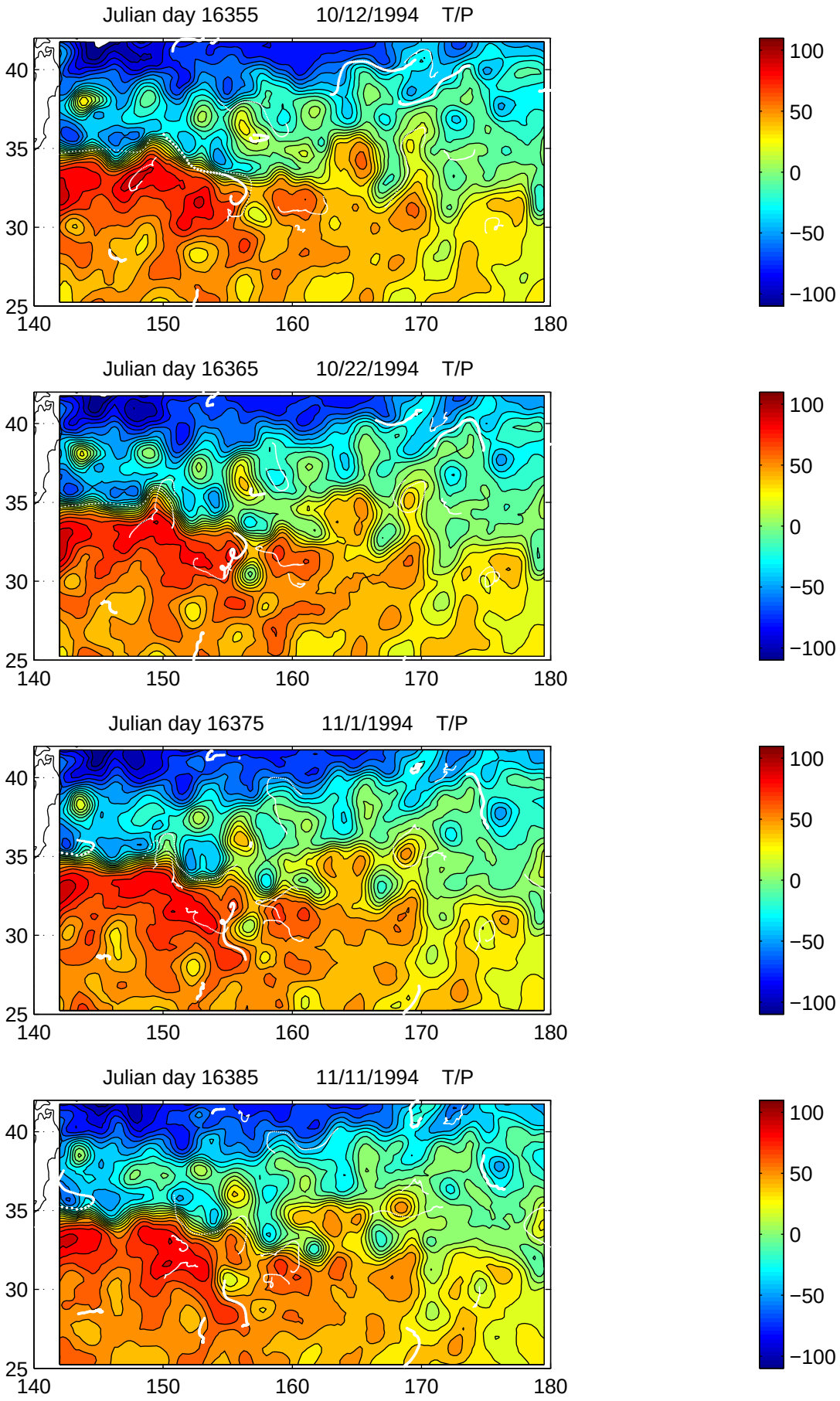

Julian day 16355 10/12/1994 T/P
Julian day 16365 10/22/1994 T/P
Julian day 16375 11/1/1994 T/P
Julian day 16385 11/11/1994 T/P
40
35
30
25
140
150
160
170
180
100
50
0
−50
−100

Fig.9−19

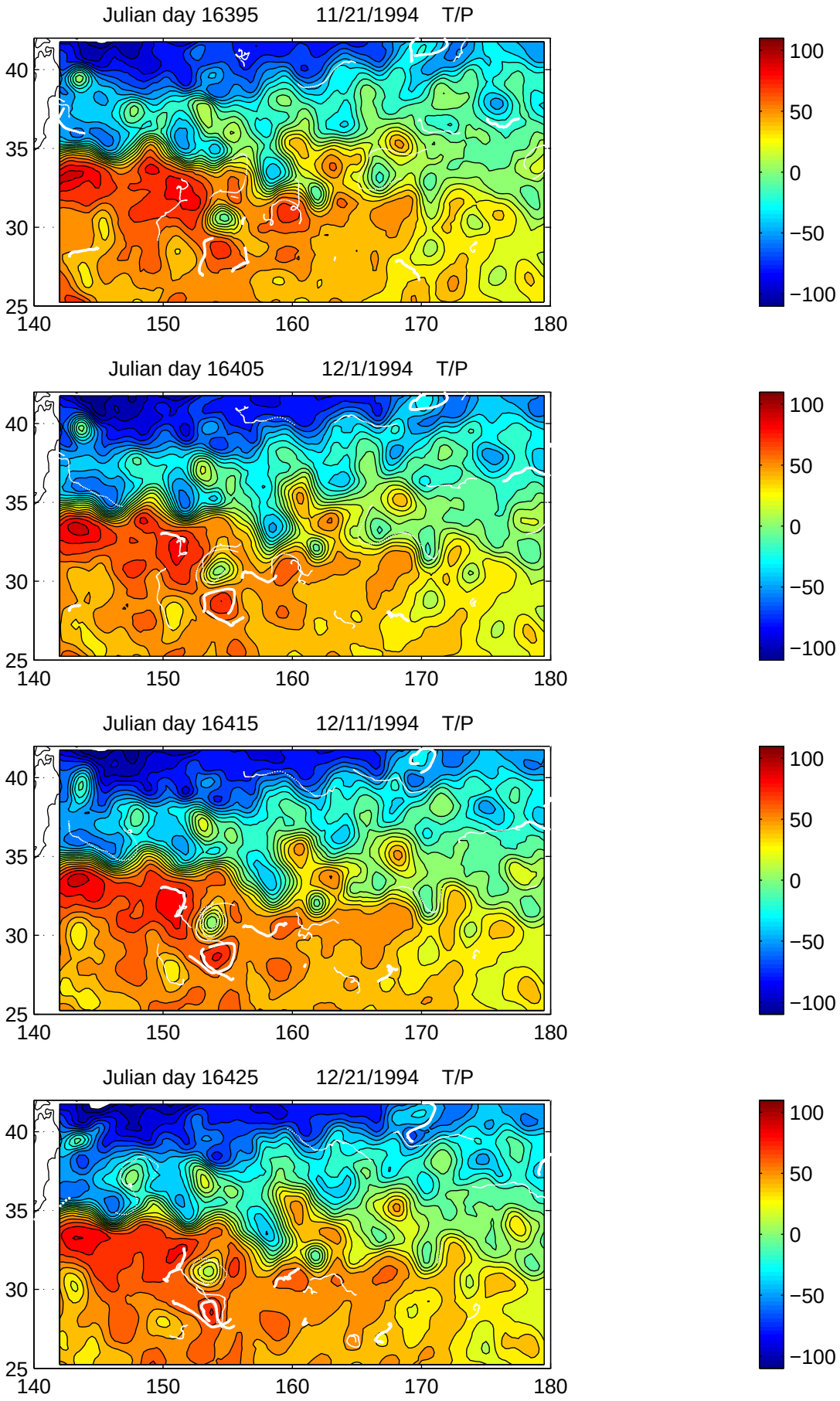

Julian day 16395 11/21/1994 T/P
Julian day 16405 12/1/1994 T/P
Julian day 16415 12/11/1994 T/P
Julian day 16425 12/21/1994 T/P
40
35
30
25
140
150
160
170
180
100
50
0
−50
−100

Fig.9−20

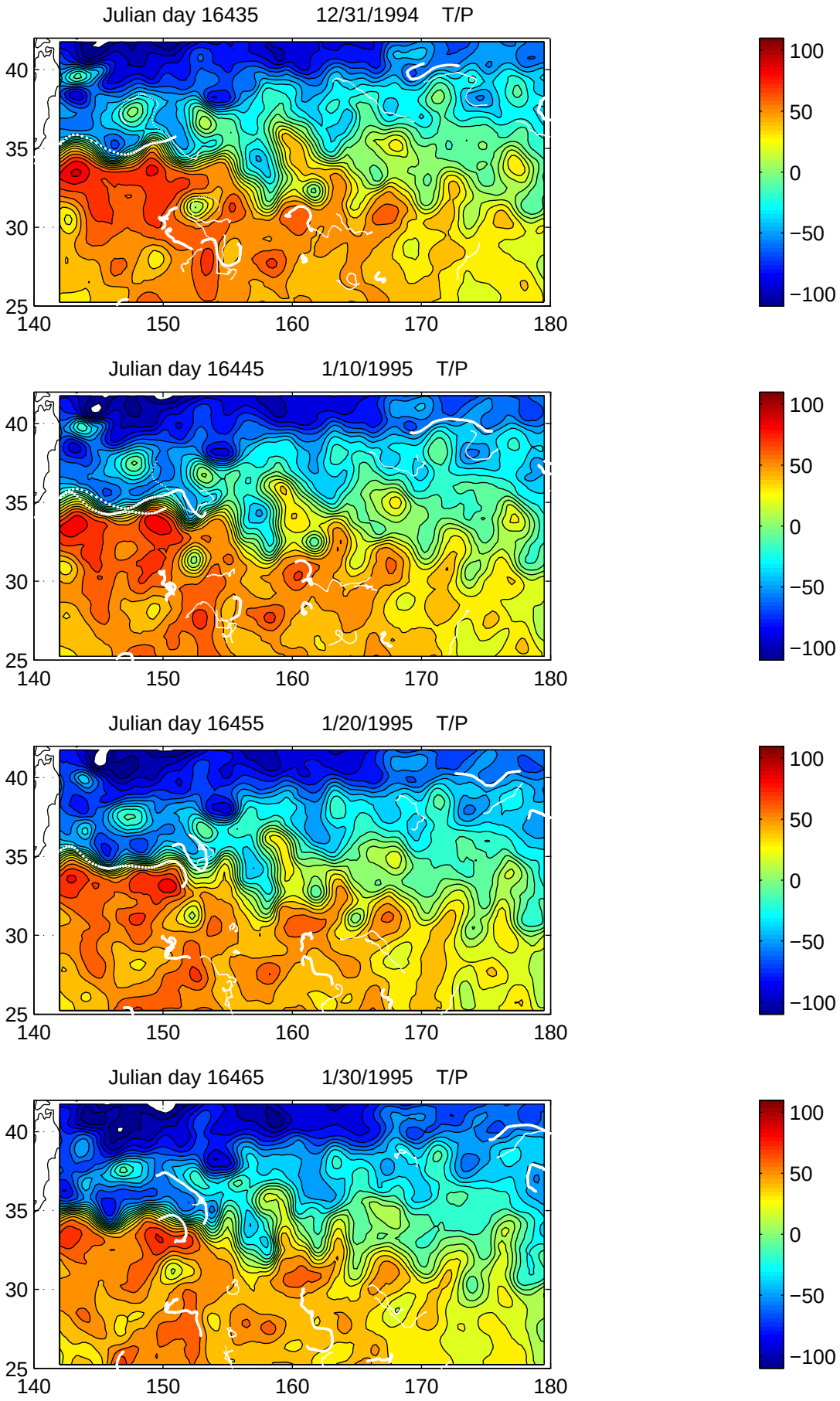

Julian day 16435 12/31/1994 T/P
Julian day 16445 1/10/1995 T/P
Julian day 16455 1/20/1995 T/P
Julian day 16465 1/30/1995 T/P
40
35
30
25
140
150
160
170
180
100
50
0
−50
−100

Fig.9−21

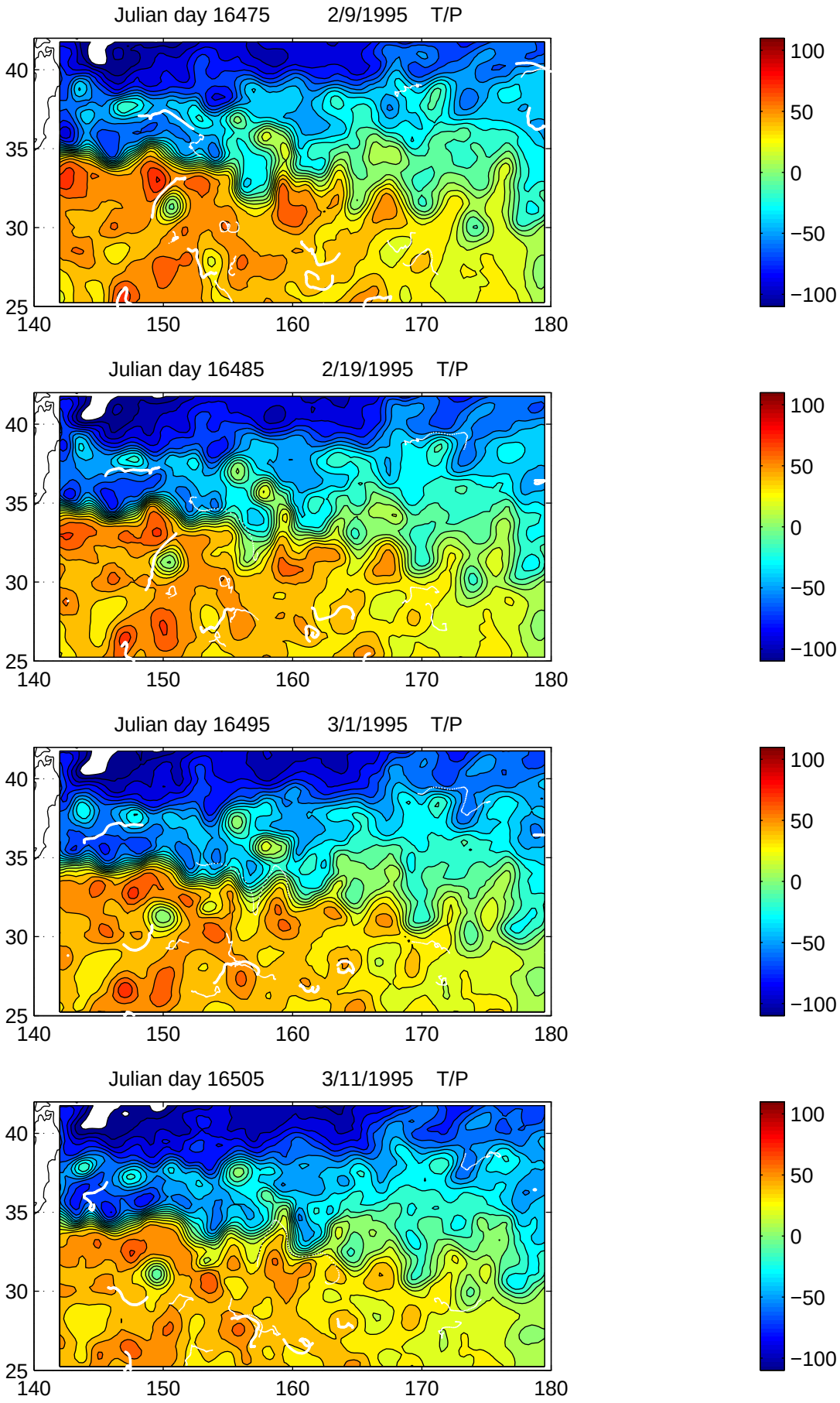

Julian day 16475 2/9/1995 T/P
Julian day 16485 2/19/1995 T/P
Julian day 16495 3/1/1995 T/P
Julian day 16505 3/11/1995 T/P
40
35
30
25
140
150
160
170
180
100
50
0
−50
−100

Fig.9−22

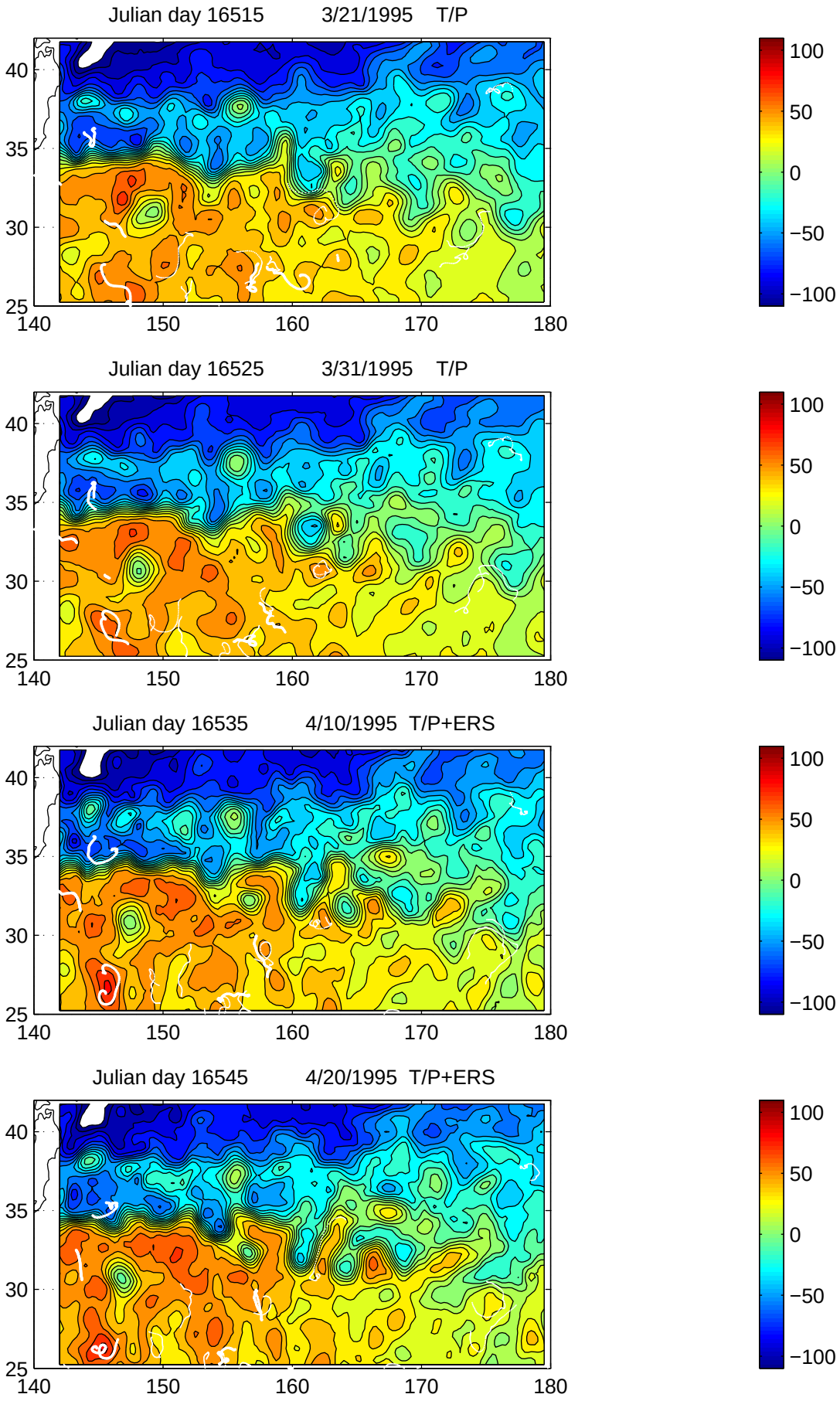

Julian day 16515 3/21/1995 T/P
Julian day 16525 3/31/1995 T/P
Julian day 16535 4/10/1995 T/P+ERS
Julian day 16545 4/20/1995 T/P+ERS
40
35
30
25
140
150
160
170
180
100
50
0
−50
−100

Fig.9−23

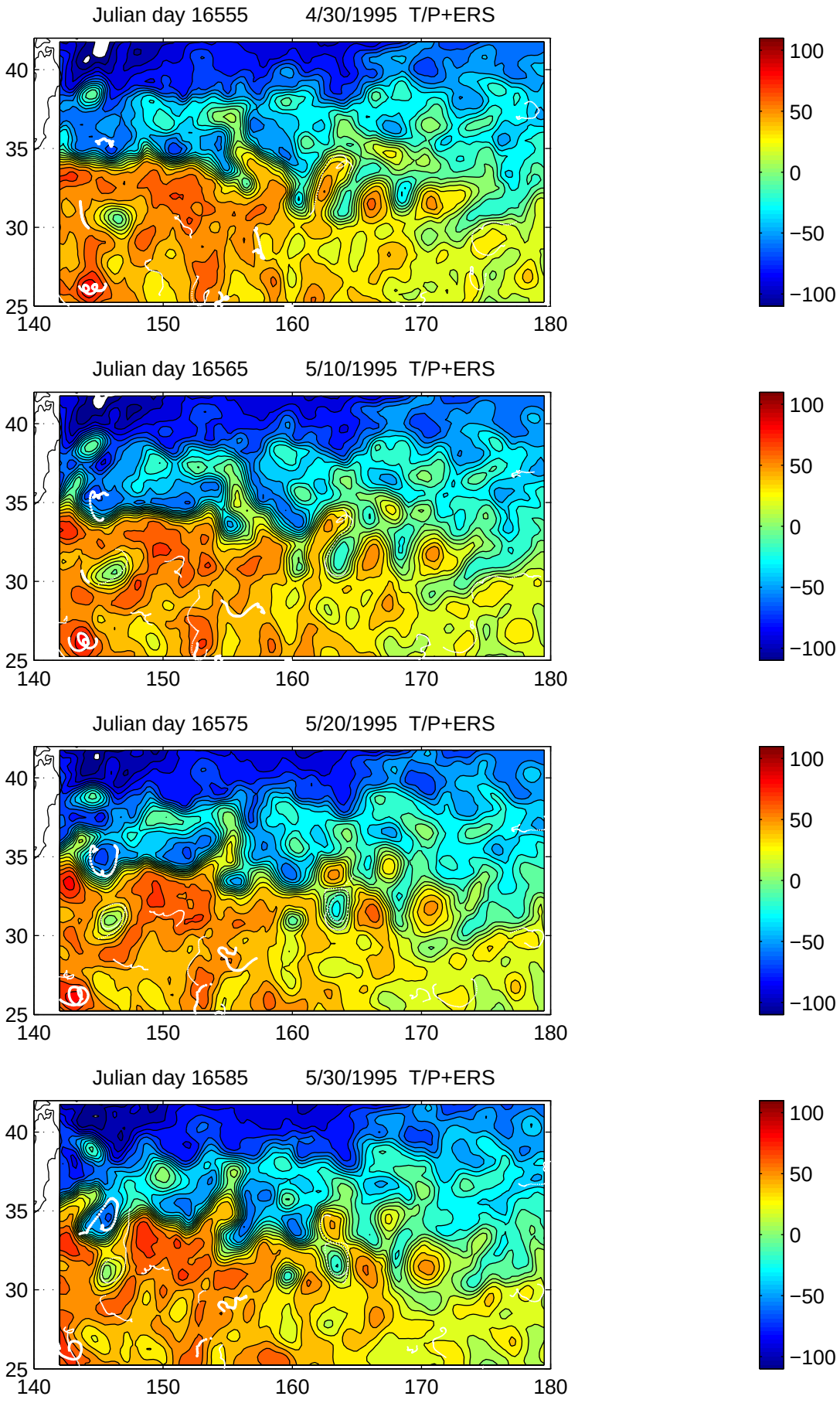

Julian day 16555 4/30/1995 T/P+ERS
Julian day 16565 5/10/1995 T/P+ERS
Julian day 16575 5/20/1995 T/P+ERS
Julian day 16585 5/30/1995 T/P+ERS
40
35
30
25
140
150
160
170
180
100
50
0
−50
−100

Fig.9−24

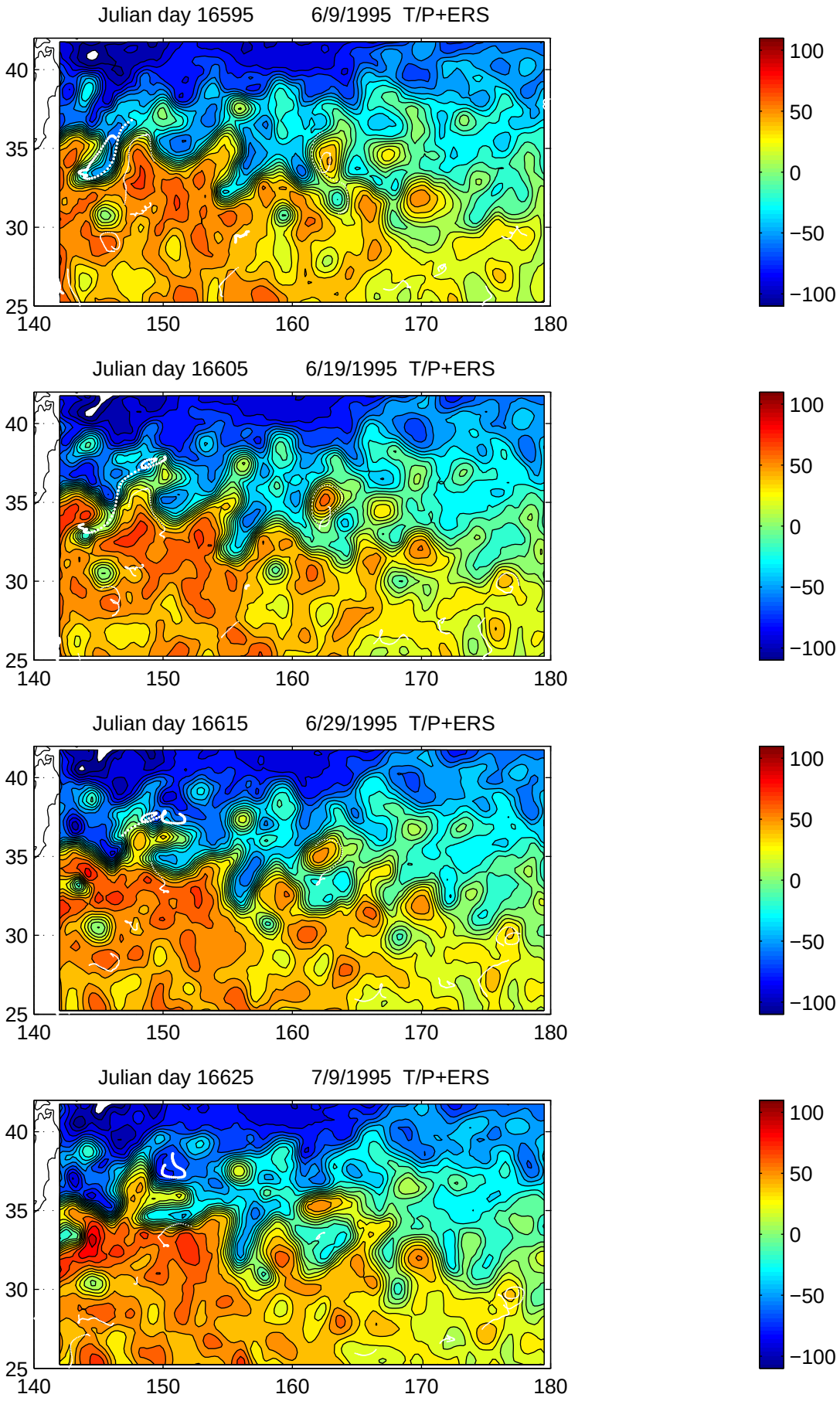

Julian day 16595 6/9/1995 T/P+ERS
Julian day 16605 6/19/1995 T/P+ERS
Julian day 16615 6/29/1995 T/P+ERS
Julian day 16625 7/9/1995 T/P+ERS
40
35
30
25
140
150
160
170
180
100
50
0
−50
−100

Fig.9−25

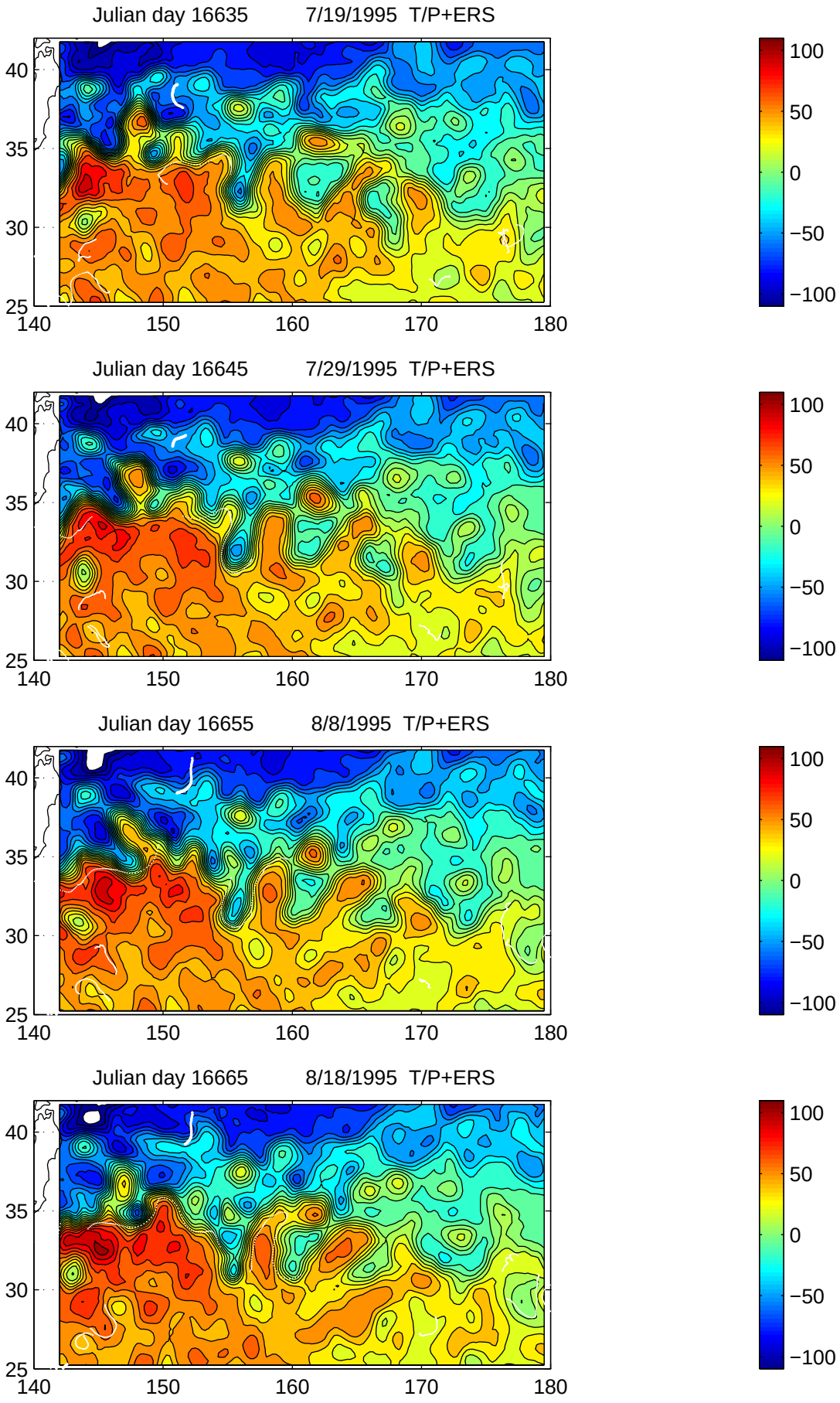

Julian day 16635 7/19/1995 T/P+ERS
Julian day 16645 7/29/1995 T/P+ERS
Julian day 16655 8/8/1995 T/P+ERS
Julian day 16665 8/18/1995 T/P+ERS
40
35
30
25
140
150
160
170
180
100
50
0
−50
−100

Fig.9−26

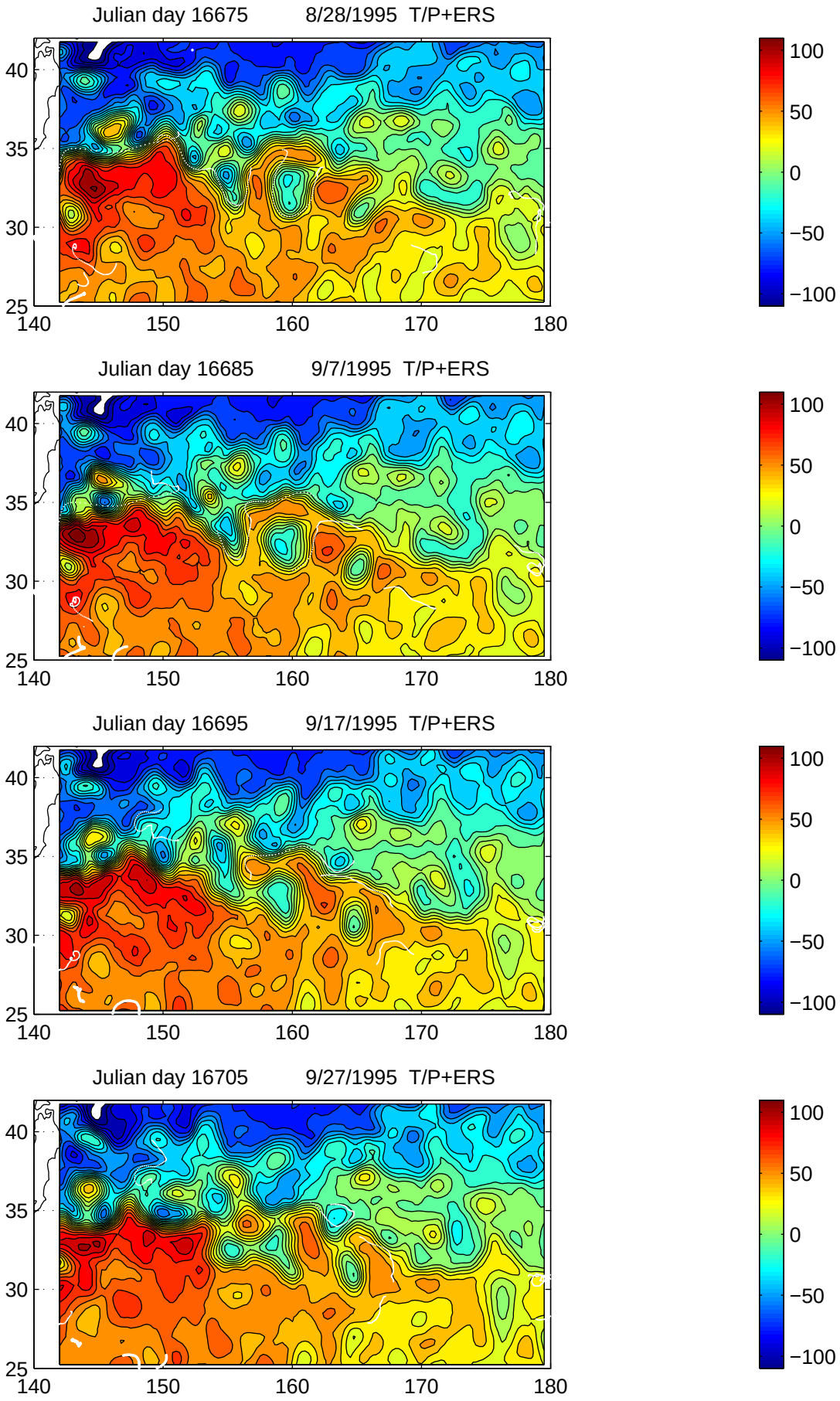

Julian day 16675 8/28/1995 T/P+ERS
Julian day 16685 9/7/1995 T/P+ERS
Julian day 16695 9/17/1995 T/P+ERS
Julian day 16705 9/27/1995 T/P+ERS
40
35
30
25
140
150
160
170
180
100
50
0
−50
−100

Fig.9−27

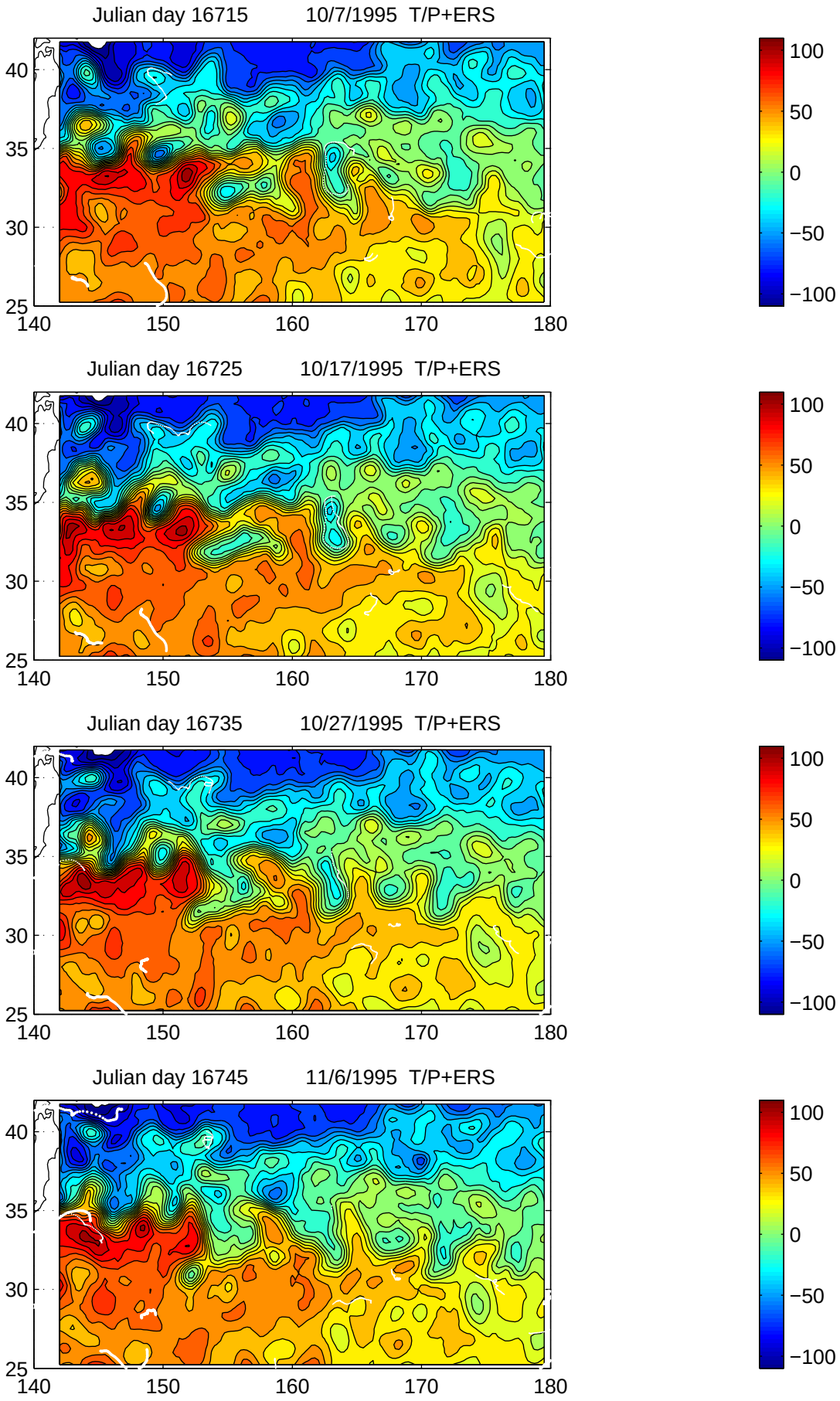

Julian day 16715 10/7/1995 T/P+ERS
Julian day 16725 10/17/1995 T/P+ERS
Julian day 16735 10/27/1995 T/P+ERS
Julian day 16745 11/6/1995 T/P+ERS
40
35
30
25
140
150
160
170
180
100
50
0
−50
−100

Fig.9−28

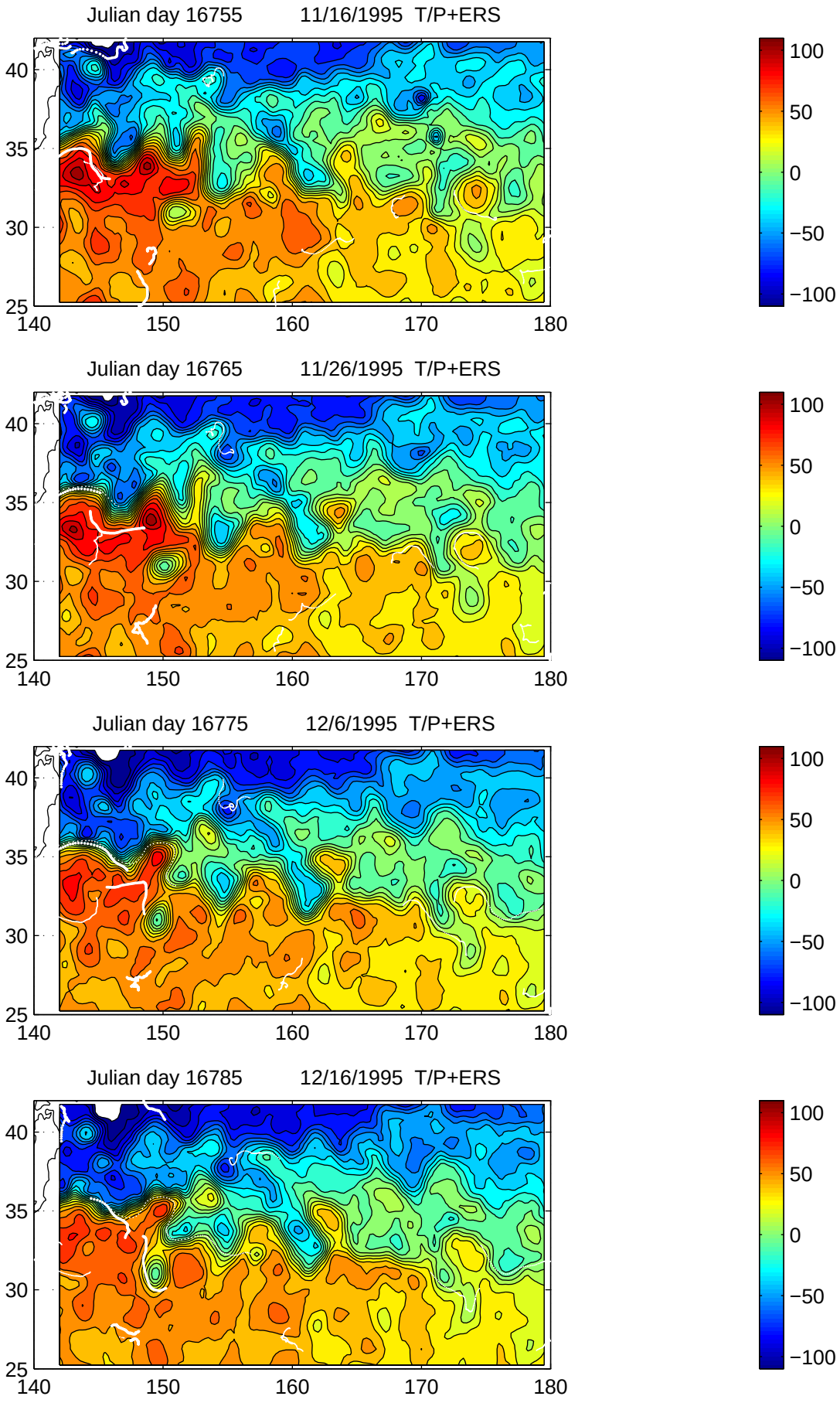

Julian day 16755 11/16/1995 T/P+ERS
Julian day 16765 11/26/1995 T/P+ERS
Julian day 16775 12/6/1995 T/P+ERS
Julian day 16785 12/16/1995 T/P+ERS
40
35
30
25
140
150
160
170
180
100
50
0
−50
−100

Fig.9−29

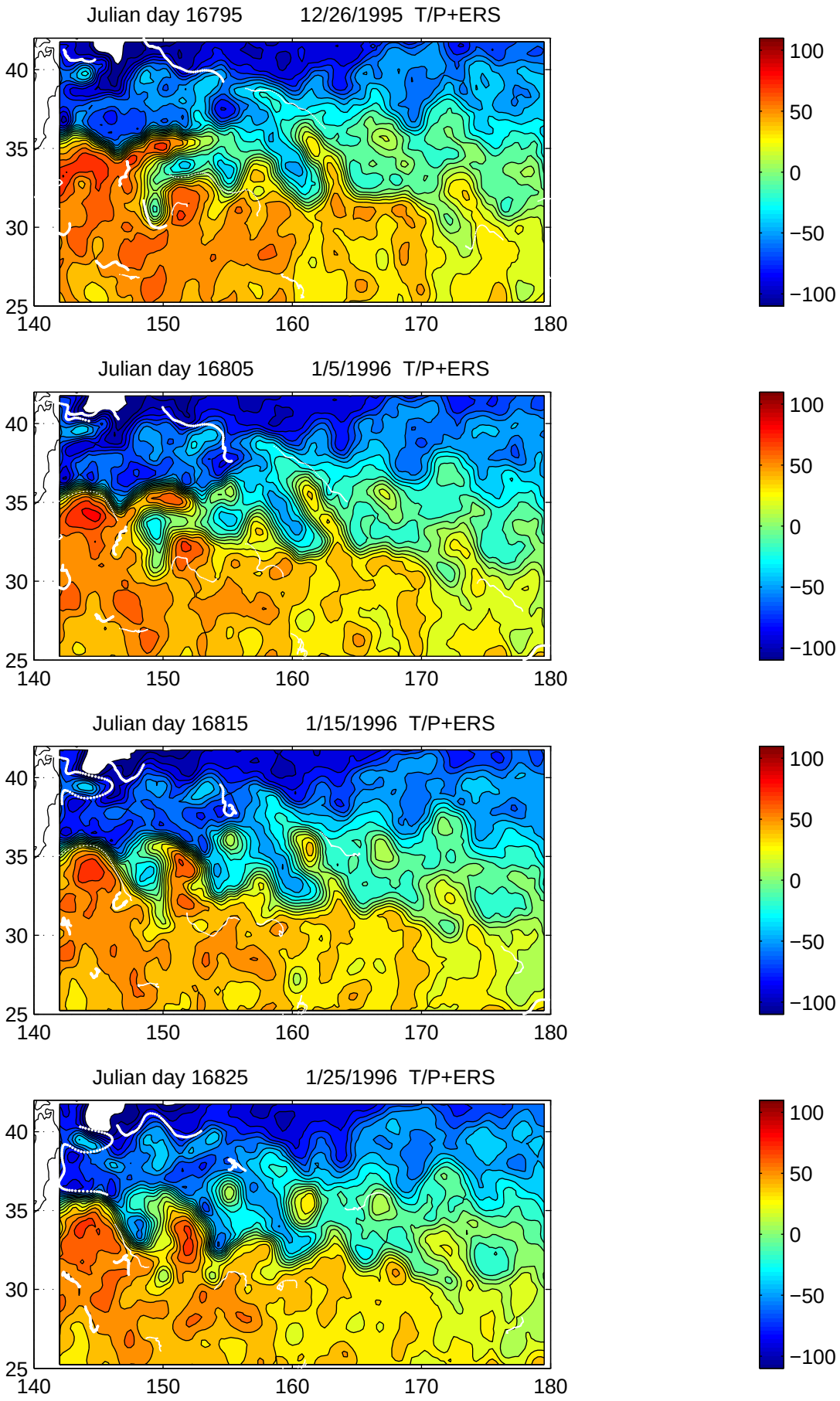

Julian day 16795 12/26/1995 T/P+ERS
Julian day 16805 1/5/1996 T/P+ERS
Julian day 16815 1/15/1996 T/P+ERS
Julian day 16825 1/25/1996 T/P+ERS
40
35
30
25
140
150
160
170
180
100
50
0
−50
−100

Fig.9−30

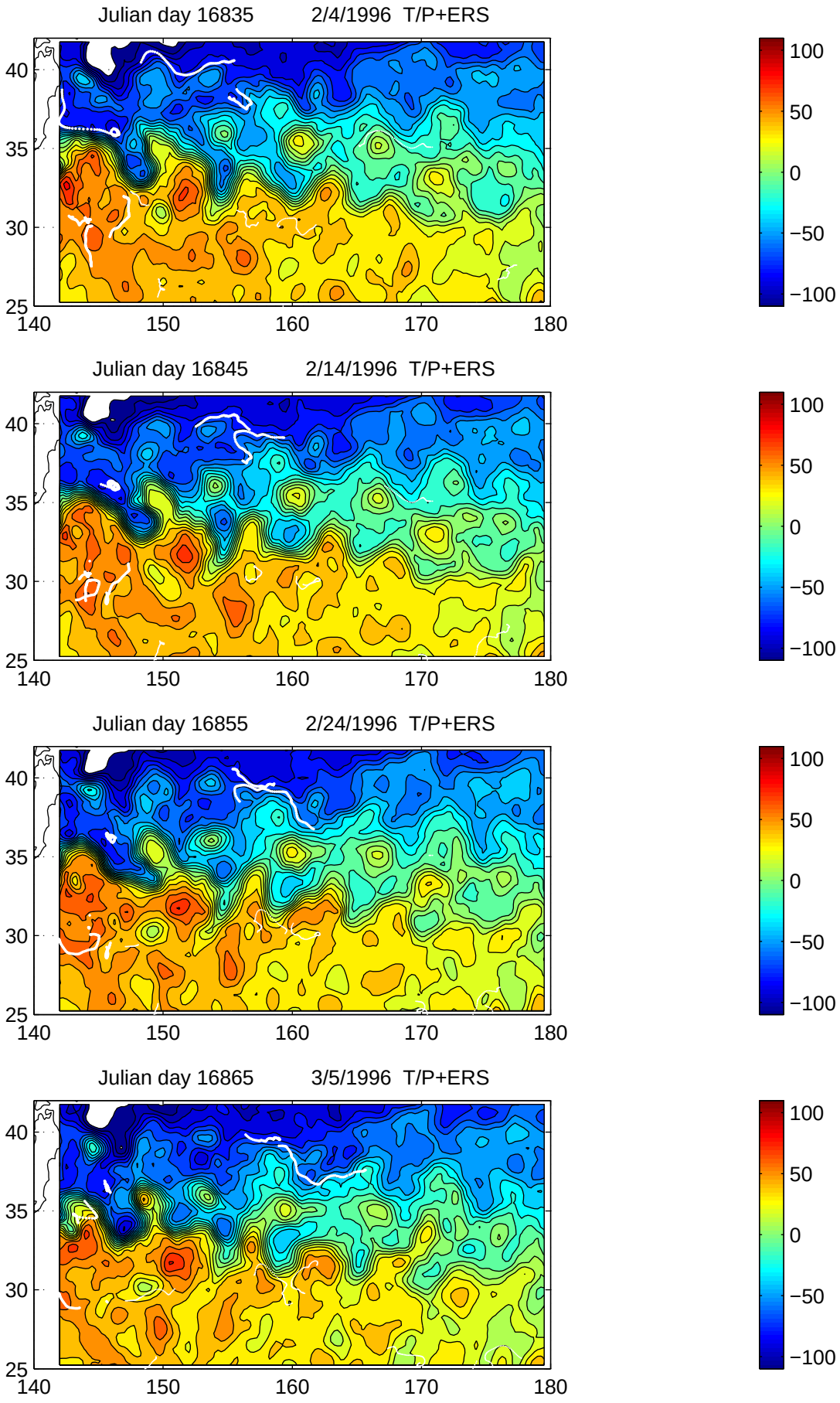

Julian day 16835 2/4/1996 T/P+ERS
Julian day 16845 2/14/1996 T/P+ERS
Julian day 16855 2/24/1996 T/P+ERS
Julian day 16865 3/5/1996 T/P+ERS
40
35
30
25
140
150
160
170
180
100
50
0
−50
−100

Fig.9−31

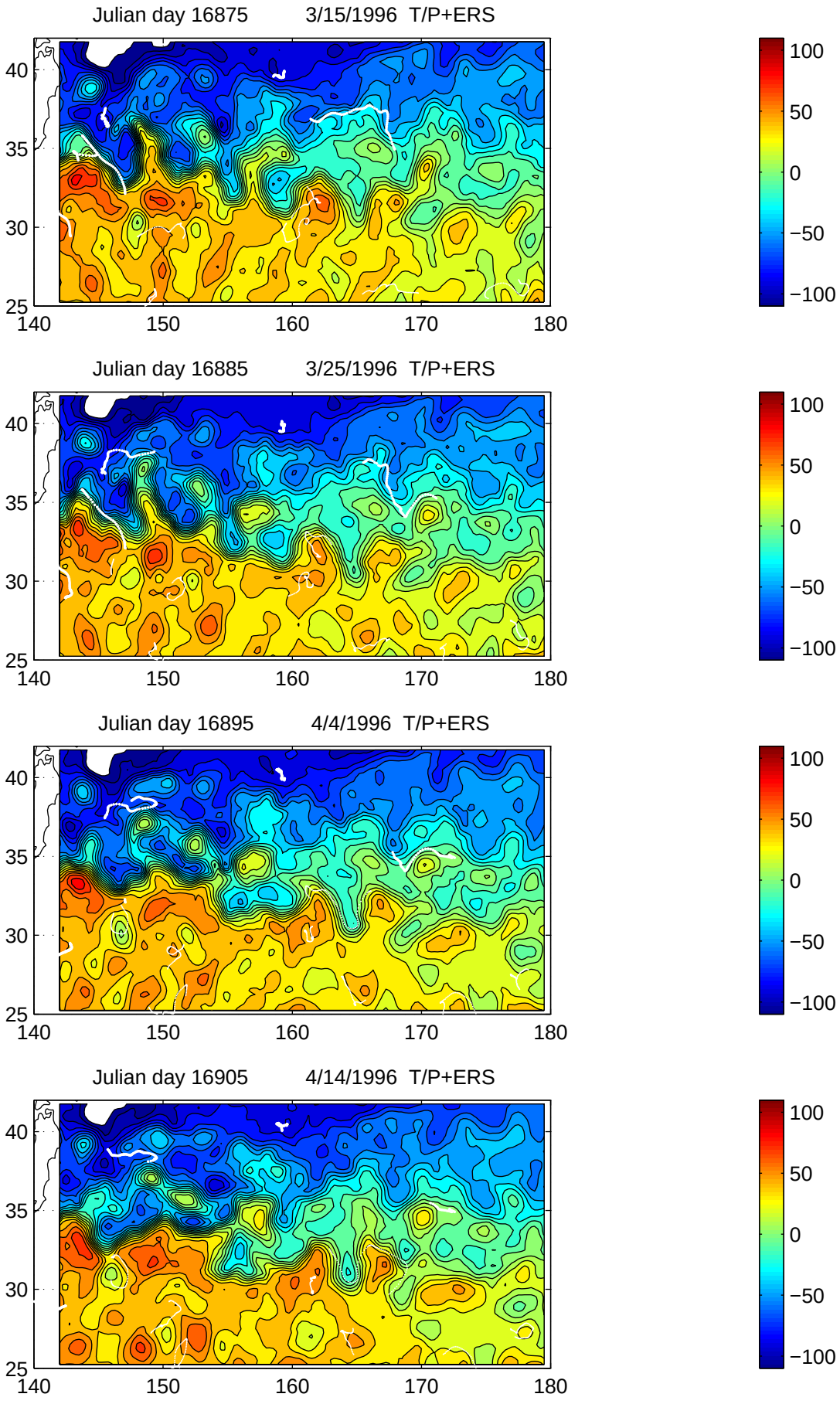

Julian day 16875 3/15/1996 T/P+ERS
Julian day 16885 3/25/1996 T/P+ERS
Julian day 16895 4/4/1996 T/P+ERS
Julian day 16905 4/14/1996 T/P+ERS
40
35
30
25
140
150
160
170
180
100
50
0
−50
−100

Fig.9−32

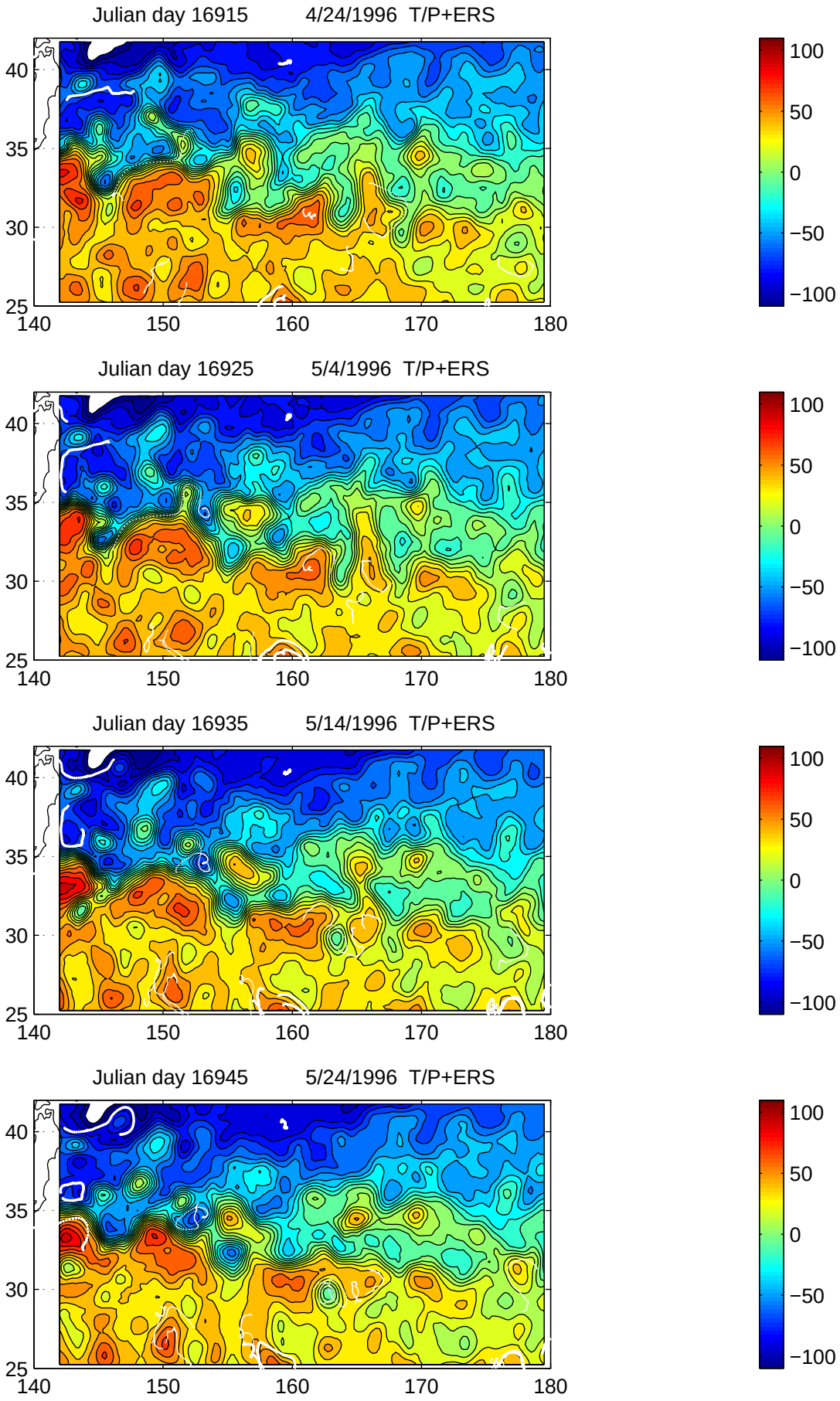

Julian day 16915 4/24/1996 T/P+ERS
Julian day 16925 5/4/1996 T/P+ERS
Julian day 16935 5/14/1996 T/P+ERS
Julian day 16945 5/24/1996 T/P+ERS
40
35
30
25
140
150
160
170
180
100
50
0
−50
−100

Fig.9−33

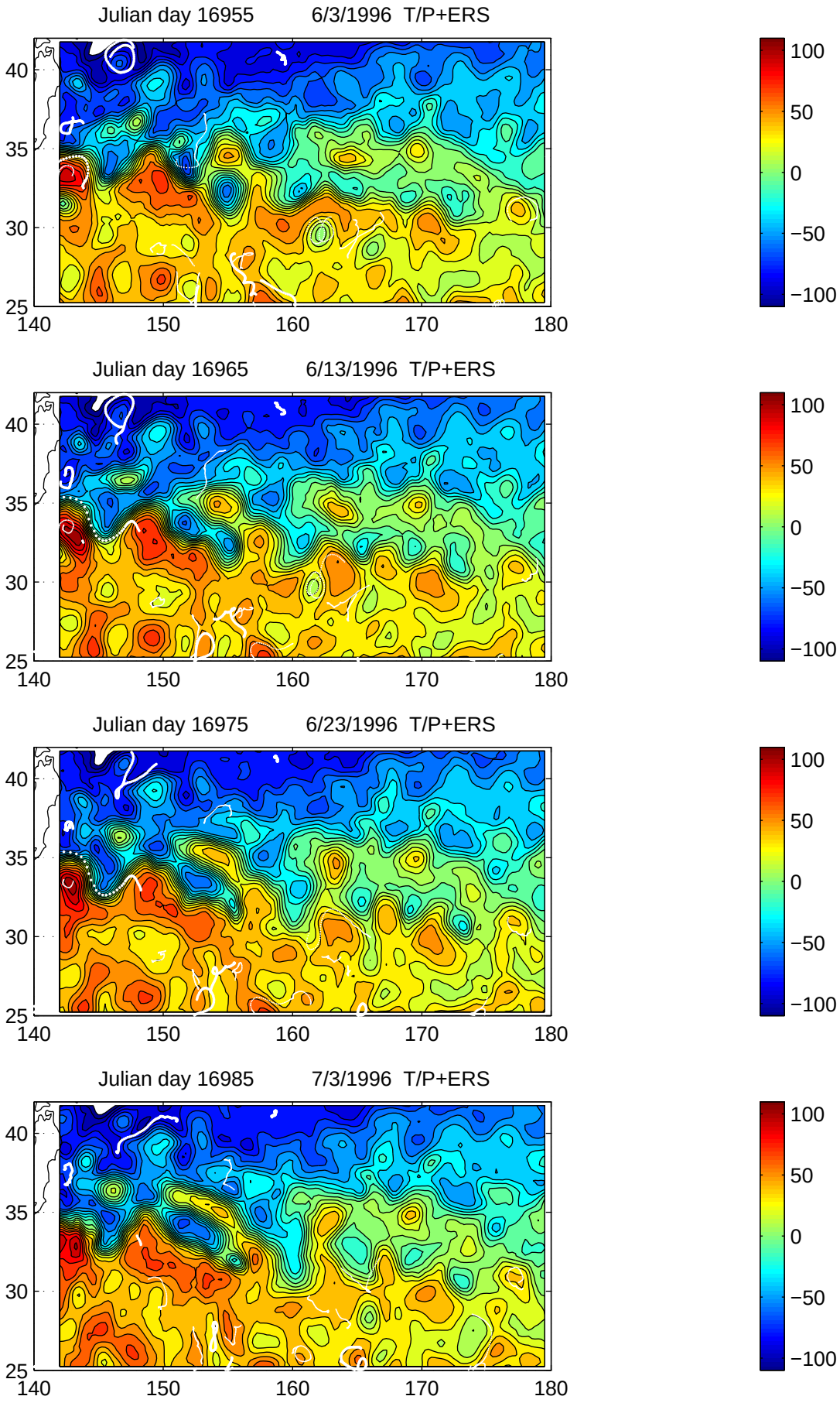

Julian day 16955 6/3/1996 T/P+ERS
Julian day 16965 6/13/1996 T/P+ERS
Julian day 16975 6/23/1996 T/P+ERS
Julian day 16985 7/3/1996 T/P+ERS
40
35
30
25
140
150
160
170
180
100
50
0
−50
−100

Fig.9−34

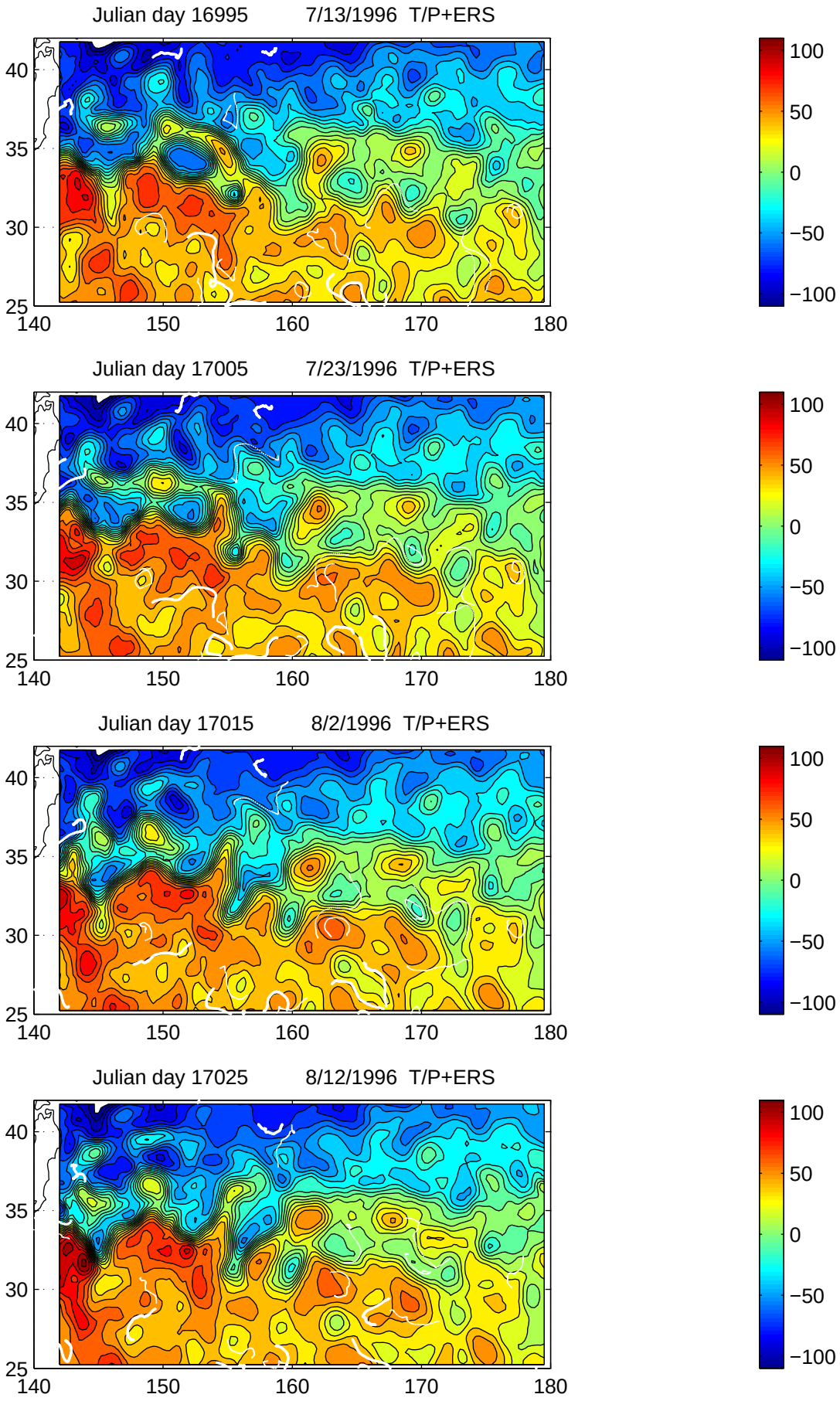

Julian day 16995 7/13/1996 T/P+ERS
Julian day 17005 7/23/1996 T/P+ERS
Julian day 17015 8/2/1996 T/P+ERS
Julian day 17025 8/12/1996 T/P+ERS
40
35
30
25
140
150
160
170
180
100
50
0
−50
−100

Fig.9−35

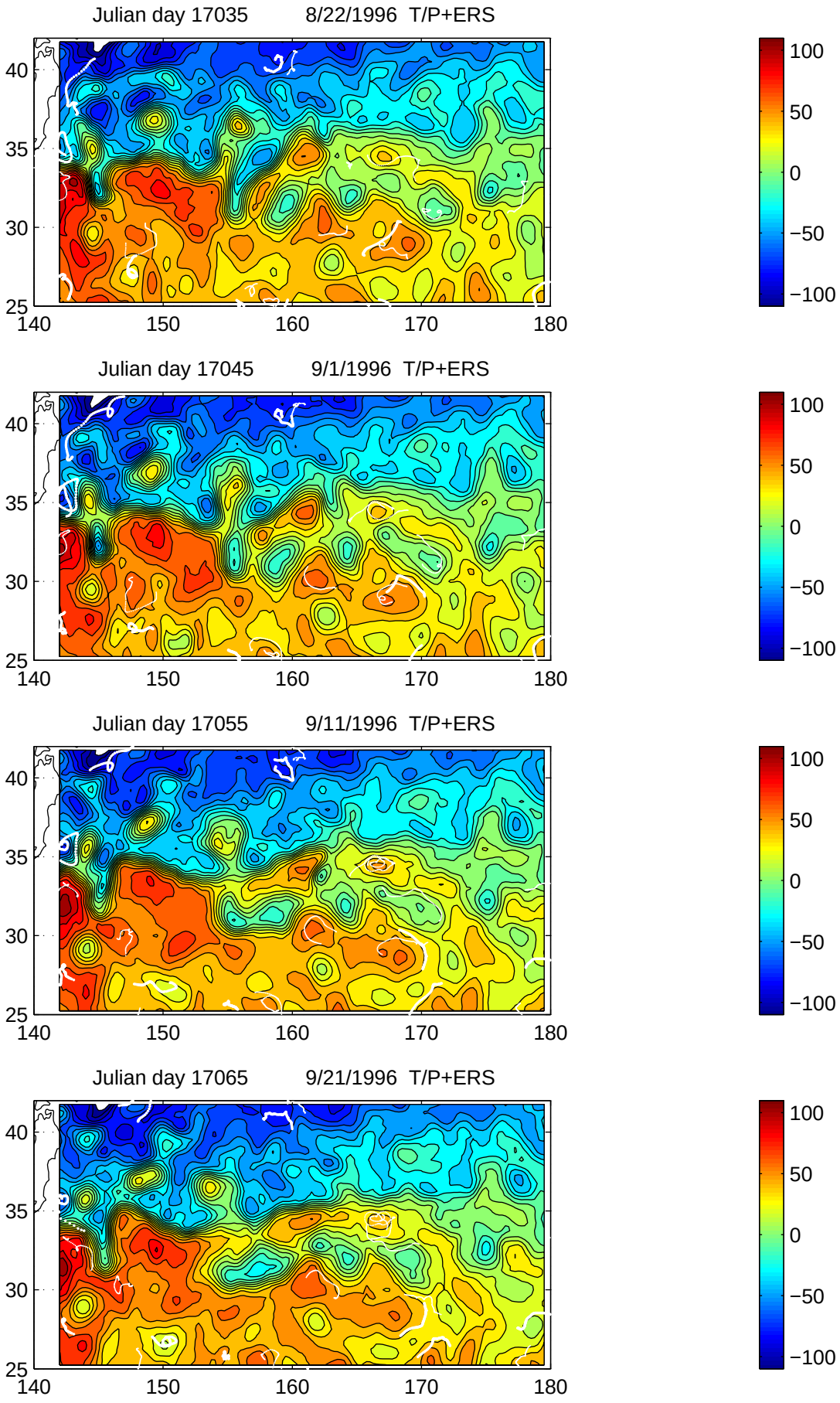

Julian day 17035 8/22/1996 T/P+ERS
Julian day 17045 9/1/1996 T/P+ERS
Julian day 17055 9/11/1996 T/P+ERS
Julian day 17065 9/21/1996 T/P+ERS
40
35
30
25
140
150
160
170
180
100
50
0
−50
−100

Fig.9−36

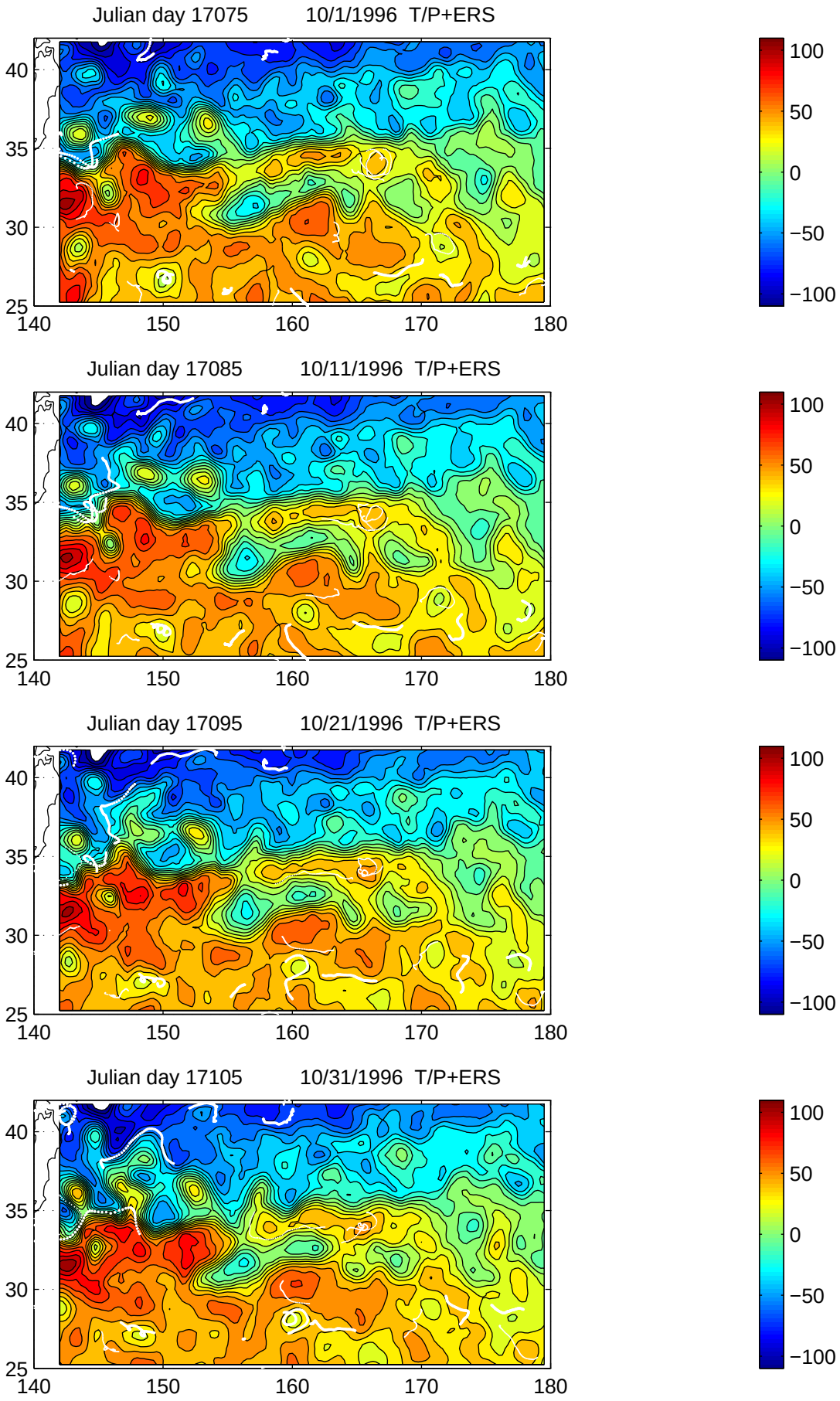

Julian day 17075 10/1/1996 T/P+ERS
Julian day 17085 10/11/1996 T/P+ERS
Julian day 17095 10/21/1996 T/P+ERS
Julian day 17105 10/31/1996 T/P+ERS
40
35
30
25
140
150
160
170
180
100
50
0
−50
−100

Fig.9−37

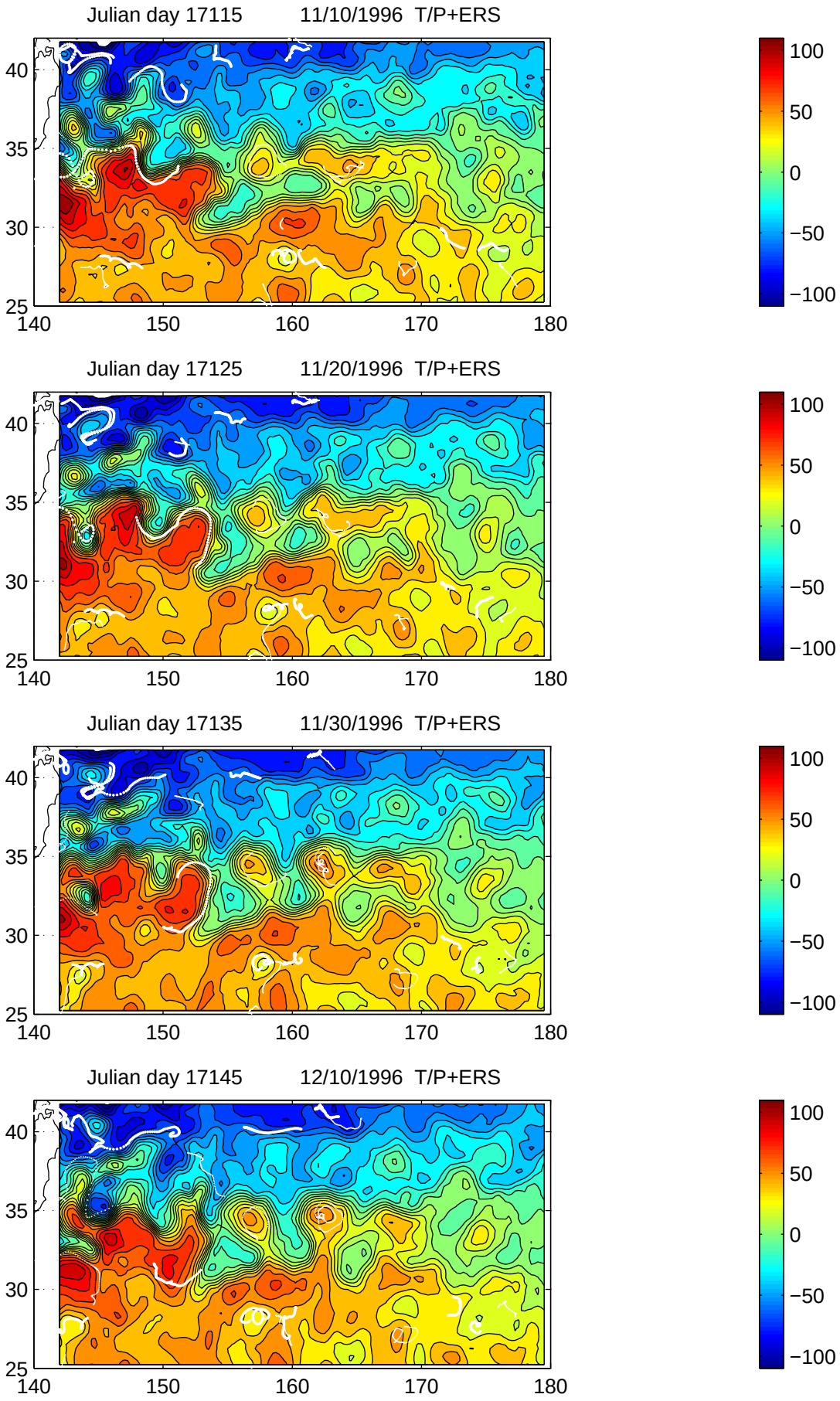

Julian day 17115 11/10/1996 T/P+ERS
Julian day 17125 11/20/1996 T/P+ERS
Julian day 17135 11/30/1996 T/P+ERS
Julian day 17145 12/10/1996 T/P+ERS
40
35
30
25
140
150
160
170
180
100
50
0
−50
−100

Fig.9−38

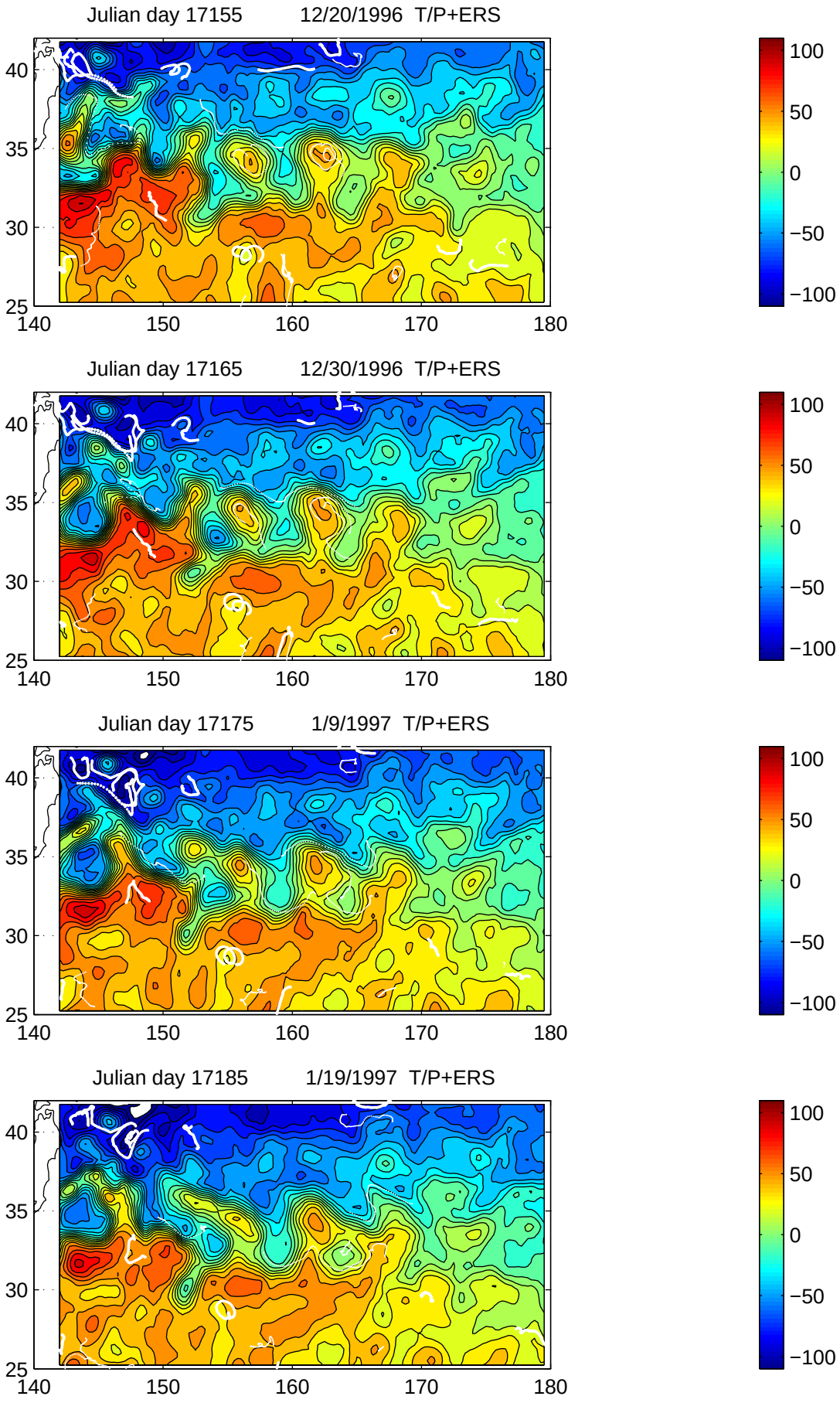

Julian day 17155 12/20/1996 T/P+ERS
Julian day 17165 12/30/1996 T/P+ERS
Julian day 17175 1/9/1997 T/P+ERS
Julian day 17185 1/19/1997 T/P+ERS
40
35
30
25
140
150
160
170
180
100
50
0
−50
−100

Fig.9−39

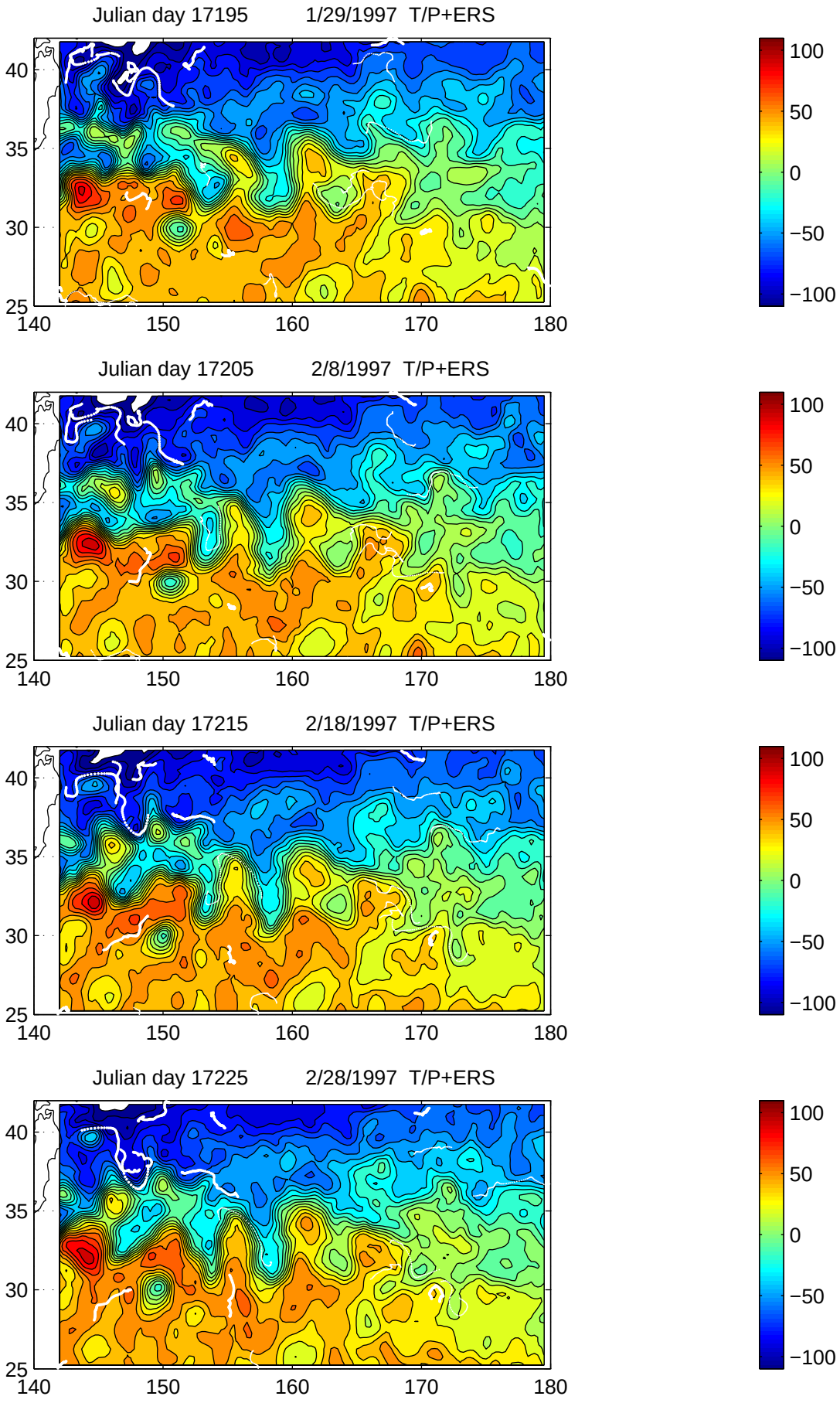

Julian day 17195 1/29/1997 T/P+ERS
Julian day 17205 2/8/1997 T/P+ERS
Julian day 17215 2/18/1997 T/P+ERS
Julian day 17225 2/28/1997 T/P+ERS
40
35
30
25
140
150
160
170
180
100
50
0
−50
−100

Fig.9−40

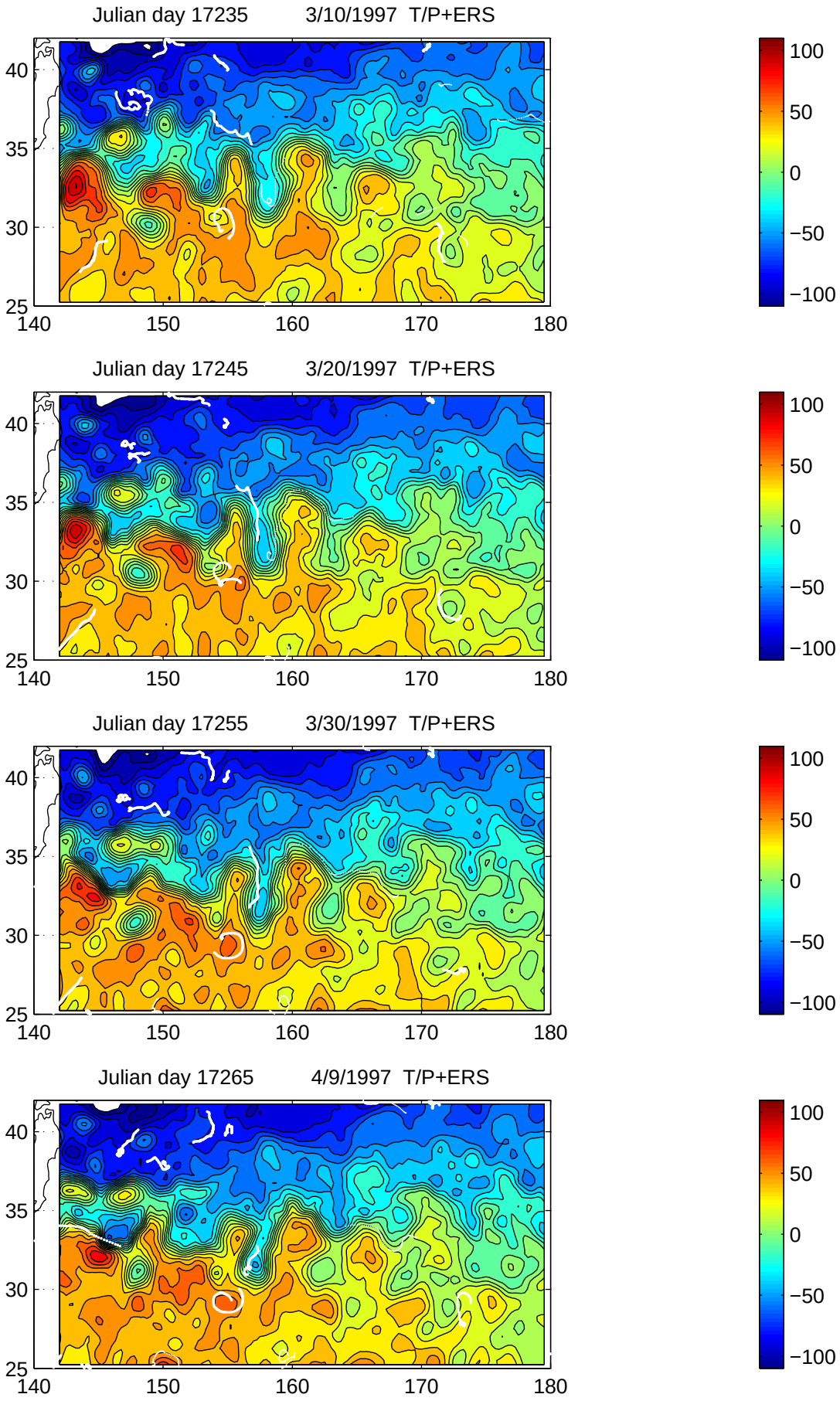

Julian day 17235 3/10/1997 T/P+ERS
Julian day 17245 3/20/1997 T/P+ERS
Julian day 17255 3/30/1997 T/P+ERS
Julian day 17265 4/9/1997 T/P+ERS
40
35
30
25
140
150
160
170
180
100
50
0
−50
−100

Fig.9−41

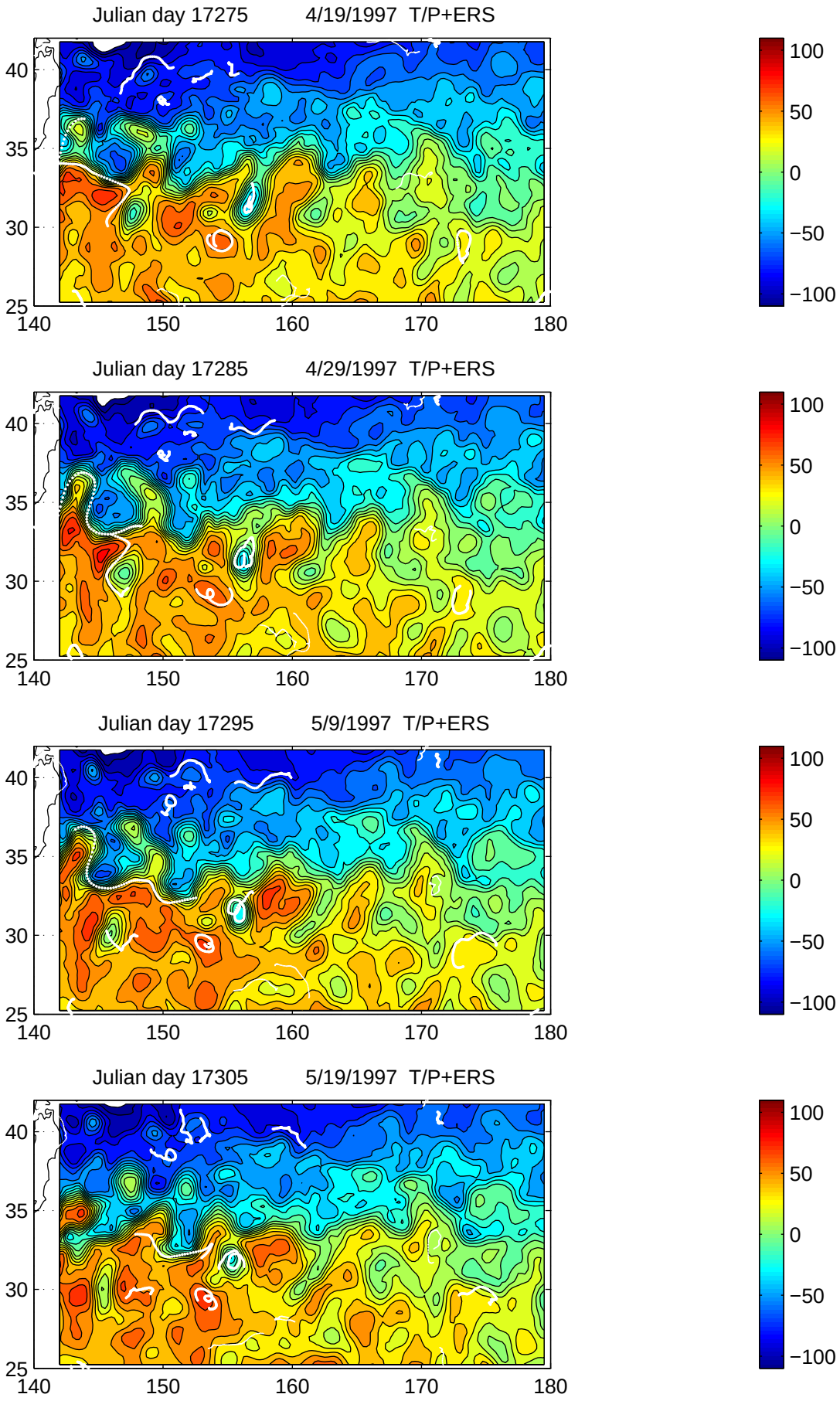

Julian day 17275 4/19/1997 T/P+ERS
Julian day 17285 4/29/1997 T/P+ERS
Julian day 17295 5/9/1997 T/P+ERS
Julian day 17305 5/19/1997 T/P+ERS
40
35
30
25
140
150
160
170
180
100
50
0
−50
−100

Fig.9−42

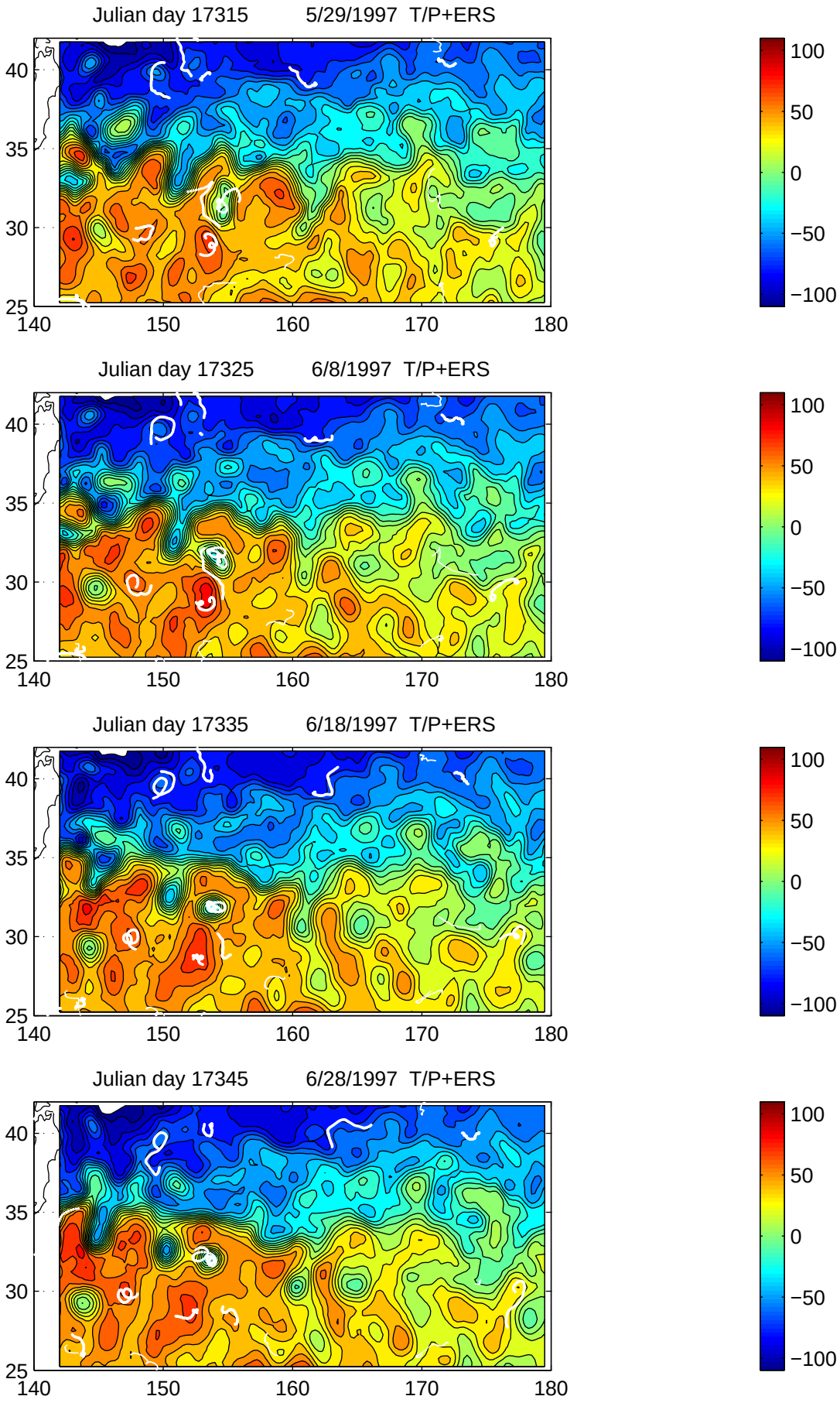

Julian day 17315 5/29/1997 T/P+ERS
Julian day 17325 6/8/1997 T/P+ERS
Julian day 17335 6/18/1997 T/P+ERS
Julian day 17345 6/28/1997 T/P+ERS
40
35
30
25
140
150
160
170
180
100
50
0
−50
−100

Fig.9−43

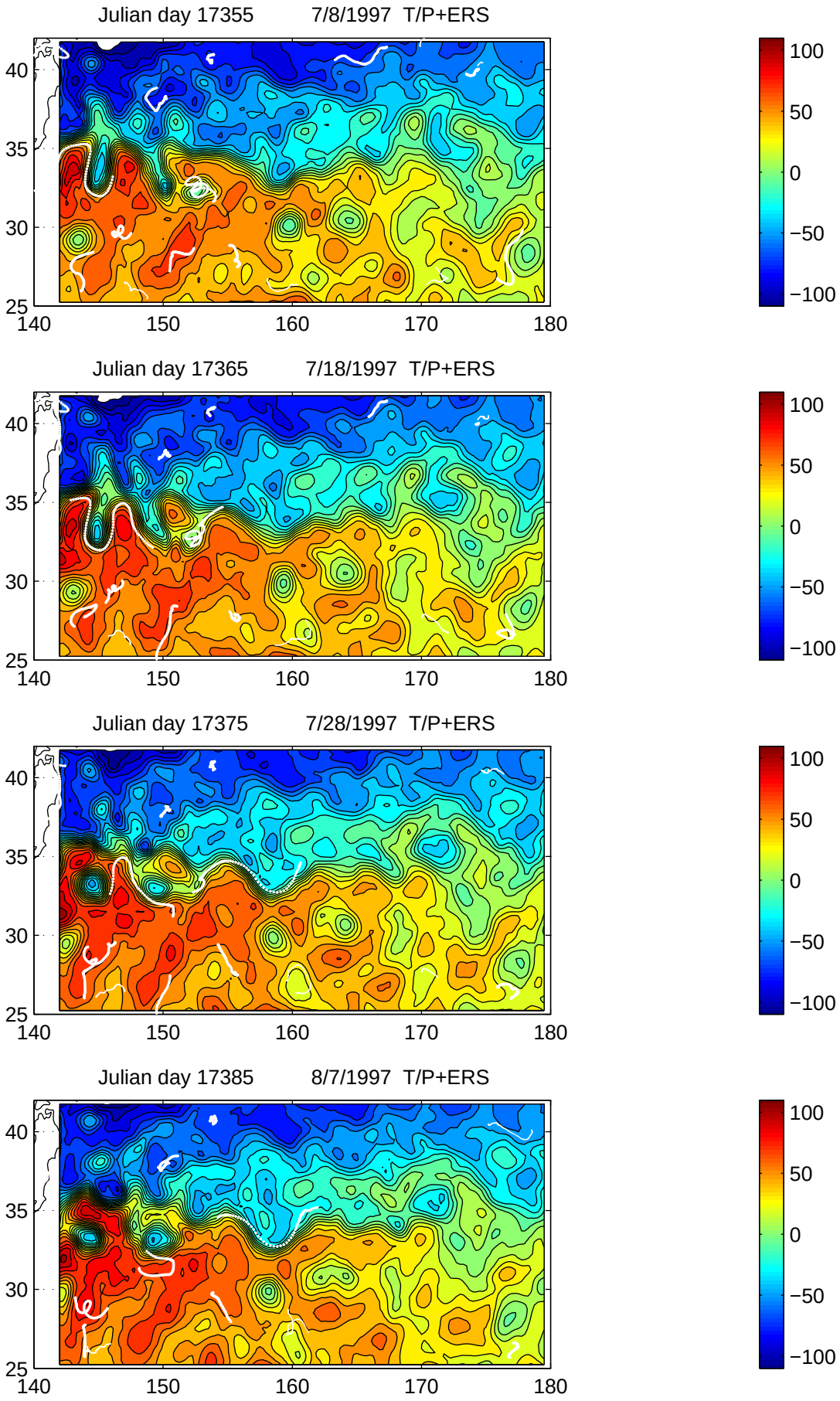

Julian day 17355 7/8/1997 T/P+ERS
Julian day 17365 7/18/1997 T/P+ERS
Julian day 17375 7/28/1997 T/P+ERS
Julian day 17385 8/7/1997 T/P+ERS
40
35
30
25
140
150
160
170
180
100
50
0
−50
−100

Fig.9−44

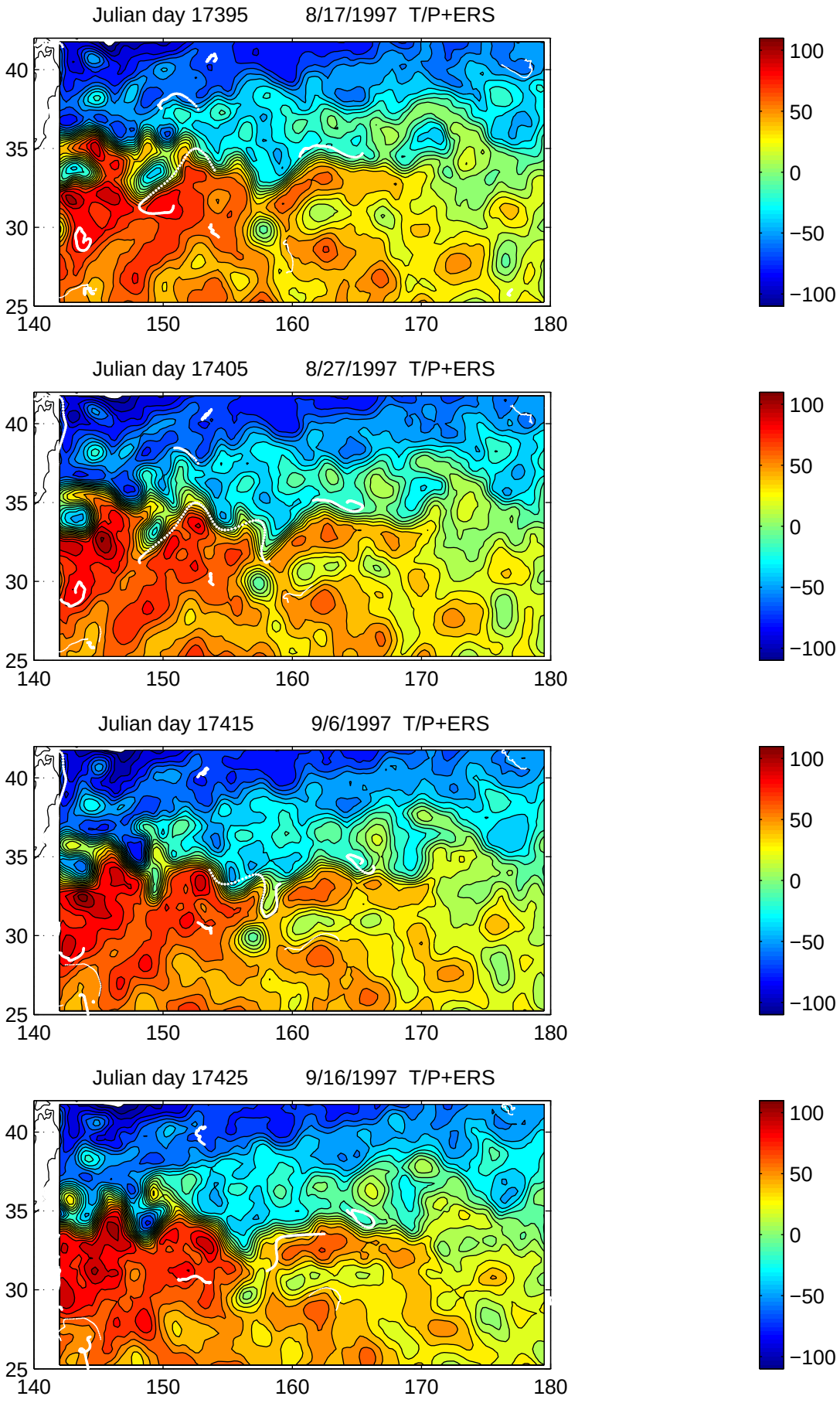

Julian day 17395 8/17/1997 T/P+ERS
Julian day 17405 8/27/1997 T/P+ERS
Julian day 17415 9/6/1997 T/P+ERS
Julian day 17425 9/16/1997 T/P+ERS
40
35
30
25
140
150
160
170
180
100
50
0
−50
−100

Fig.9−45

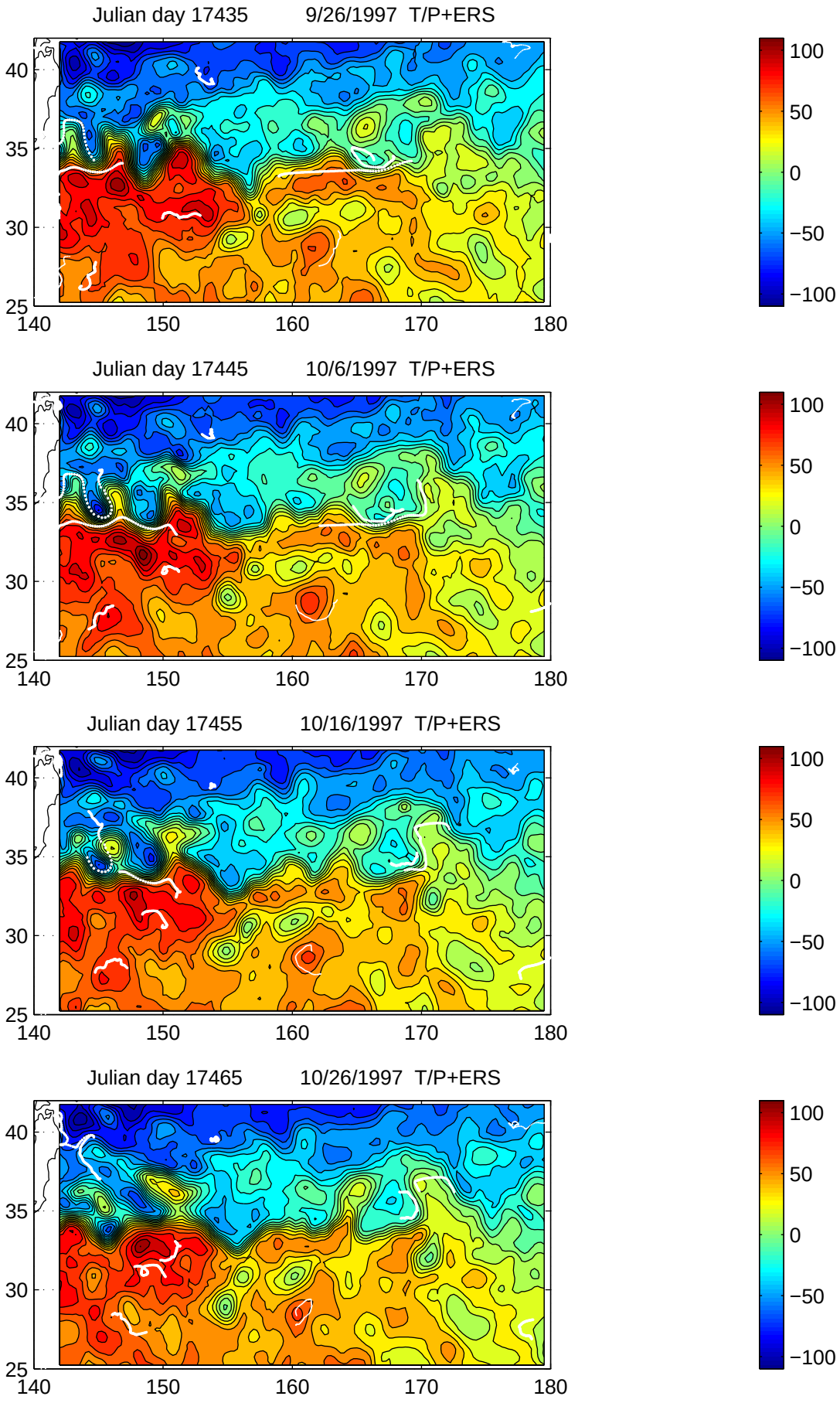

Julian day 17435 9/26/1997 T/P+ERS
Julian day 17445 10/6/1997 T/P+ERS
Julian day 17455 10/16/1997 T/P+ERS
Julian day 17465 10/26/1997 T/P+ERS
40
35
30
25
140
150
160
170
180
100
50
0
−50
−100

Fig.9−46

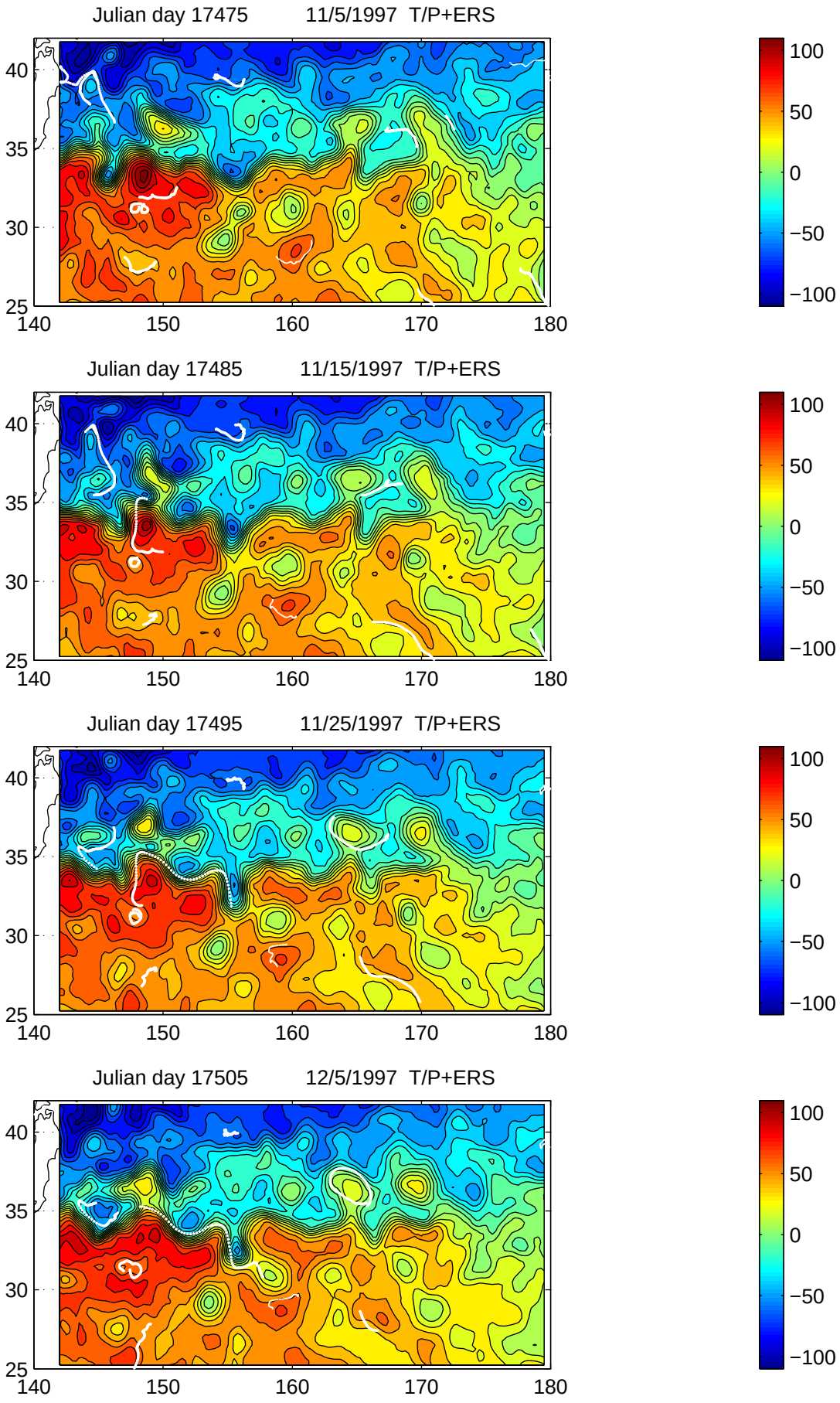

Julian day 17475 11/5/1997 T/P+ERS
Julian day 17485 11/15/1997 T/P+ERS
Julian day 17495 11/25/1997 T/P+ERS
Julian day 17505 12/5/1997 T/P+ERS
40
35
30
25
140
150
160
170
180
100
50
0
−50
−100

Fig.9−47

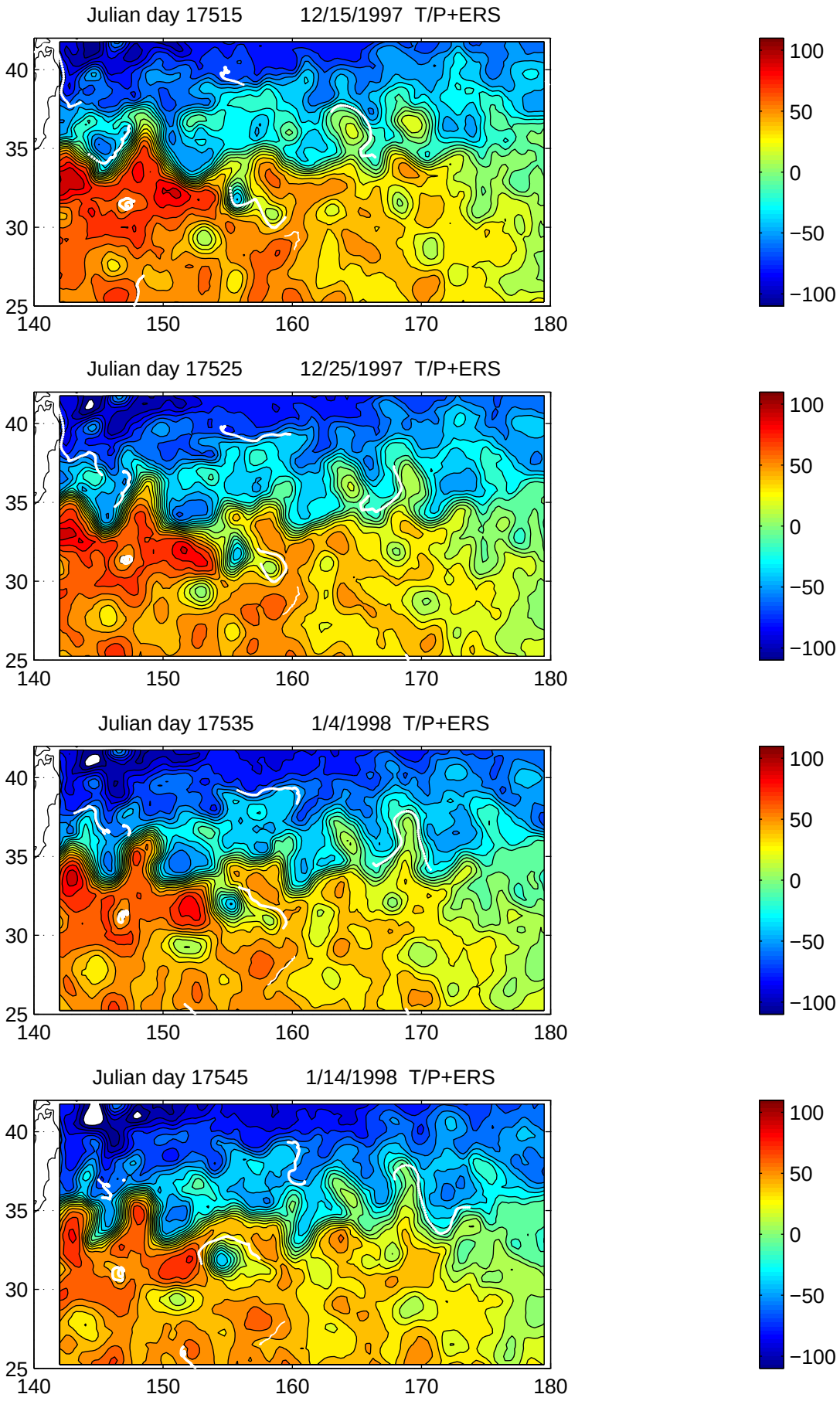

Julian day 17515 12/15/1997 T/P+ERS
Julian day 17525 12/25/1997 T/P+ERS
Julian day 17535 1/4/1998 T/P+ERS
Julian day 17545 1/14/1998 T/P+ERS
40
35
30
25
140
150
160
170
180
100
50
0
−50
−100

Fig.9−48

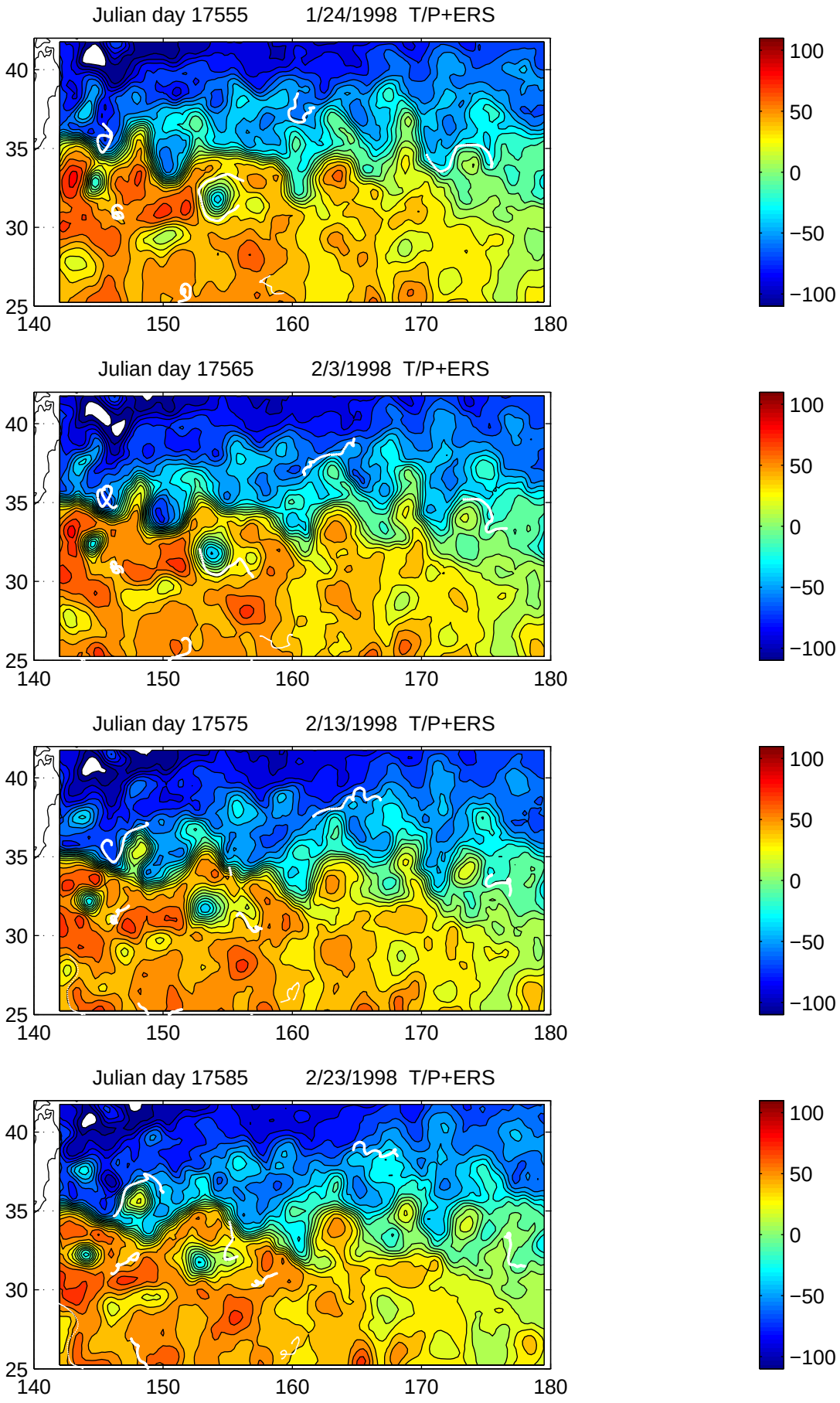

Julian day 17555 1/24/1998 T/P+ERS
Julian day 17565 2/3/1998 T/P+ERS
Julian day 17575 2/13/1998 T/P+ERS
Julian day 17585 2/23/1998 T/P+ERS
40
35
30
25
140
150
160
170
180
100
50
0
−50
−100

Fig.9−49

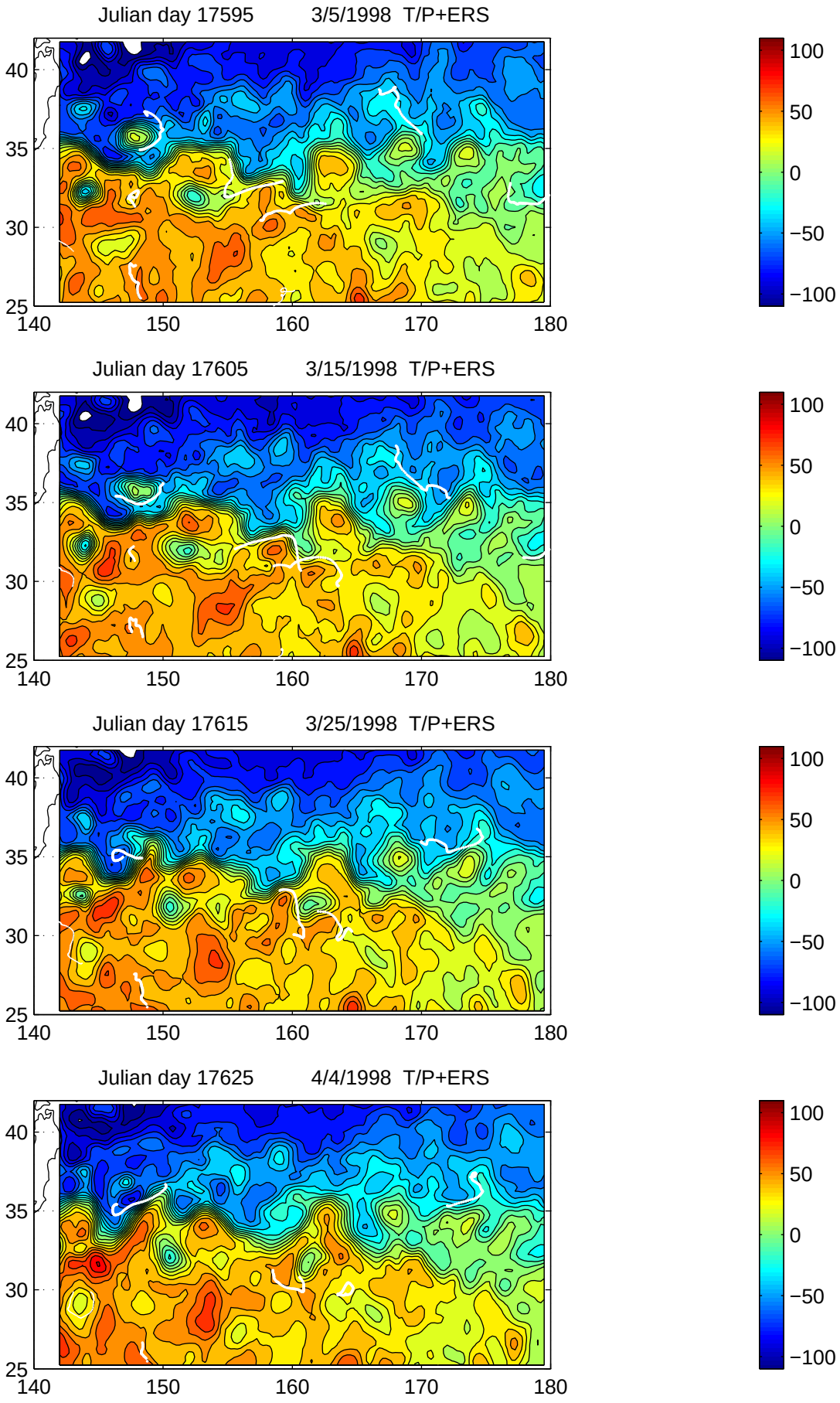

Julian day 17595 3/5/1998 T/P+ERS
Julian day 17605 3/15/1998 T/P+ERS
Julian day 17615 3/25/1998 T/P+ERS
Julian day 17625 4/4/1998 T/P+ERS
40
35
30
25
140
150
160
170
180
100
50
0
−50
−100

Fig.9−50

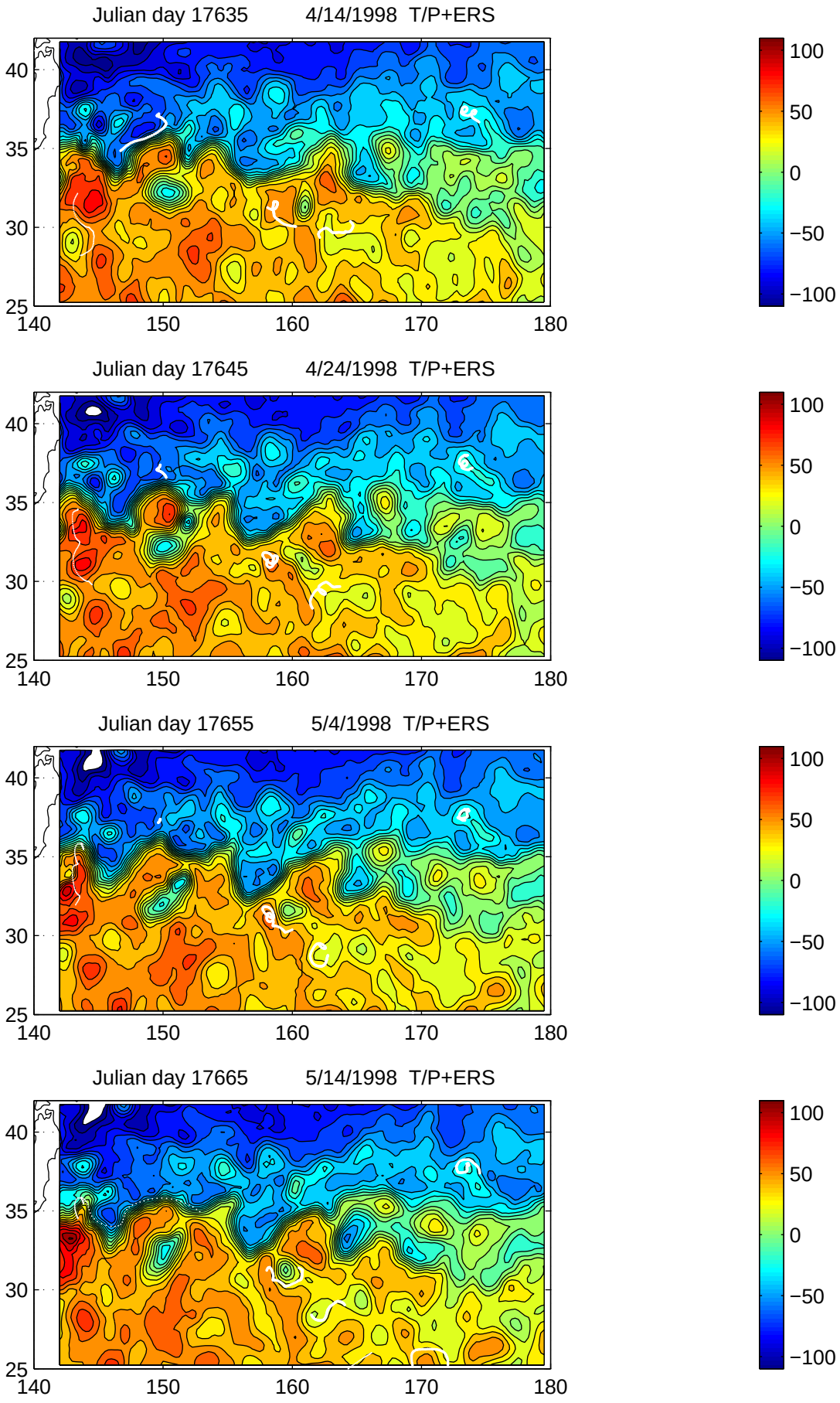

Julian day 17635 4/14/1998 T/P+ERS
Julian day 17645 4/24/1998 T/P+ERS
Julian day 17655 5/4/1998 T/P+ERS
Julian day 17665 5/14/1998 T/P+ERS
40
35
30
25
140
150
160
170
180
100
50
0
−50
−100

Fig.9−51

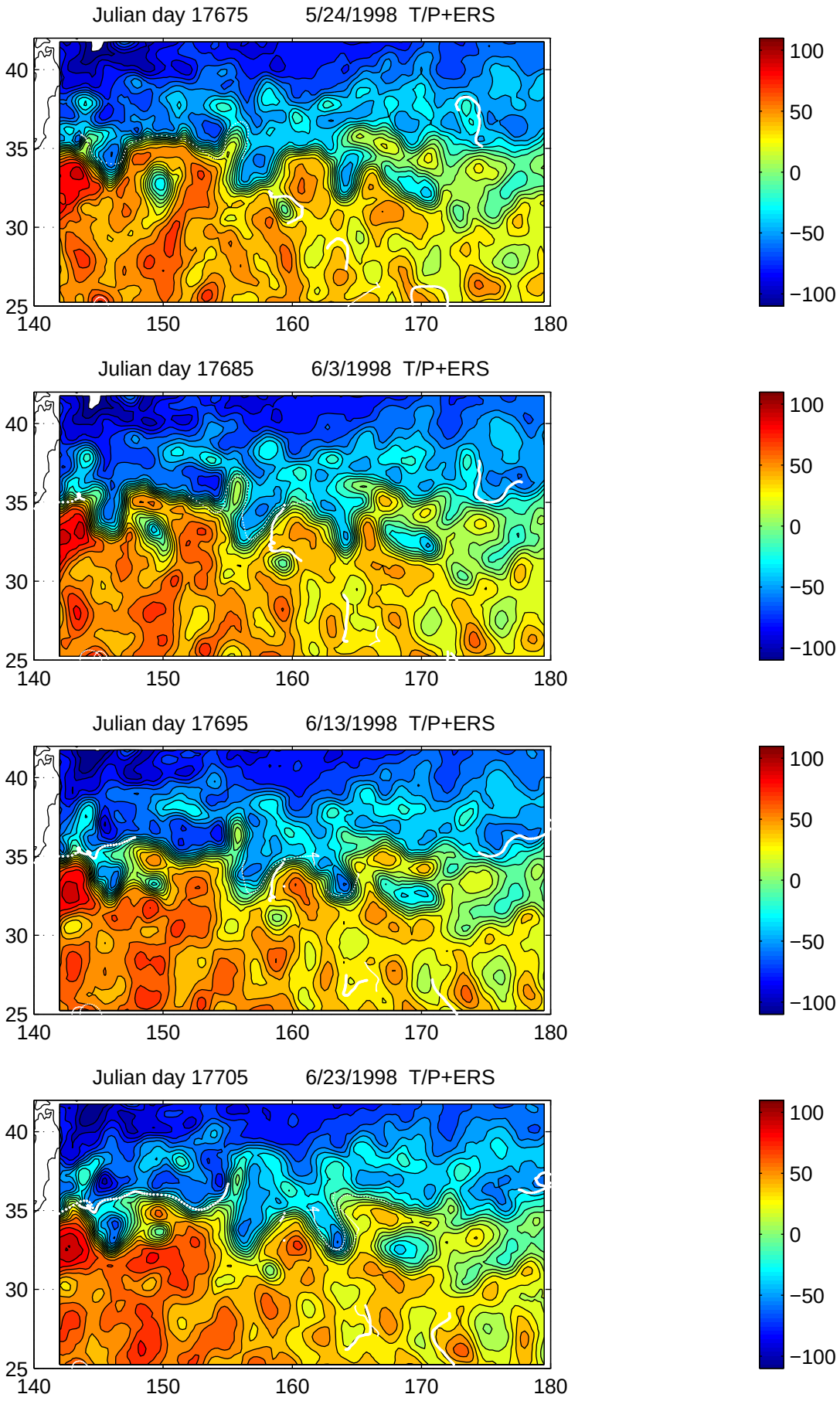

Julian day 17675 5/24/1998 T/P+ERS
Julian day 17685 6/3/1998 T/P+ERS
Julian day 17695 6/13/1998 T/P+ERS
Julian day 17705 6/23/1998 T/P+ERS
40
35
30
25
140
150
160
170
180
100
50
0
−50
−100

Fig.9−52

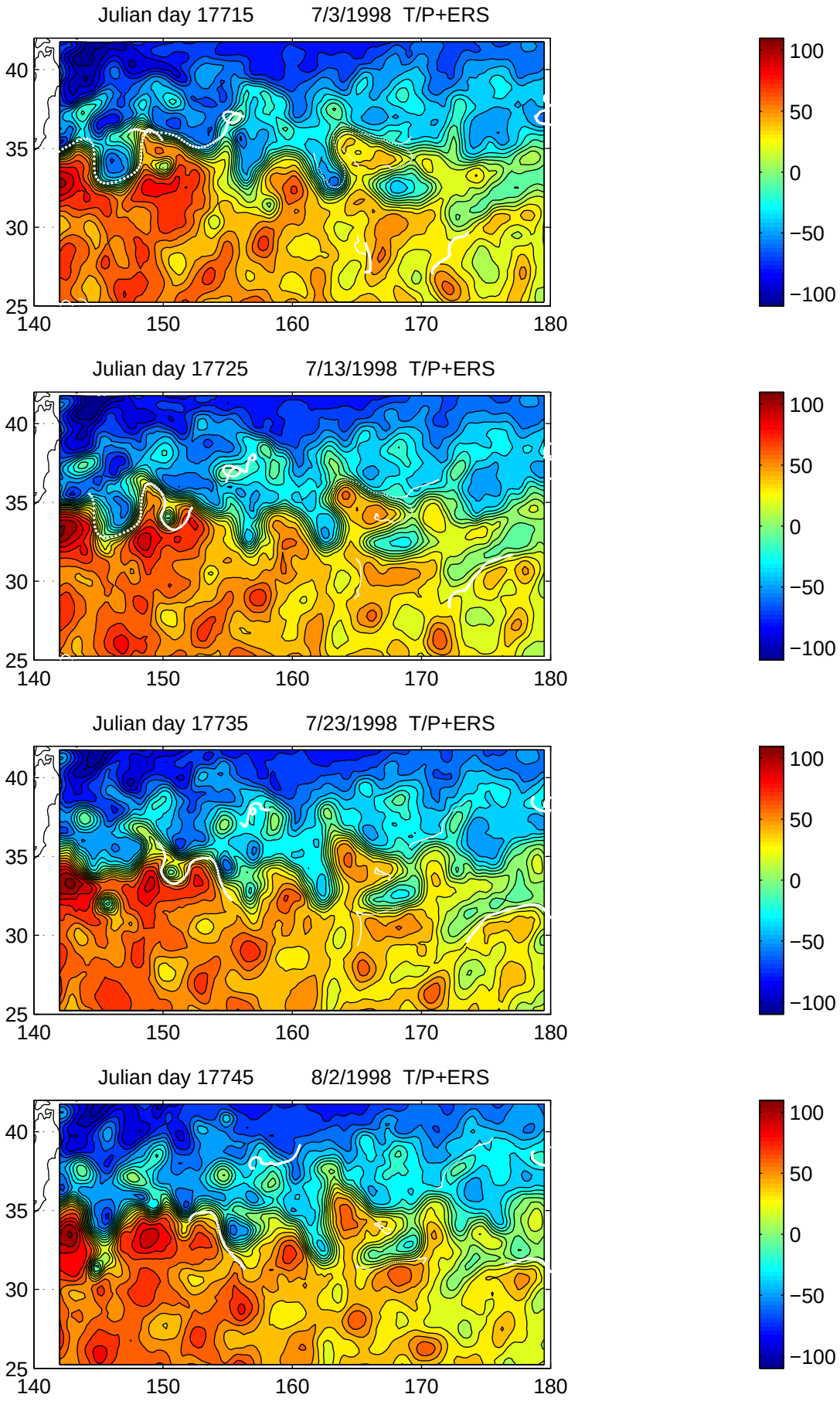

Julian day 17715 7/3/1998 T/P+ERS
Julian day 17725 7/13/1998 T/P+ERS
Julian day 17735 7/23/1998 T/P+ERS
Julian day 17745 8/2/1998 T/P+ERS
40
35
30
25
140
150
160
170
180
100
50
0
−50
−100

Fig.9−53

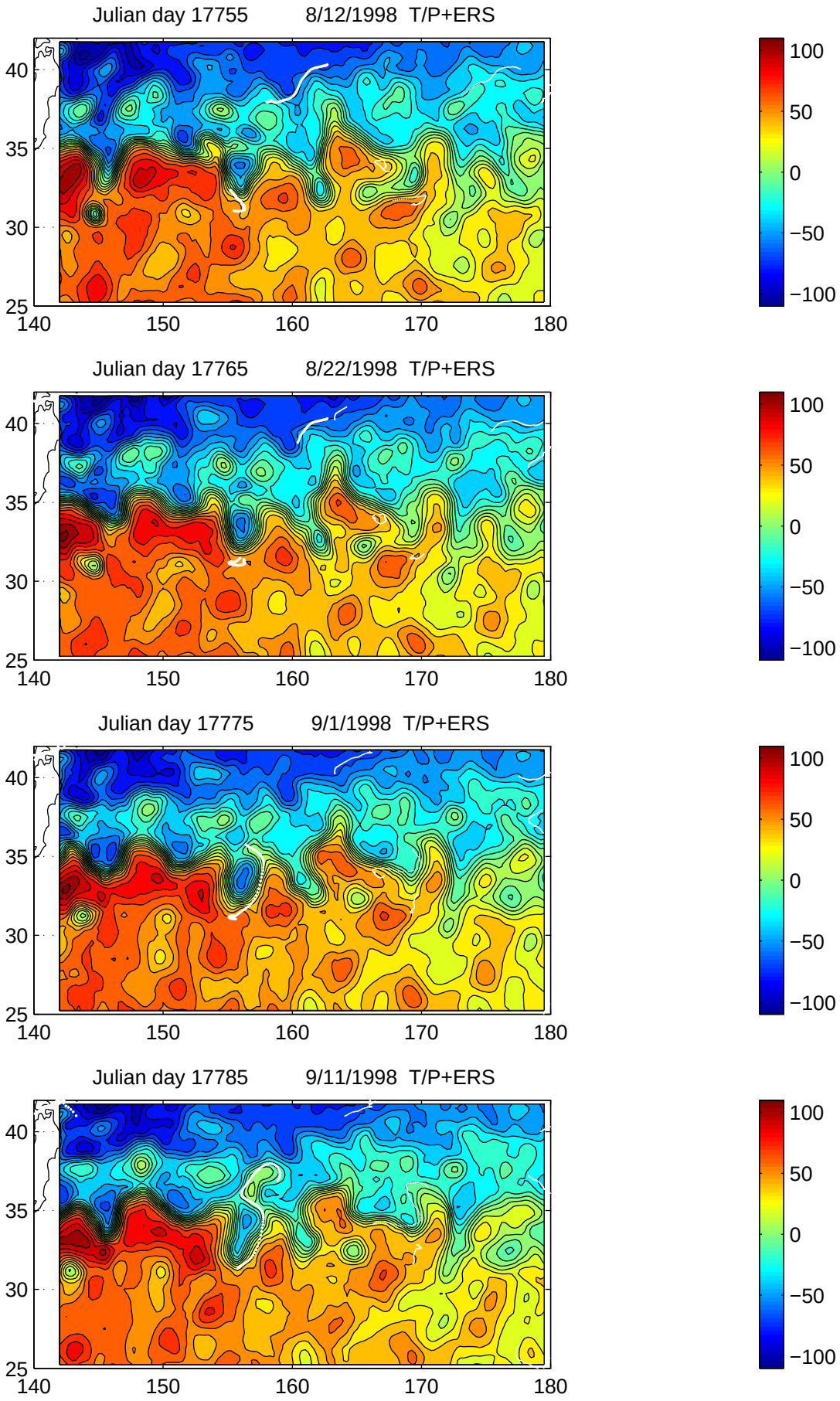

Julian day 17755 8/12/1998 T/P+ERS
Julian day 17765 8/22/1998 T/P+ERS
Julian day 17775 9/1/1998 T/P+ERS
Julian day 17785 9/11/1998 T/P+ERS
40
35
30
25
140
150
160
170
180
100
50
0
−50
−100

Fig.9−54

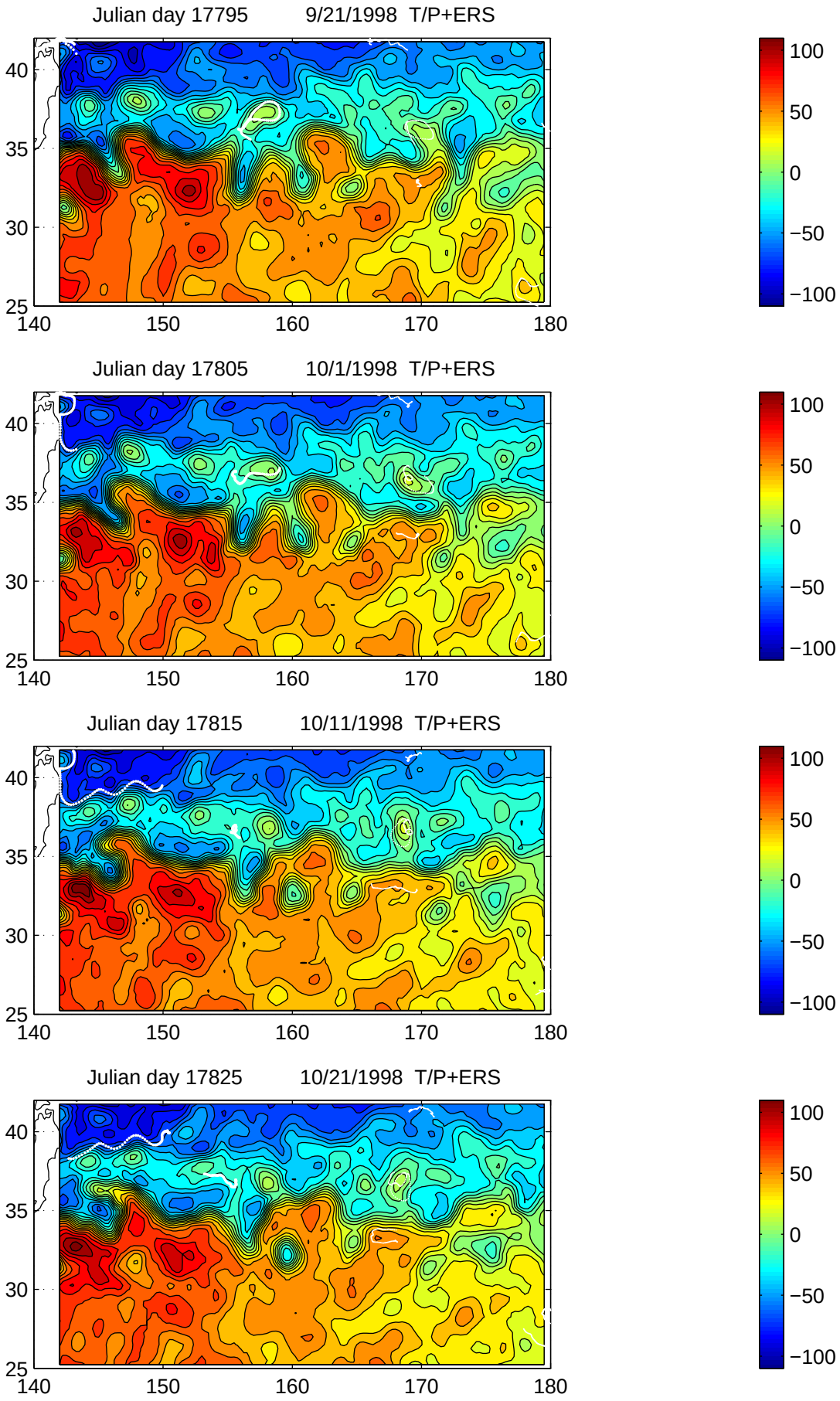

Julian day 17795 9/21/1998 T/P+ERS
Julian day 17805 10/1/1998 T/P+ERS
Julian day 17815 10/11/1998 T/P+ERS
Julian day 17825 10/21/1998 T/P+ERS
40
35
30
25
140
150
160
170
180
100
50
0
−50
−100

Fig.9−55

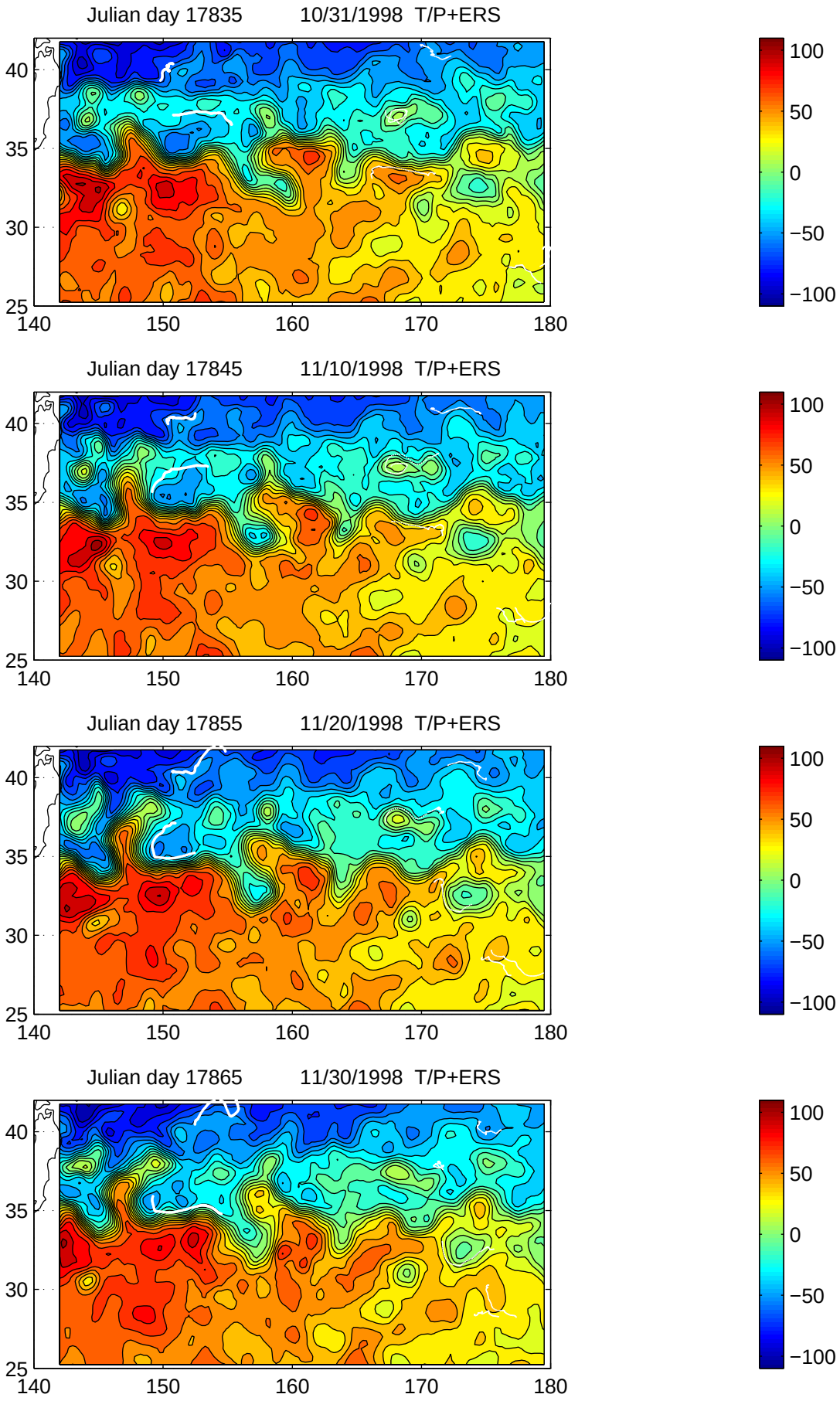

Julian day 17835 10/31/1998 T/P+ERS
Julian day 17845 11/10/1998 T/P+ERS
Julian day 17855 11/20/1998 T/P+ERS
Julian day 17865 11/30/1998 T/P+ERS
40
35
30
25
140
150
160
170
180
100
50
0
−50
−100

Fig.9−56

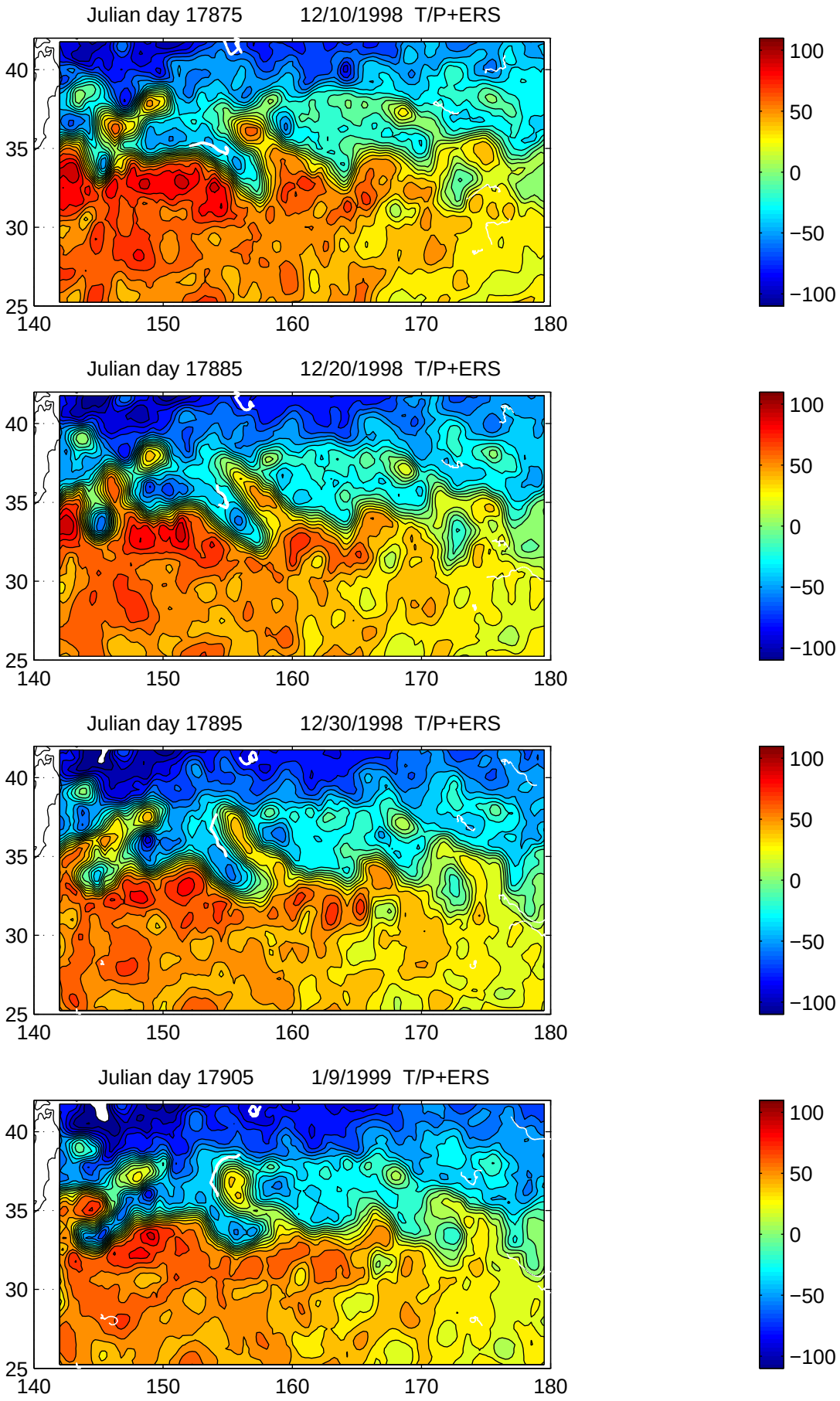

Julian day 17875 12/10/1998 T/P+ERS
Julian day 17885 12/20/1998 T/P+ERS
Julian day 17895 12/30/1998 T/P+ERS
Julian day 17905 1/9/1999 T/P+ERS
40
35
30
25
140
150
160
170
180
100
50
0
−50
−100

Fig.9−57

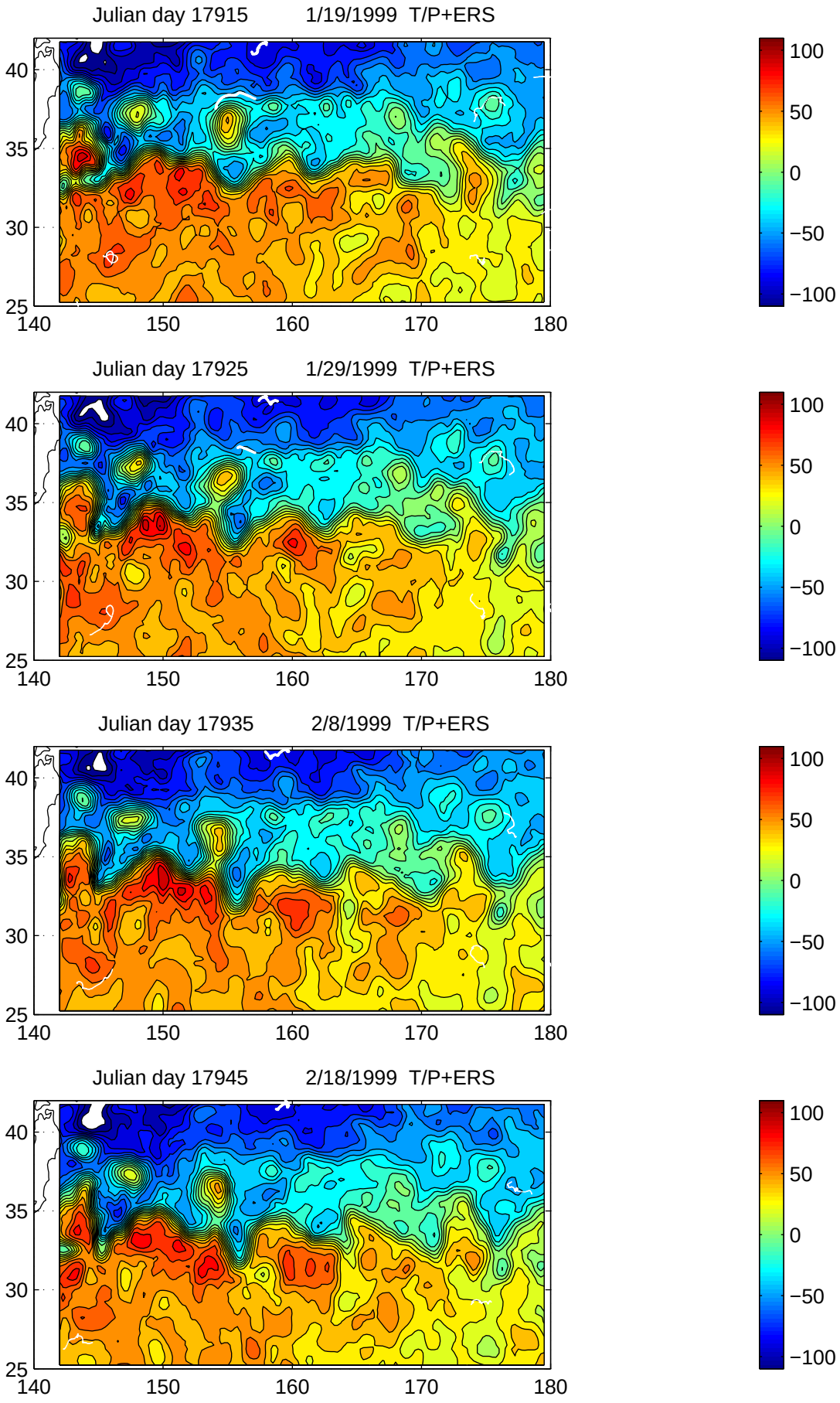

Julian day 17915 1/19/1999 T/P+ERS
Julian day 17925 1/29/1999 T/P+ERS
Julian day 17935 2/8/1999 T/P+ERS
Julian day 17945 2/18/1999 T/P+ERS
40
35
30
25
140
150
160
170
180
100
50
0
−50
−100

Fig.9−58

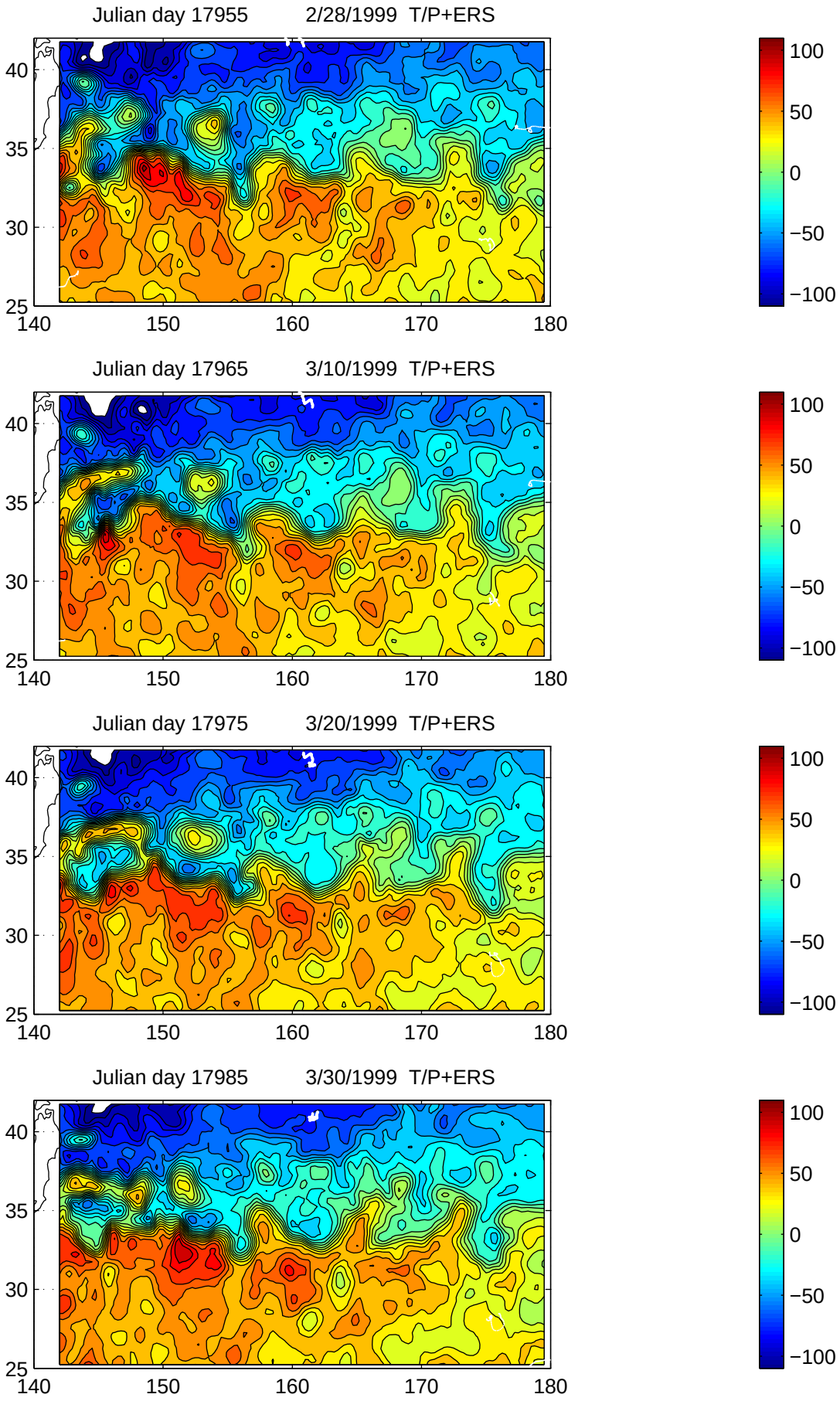

Julian day 17955 2/28/1999 T/P+ERS
Julian day 17965 3/10/1999 T/P+ERS
Julian day 17975 3/20/1999 T/P+ERS
Julian day 17985 3/30/1999 T/P+ERS
40
35
30
25
140
150
160
170
180
100
50
0
−50
−100

Fig.9−59

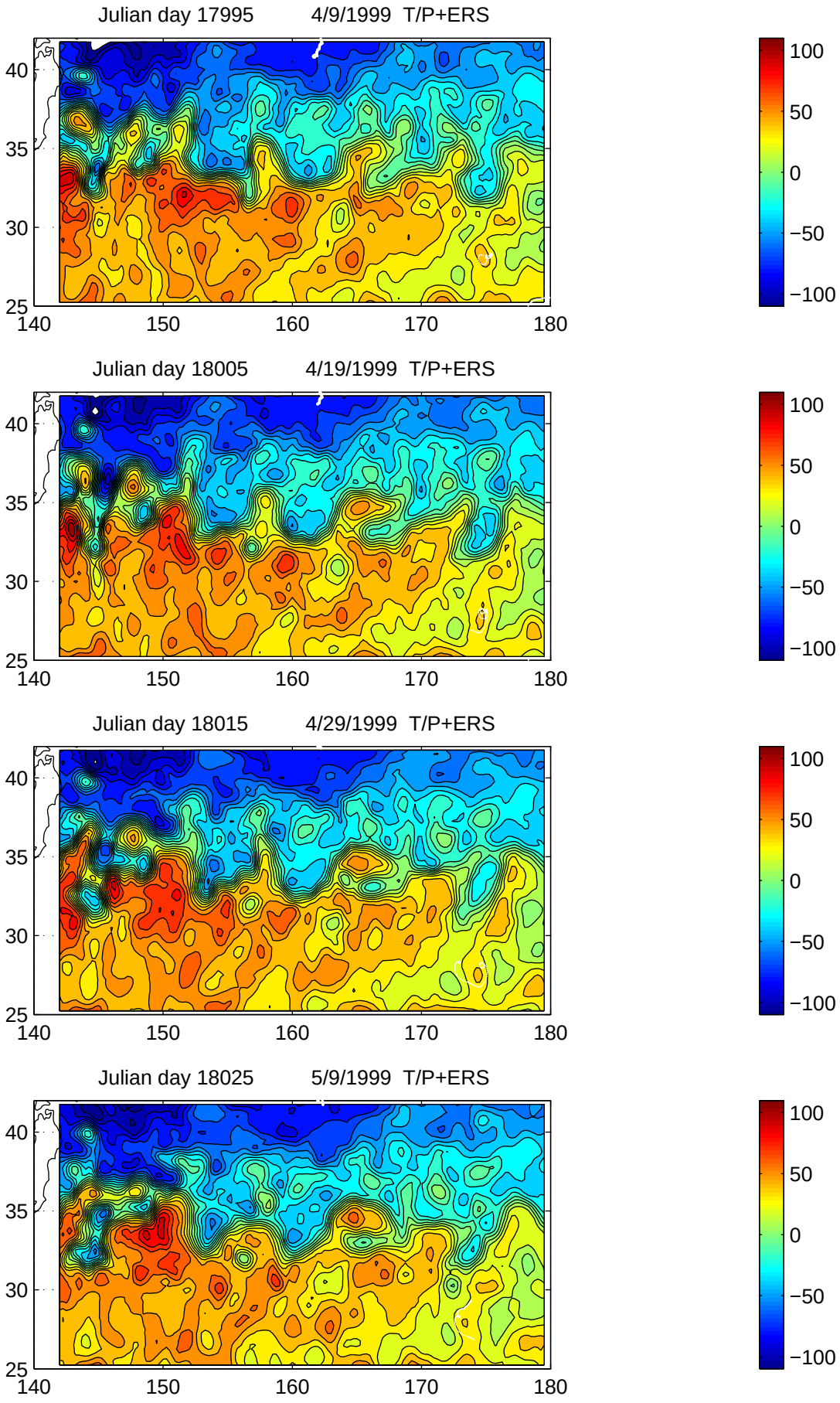

Julian day 17995 4/9/1999 T/P+ERS
Julian day 18005 4/19/1999 T/P+ERS
Julian day 18015 4/29/1999 T/P+ERS
Julian day 18025 5/9/1999 T/P+ERS
40
35
30
25
140
150
160
170
180
100
50
0
−50
−100

Fig.9−60

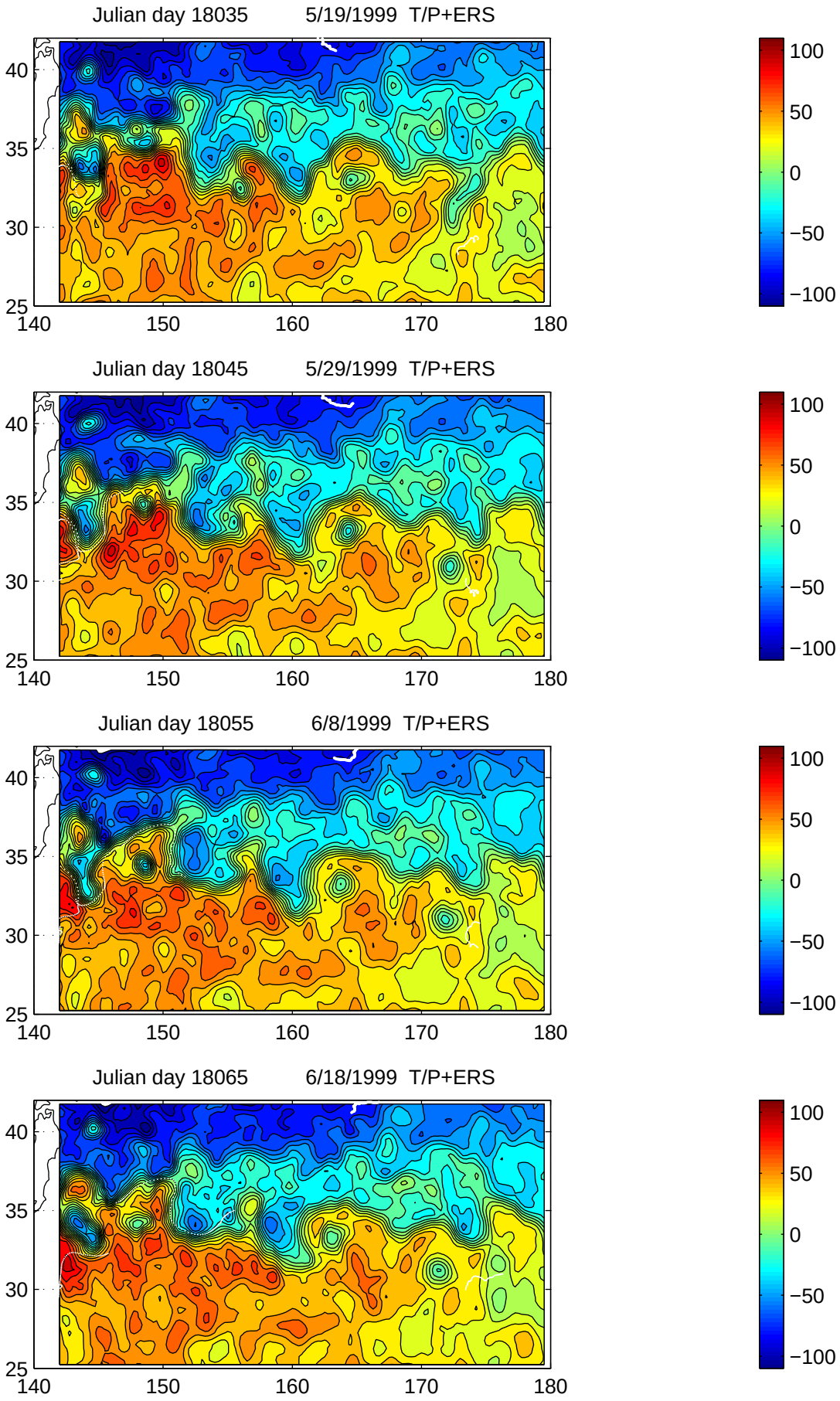

Julian day 18035 5/19/1999 T/P+ERS
Julian day 18045 5/29/1999 T/P+ERS
Julian day 18055 6/8/1999 T/P+ERS
Julian day 18065 6/18/1999 T/P+ERS
40
35
30
25
140
150
160
170
180
100
50
0
−50
−100

Fig.9−61

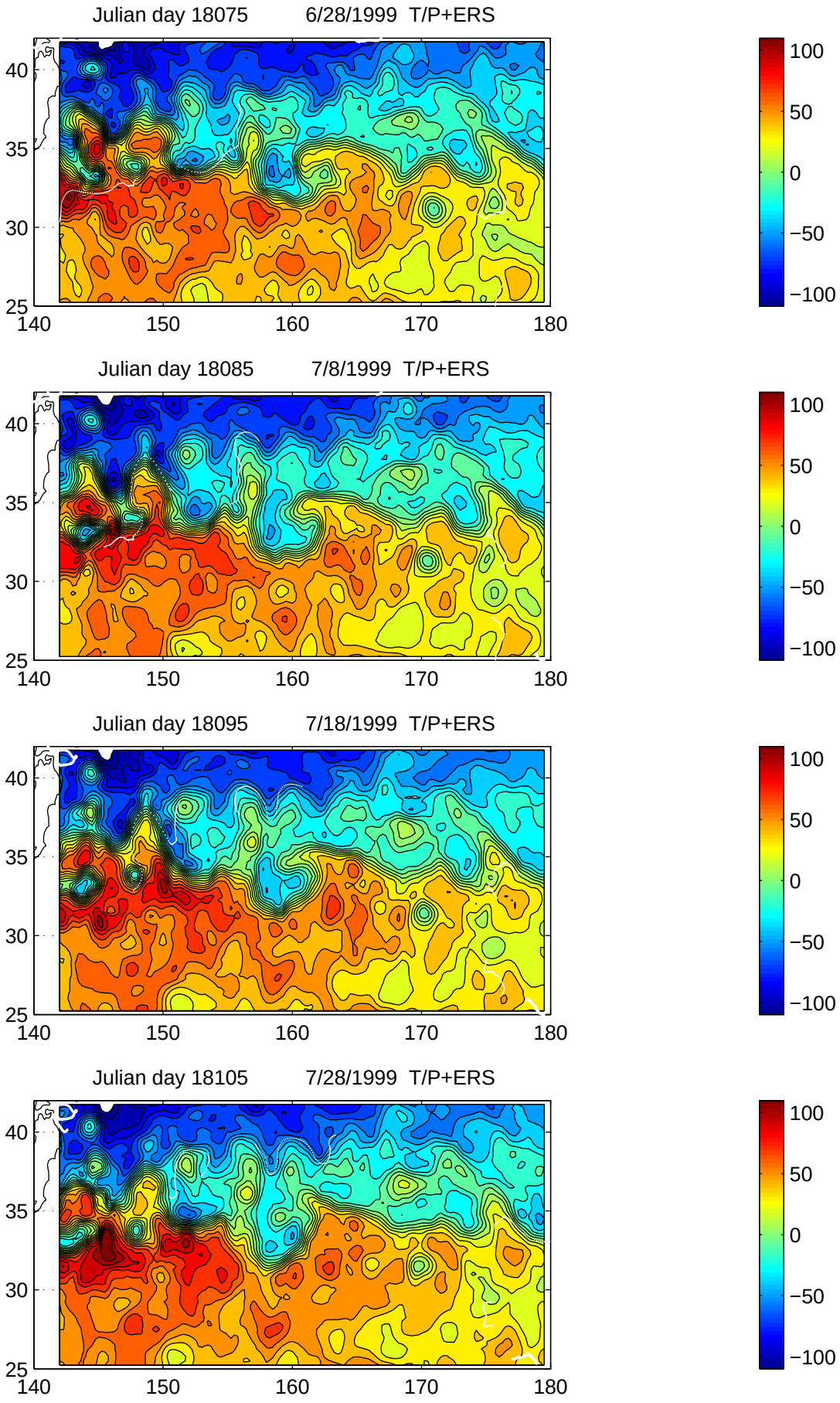

Julian day 18075 6/28/1999 T/P+ERS
Julian day 18085 7/8/1999 T/P+ERS
Julian day 18095 7/18/1999 T/P+ERS
Julian day 18105 7/28/1999 T/P+ERS
40
35
30
25
140
150
160
170
180
100
50
0
−50
−100

Fig.9−62

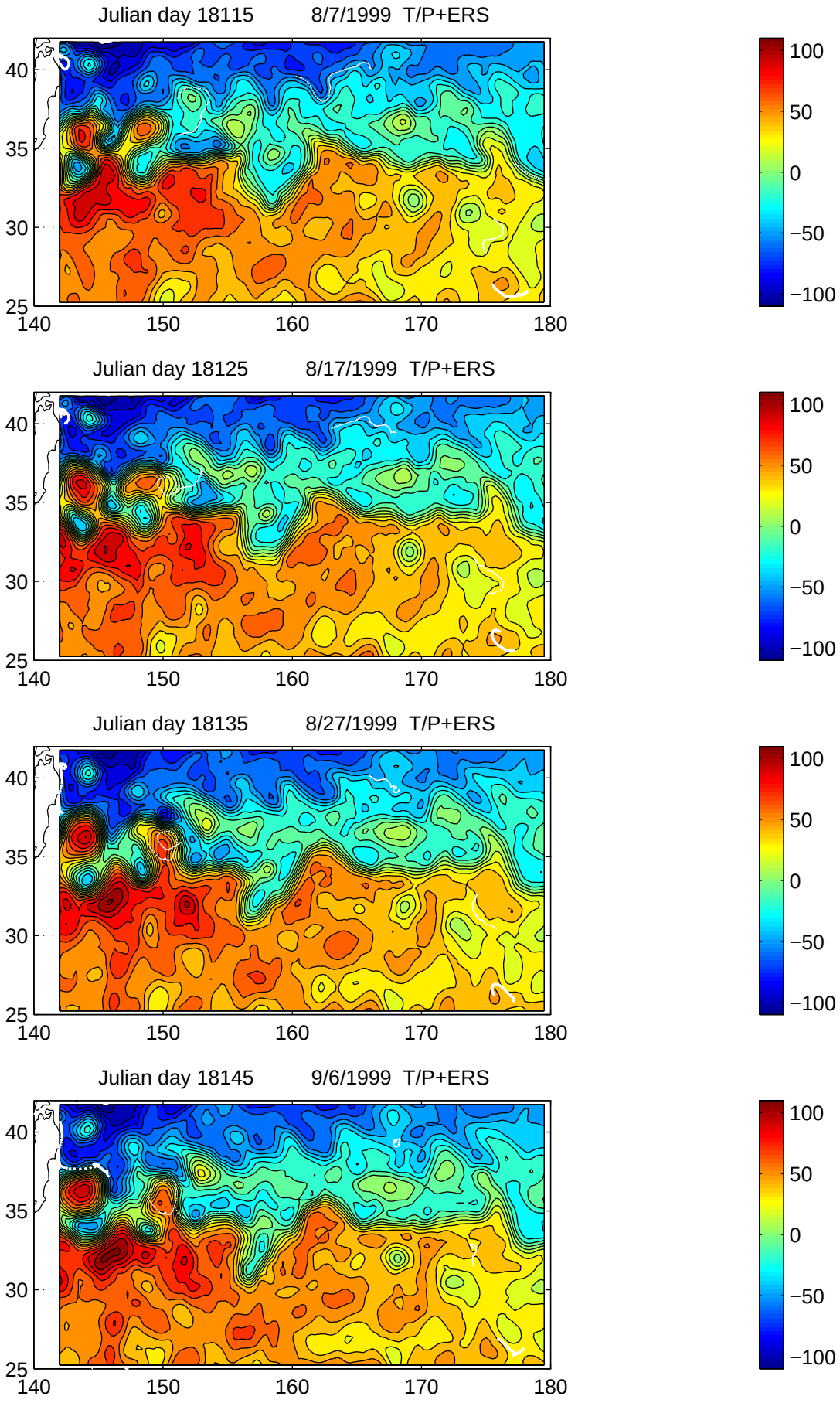

Julian day 18115 8/7/1999 T/P+ERS
Julian day 18125 8/17/1999 T/P+ERS
Julian day 18135 8/27/1999 T/P+ERS
Julian day 18145 9/6/1999 T/P+ERS
40
35
30
25
140
150
160
170
180
100
50
0
−50
−100

Fig.9−63

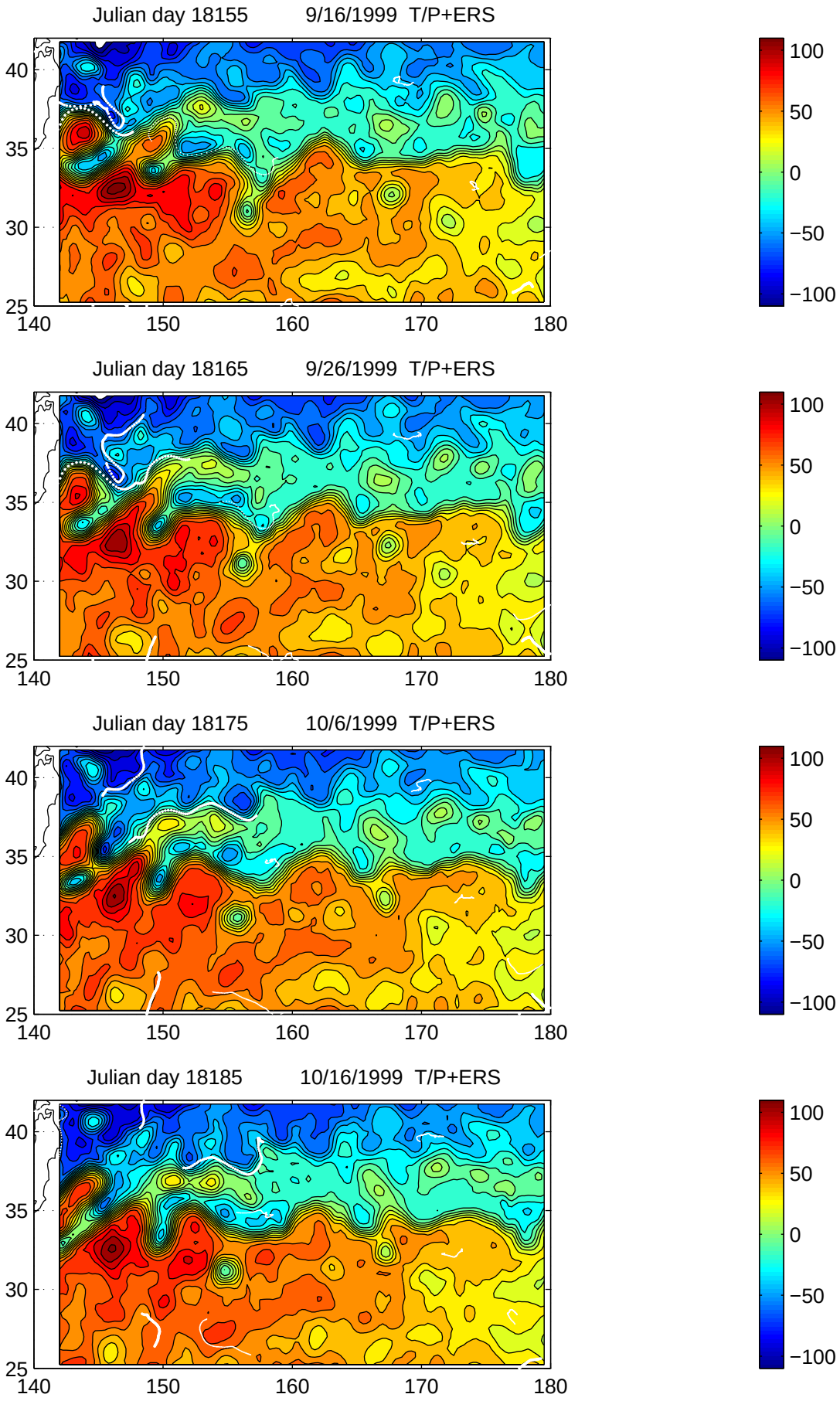

Julian day 18155 9/16/1999 T/P+ERS
Julian day 18165 9/26/1999 T/P+ERS
Julian day 18175 10/6/1999 T/P+ERS
Julian day 18185 10/16/1999 T/P+ERS
40
35
30
25
140
150
160
170
180
100
50
0
−50
−100

Fig.9−64

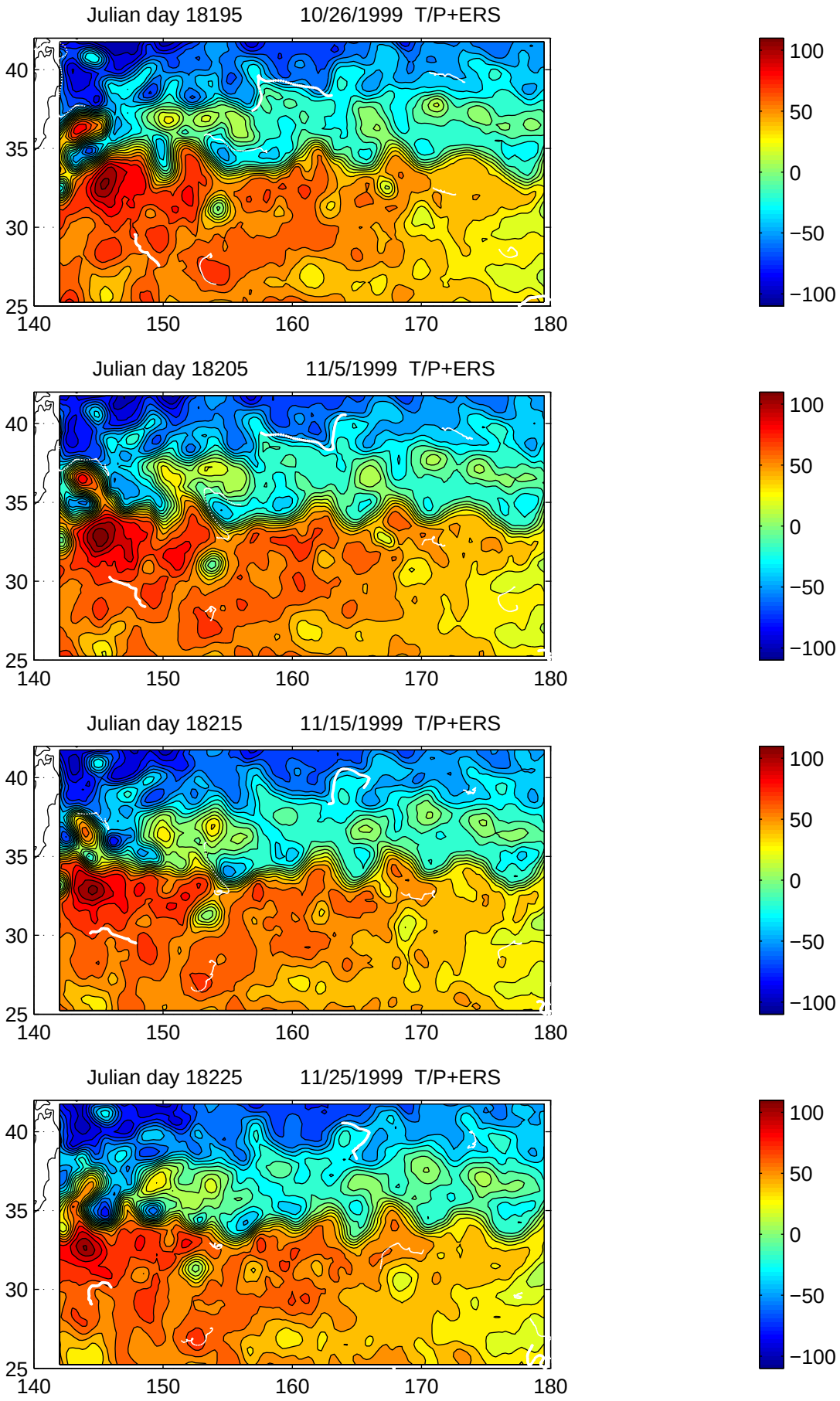

Julian day 18195 10/26/1999 T/P+ERS
Julian day 18205 11/5/1999 T/P+ERS
Julian day 18215 11/15/1999 T/P+ERS
Julian day 18225 11/25/1999 T/P+ERS
40
35
30
25
140
150
160
170
180
100
50
0
−50
−100

Fig.9−65

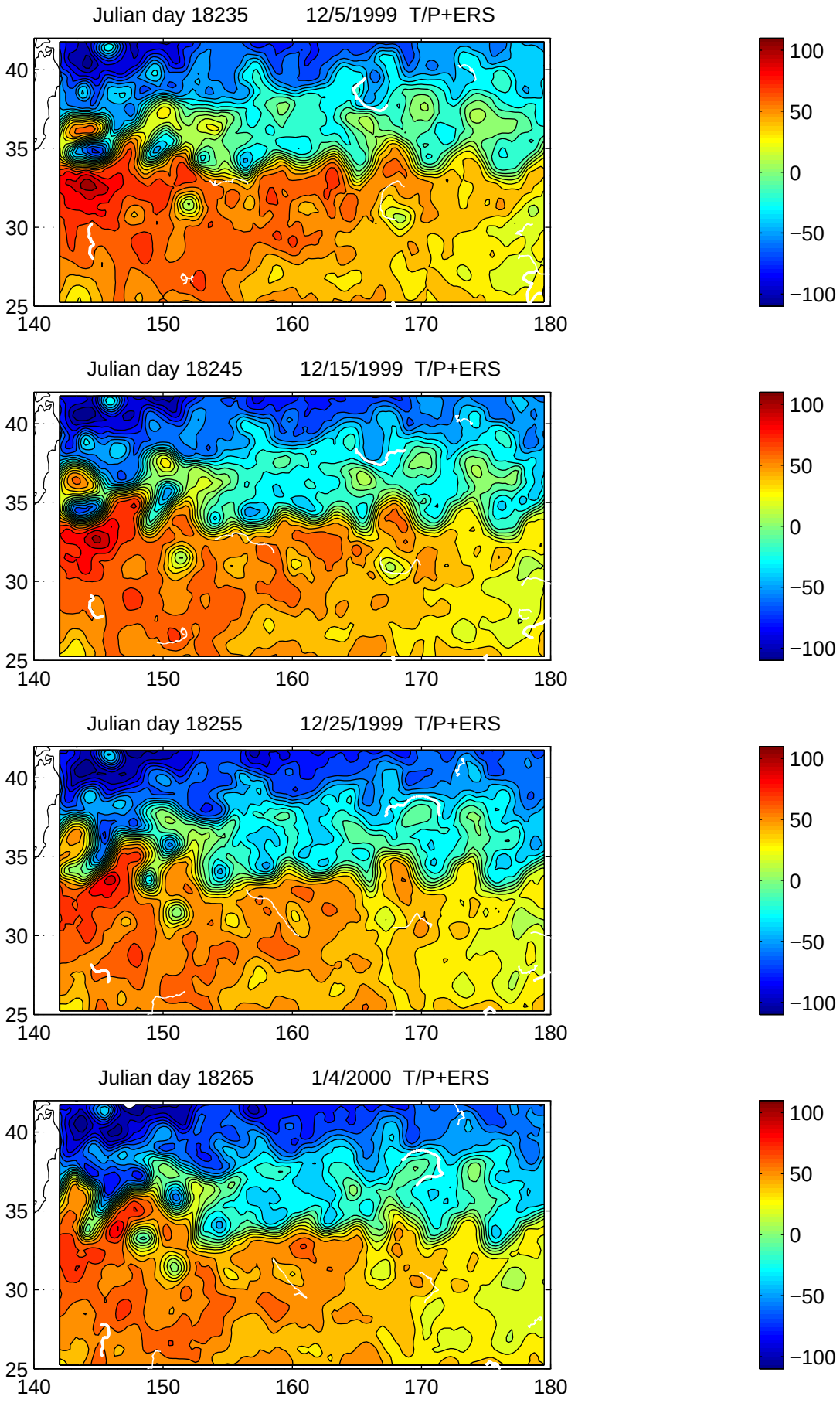

Julian day 18235 12/5/1999 T/P+ERS
Julian day 18245 12/15/1999 T/P+ERS
Julian day 18255 12/25/1999 T/P+ERS
Julian day 18265 1/4/2000 T/P+ERS
40
35
30
25
140
150
160
170
180
100
50
0
−50
−100

Fig.9−66

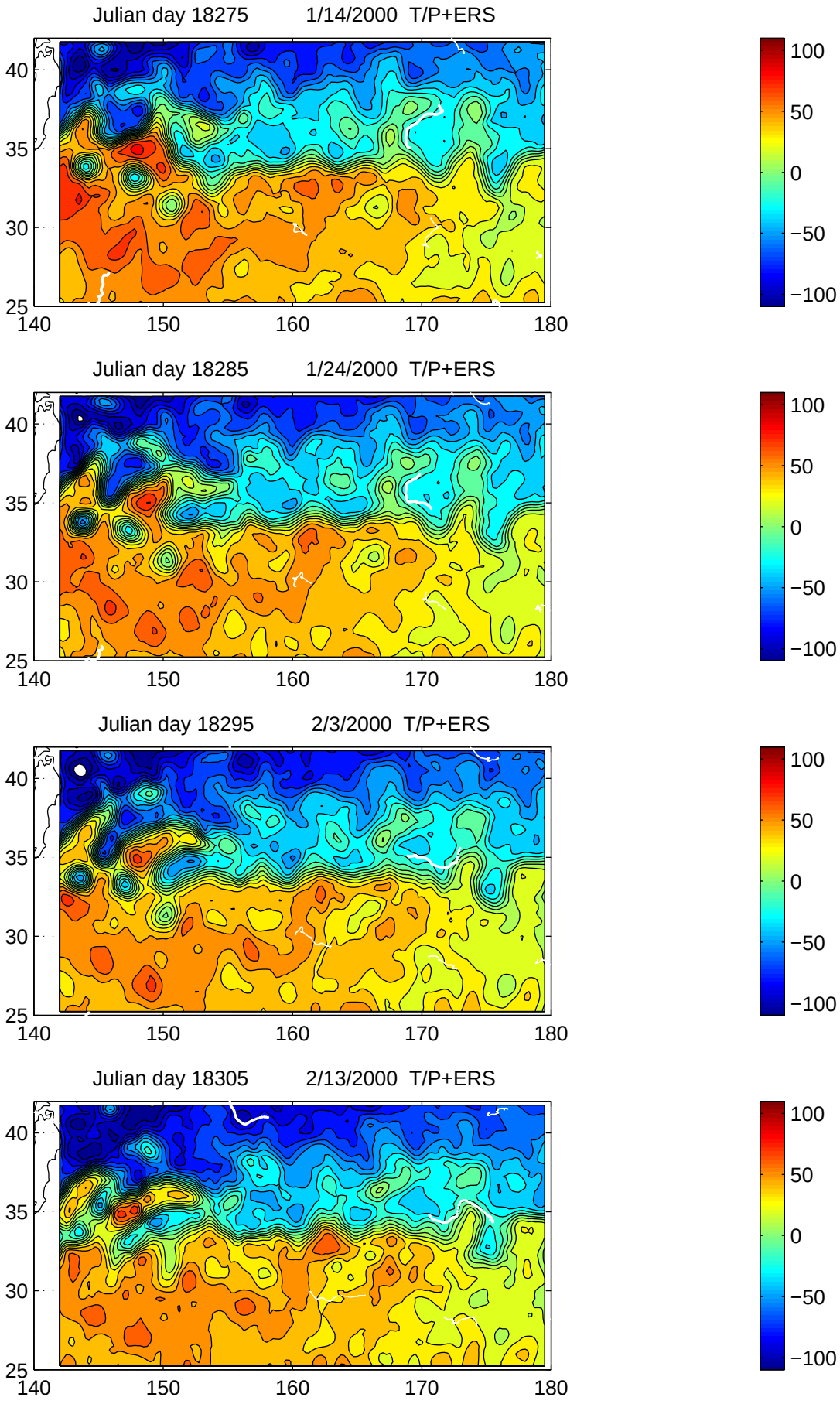

Julian day 18275 1/14/2000 T/P+ERS
Julian day 18285 1/24/2000 T/P+ERS
Julian day 18295 2/3/2000 T/P+ERS
Julian day 18305 2/13/2000 T/P+ERS
40
35
30
25
140
150
160
170
180
100
50
0
−50
−100

Fig.9−67

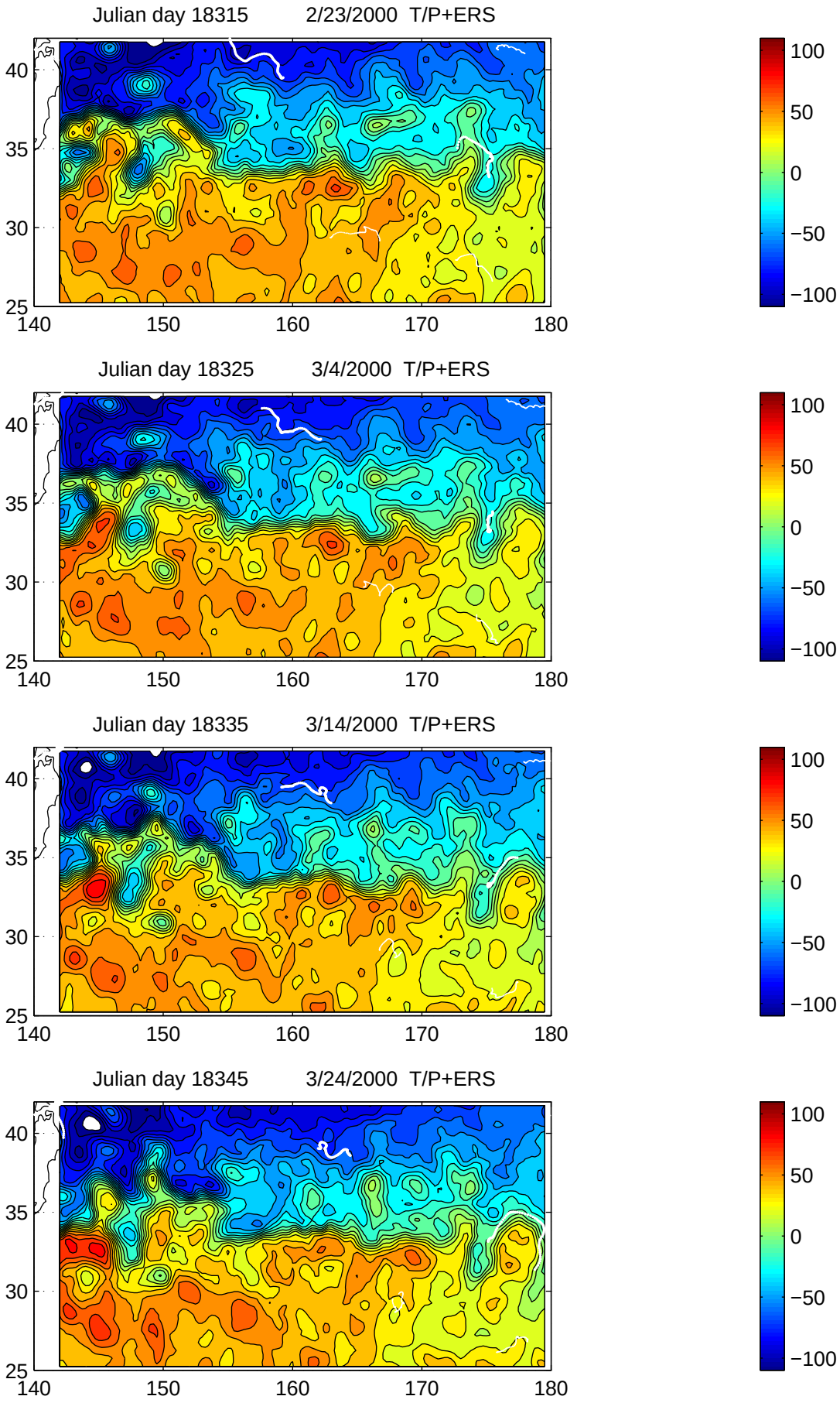

Julian day 18315 2/23/2000 T/P+ERS
Julian day 18325 3/4/2000 T/P+ERS
Julian day 18335 3/14/2000 T/P+ERS
Julian day 18345 3/24/2000 T/P+ERS
40
35
30
25
140
150
160
170
180
100
50
0
−50
−100

Fig.9−68

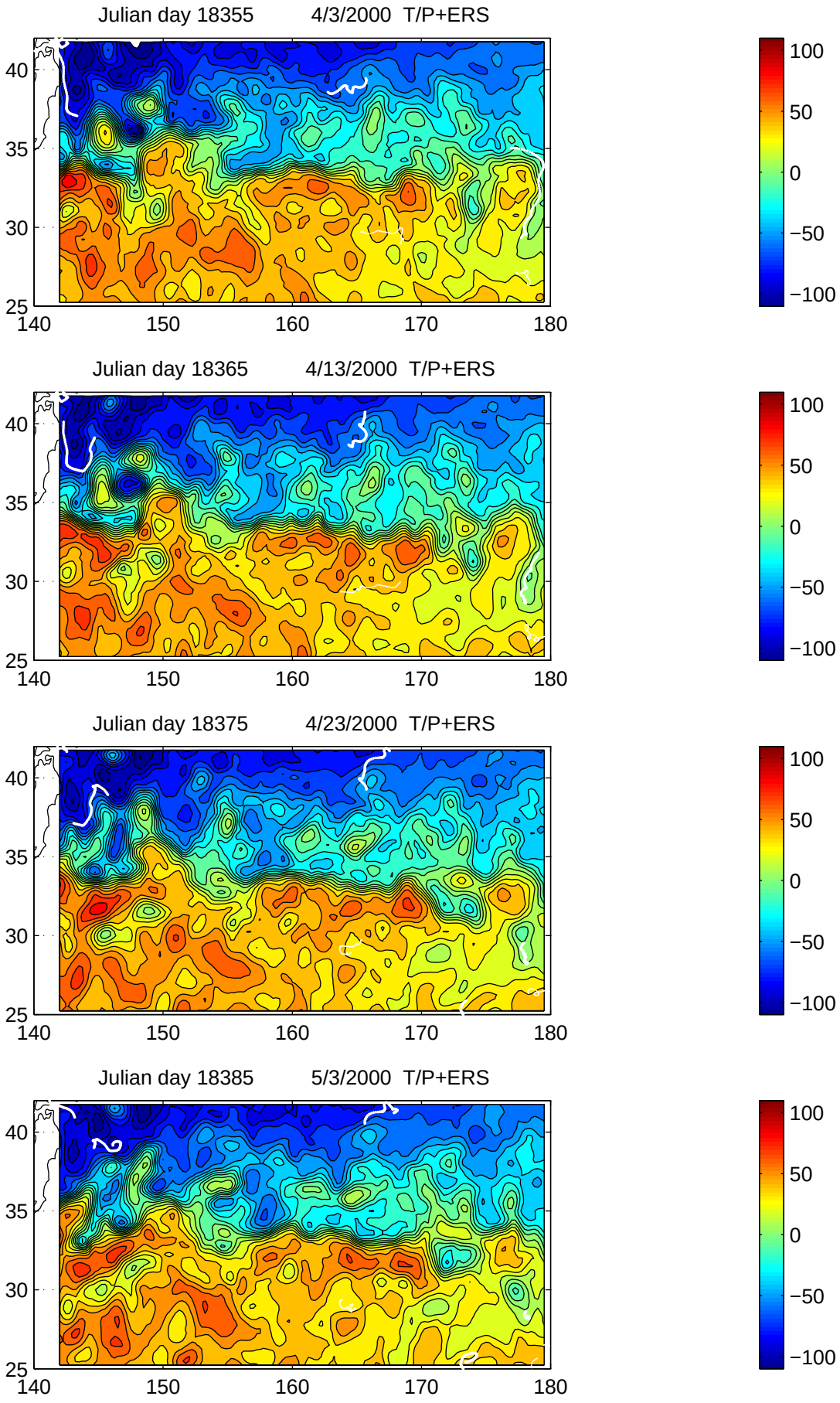

Julian day 18355 4/3/2000 T/P+ERS
Julian day 18365 4/13/2000 T/P+ERS
Julian day 18375 4/23/2000 T/P+ERS
Julian day 18385 5/3/2000 T/P+ERS
40
35
30
25
140
150
160
170
180
100
50
0
−50
−100

Fig.9−69

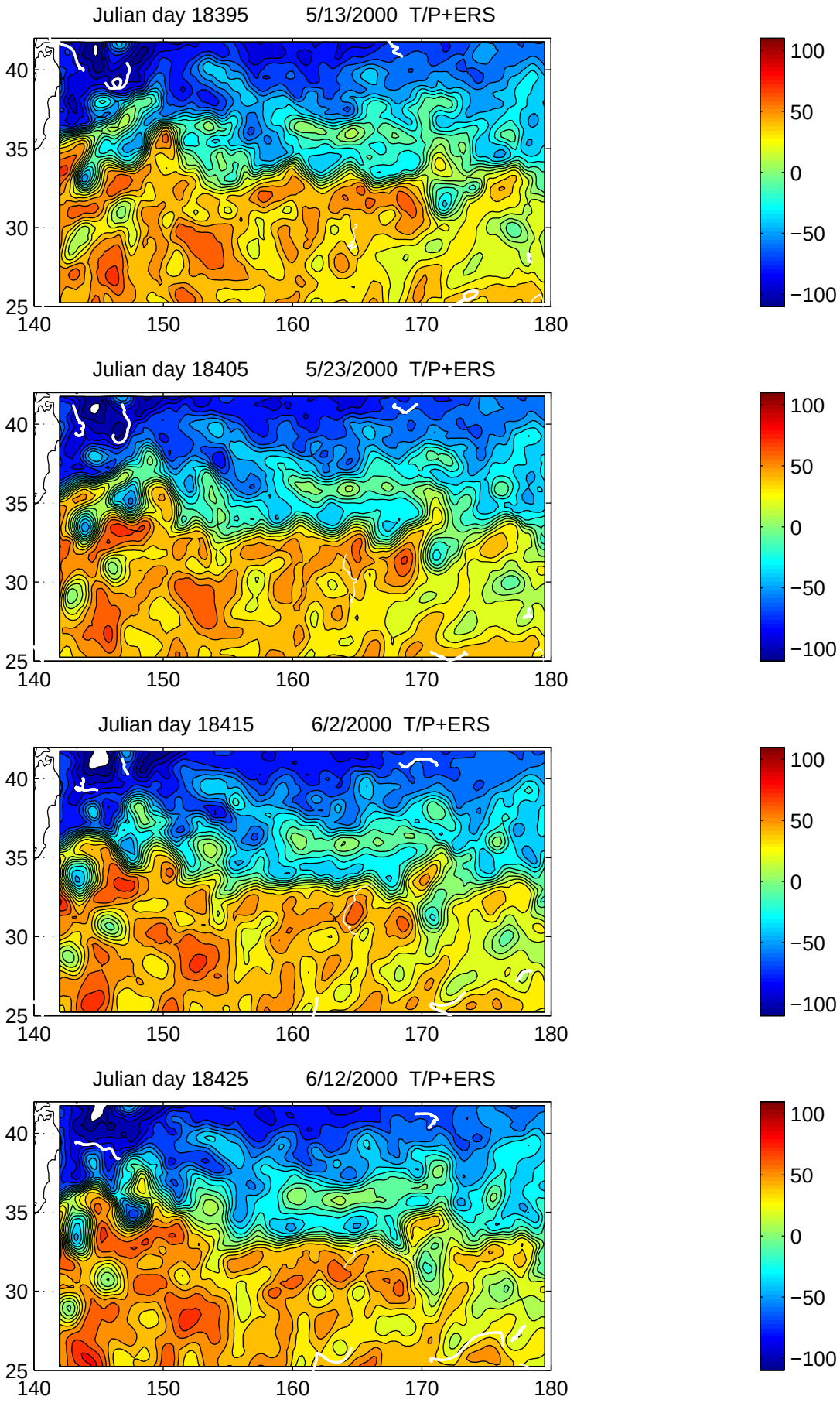

Julian day 18395 5/13/2000 T/P+ERS
Julian day 18405 5/23/2000 T/P+ERS
Julian day 18415 6/2/2000 T/P+ERS
Julian day 18425 6/12/2000 T/P+ERS
40
35
30
25
140
150
160
170
180
100
50
0
−50
−100

Fig.9−70

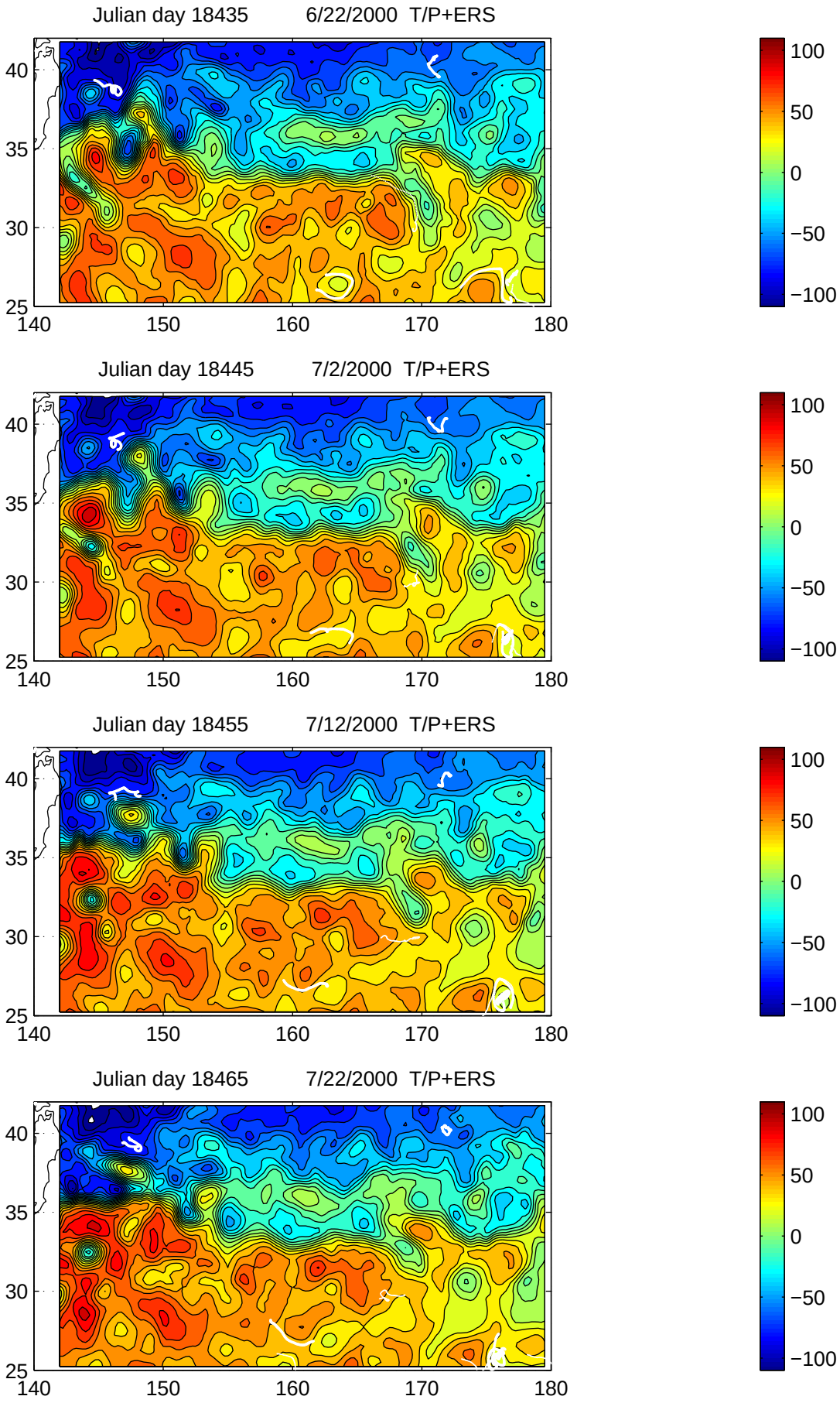

Julian day 18435 6/22/2000 T/P+ERS
Julian day 18445 7/2/2000 T/P+ERS
Julian day 18455 7/12/2000 T/P+ERS
Julian day 18465 7/22/2000 T/P+ERS
40
35
30
25
140
150
160
170
180
100
50
0
−50
−100

Fig.9−71

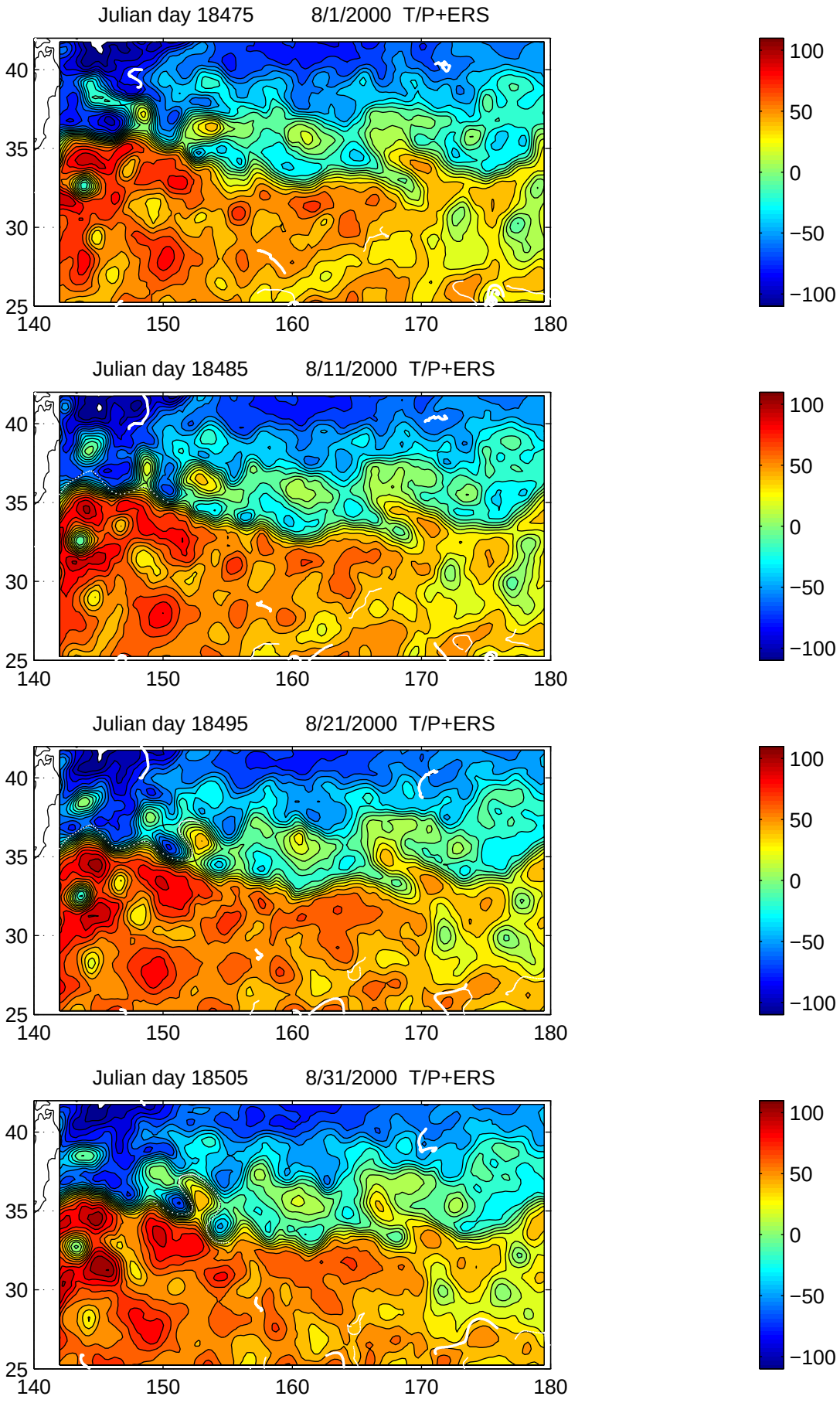

Julian day 18475 8/1/2000 T/P+ERS
Julian day 18485 8/11/2000 T/P+ERS
Julian day 18495 8/21/2000 T/P+ERS
Julian day 18505 8/31/2000 T/P+ERS
40
35
30
25
140
150
160
170
180
100
50
0
−50
−100

Fig.9−72

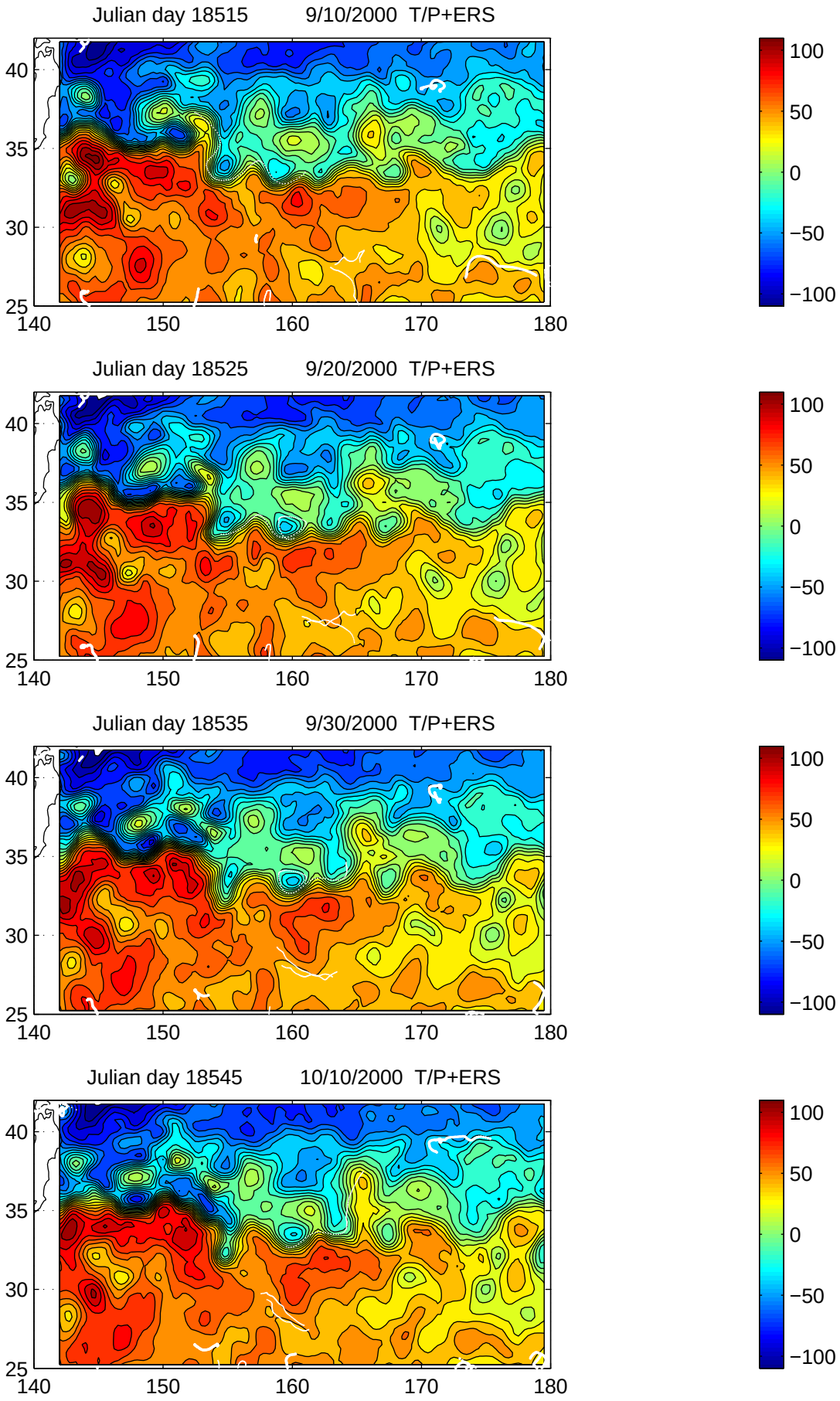

Julian day 18515 9/10/2000 T/P+ERS
Julian day 18525 9/20/2000 T/P+ERS
Julian day 18535 9/30/2000 T/P+ERS
Julian day 18545 10/10/2000 T/P+ERS
40
35
30
25
140
150
160
170
180
100
50
0
−50
−100

Fig.9−73

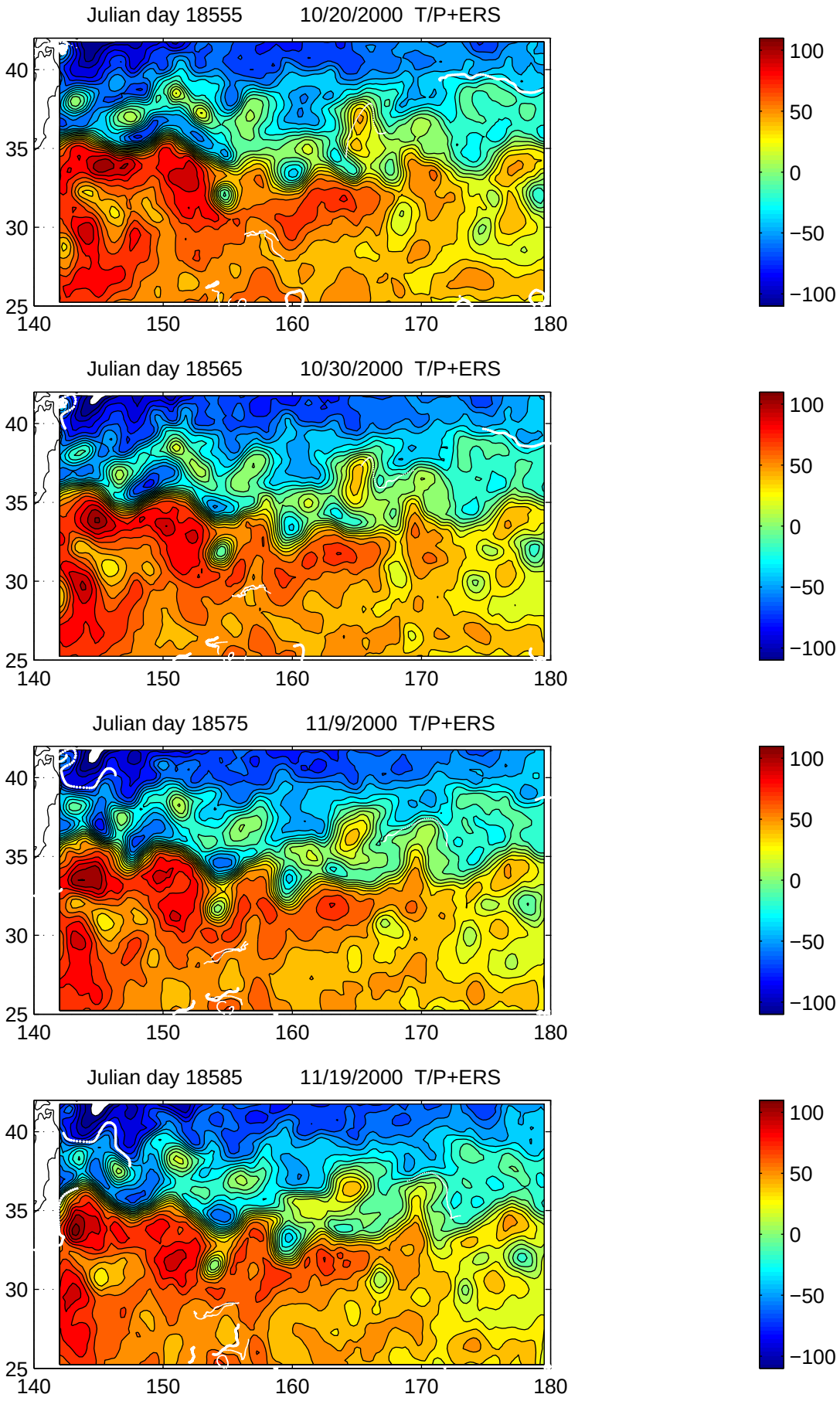

Julian day 18555 10/20/2000 T/P+ERS
Julian day 18565 10/30/2000 T/P+ERS
Julian day 18575 11/9/2000 T/P+ERS
Julian day 18585 11/19/2000 T/P+ERS
40
35
30
25
140
150
160
170
180
100
50
0
−50
−100

Fig.9−74

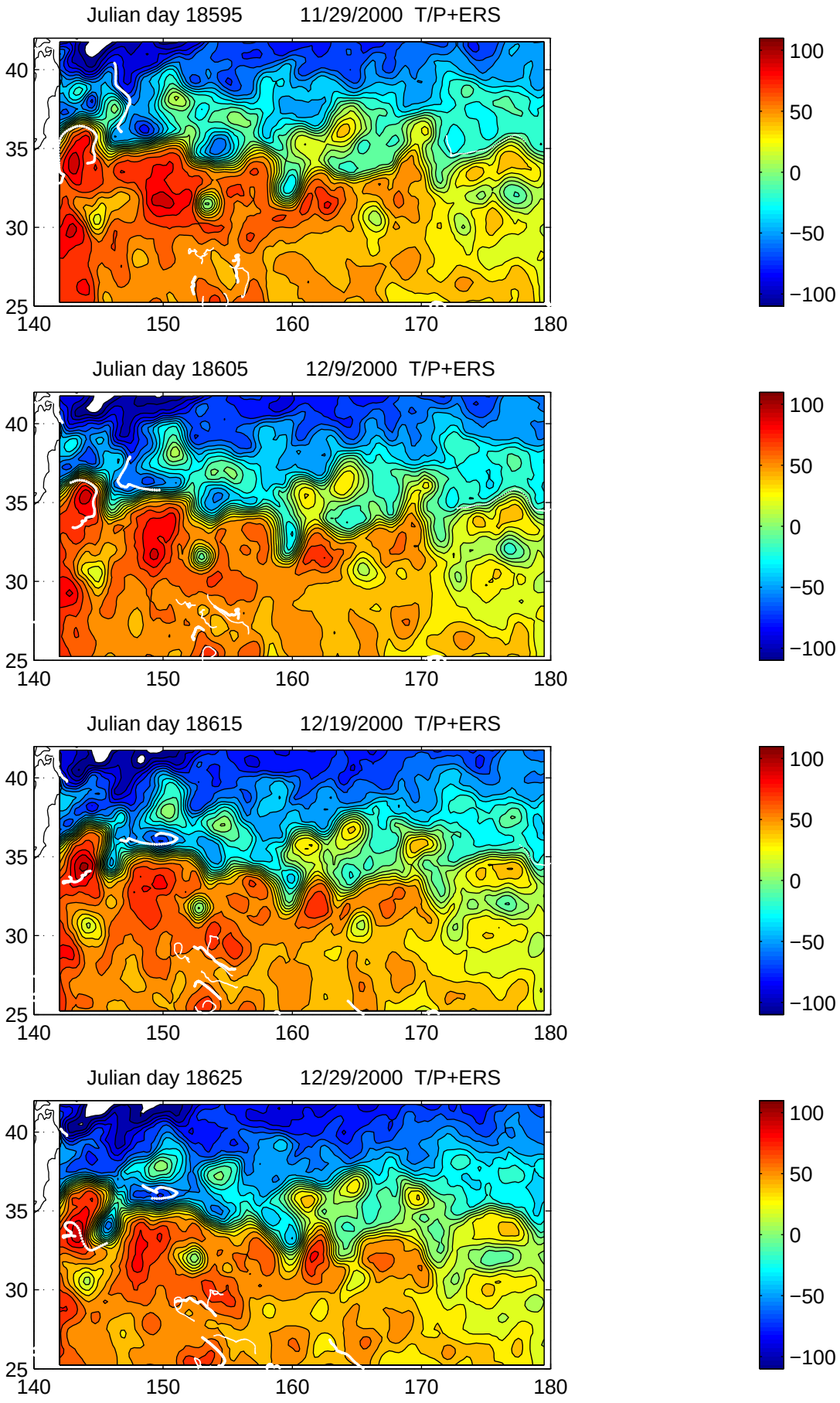

Julian day 18595 11/29/2000 T/P+ERS
Julian day 18605 12/9/2000 T/P+ERS
Julian day 18615 12/19/2000 T/P+ERS
Julian day 18625 12/29/2000 T/P+ERS
40
35
30
25
140
150
160
170
180
100
50
0
−50
−100

Fig.9−75

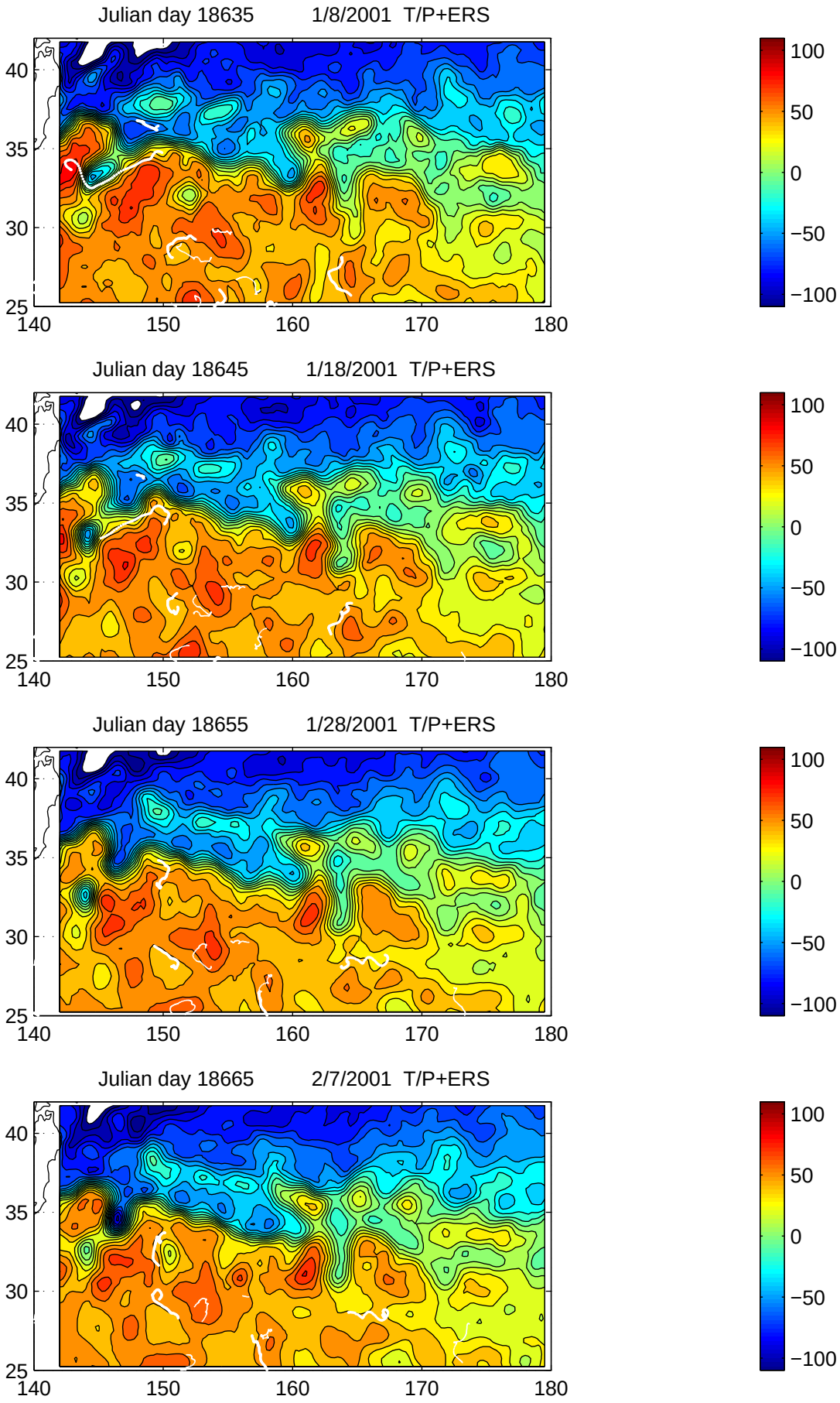

Julian day 18635 1/8/2001 T/P+ERS
Julian day 18645 1/18/2001 T/P+ERS
Julian day 18655 1/28/2001 T/P+ERS
Julian day 18665 2/7/2001 T/P+ERS
40
35
30
25
140
150
160
170
180
100
50
0
−50
−100

Fig.9−76

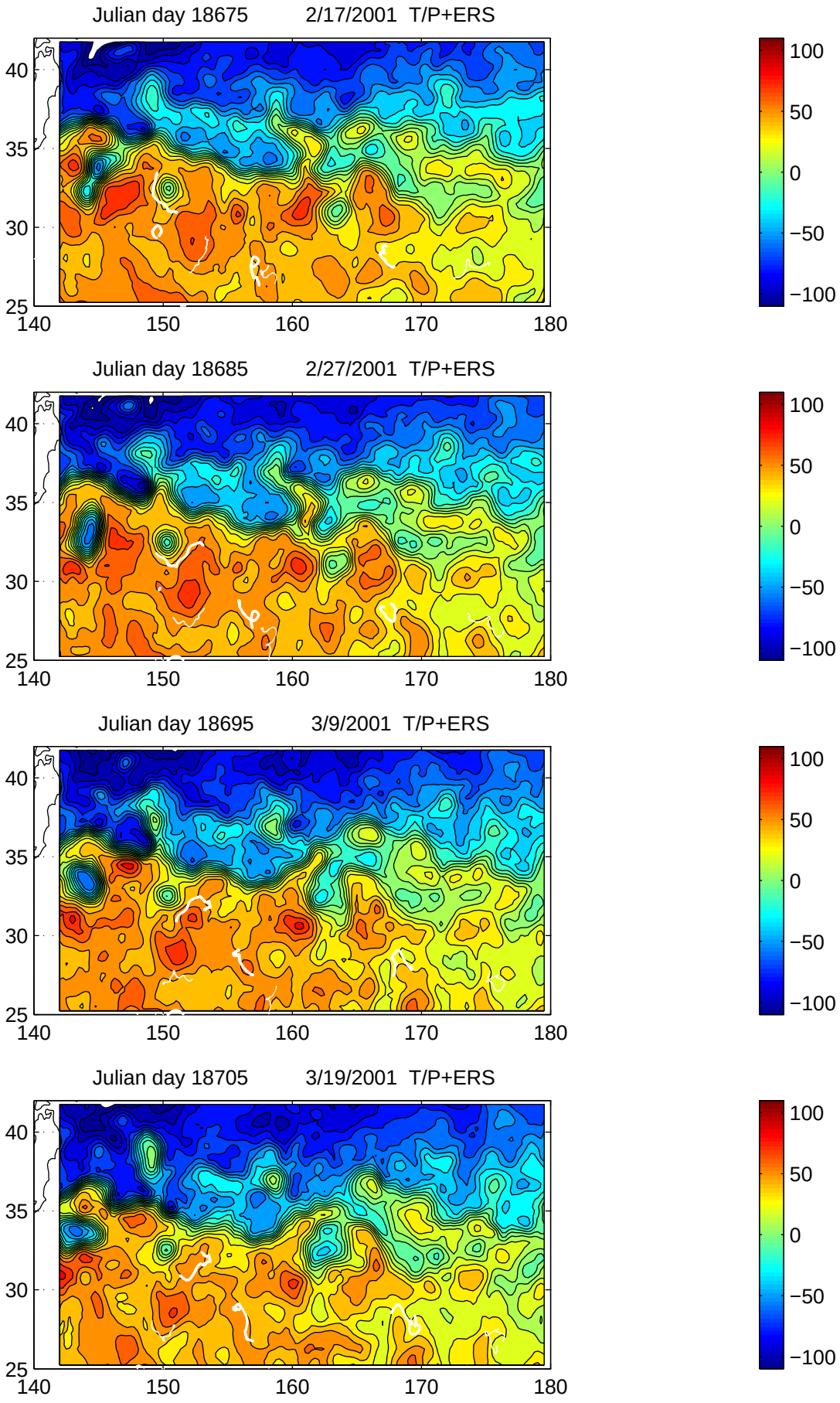

Julian day 18675 2/17/2001 T/P+ERS
Julian day 18685 2/27/2001 T/P+ERS
Julian day 18695 3/9/2001 T/P+ERS
Julian day 18705 3/19/2001 T/P+ERS
40
35
30
25
140
150
160
170
180
100
50
0
−50
−100

Fig.9−77

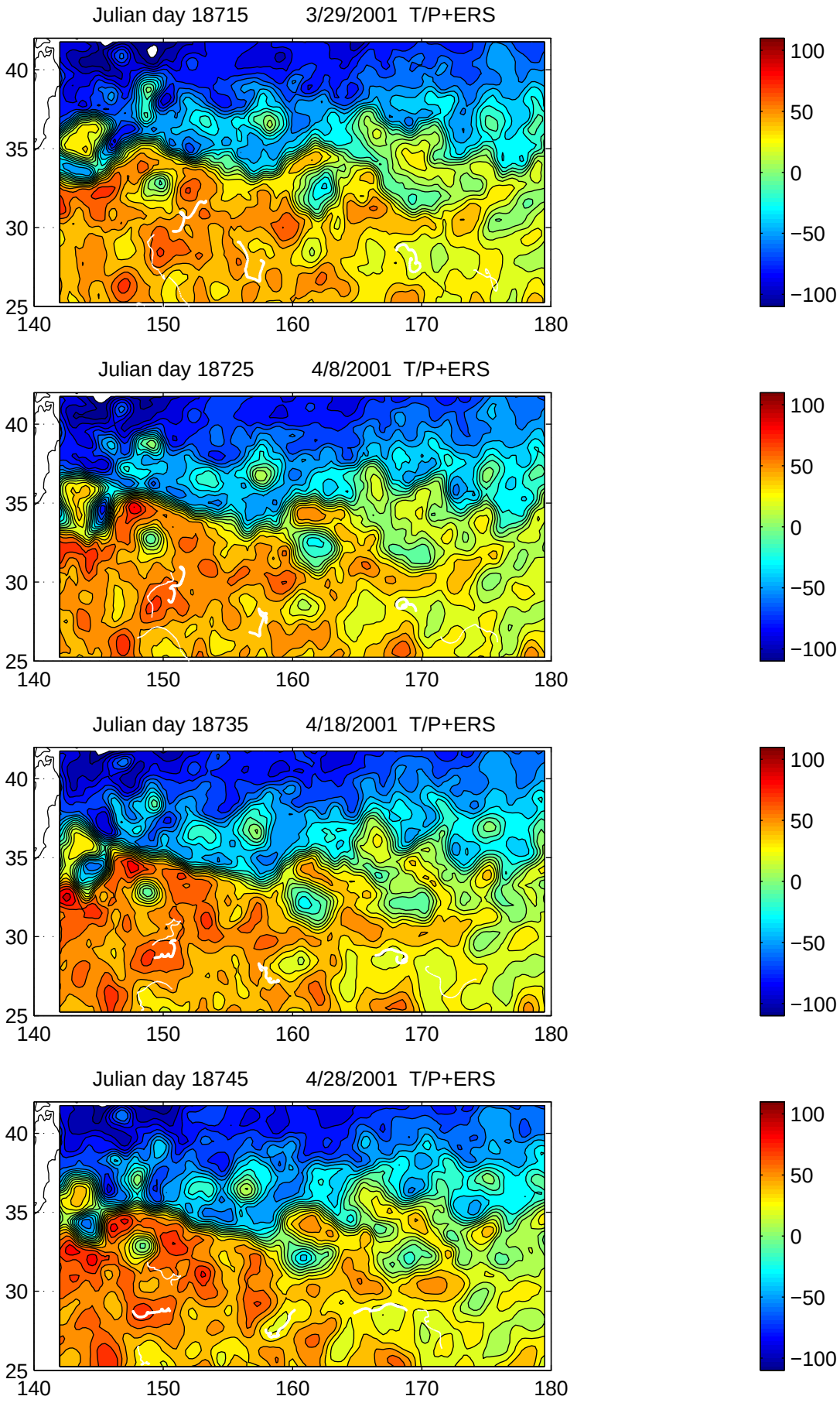

Julian day 18715 3/29/2001 T/P+ERS
Julian day 18725 4/8/2001 T/P+ERS
Julian day 18735 4/18/2001 T/P+ERS
Julian day 18745 4/28/2001 T/P+ERS
40
35
30
25
140
150
160
170
180
100
50
0
−50
−100

Fig.9−78

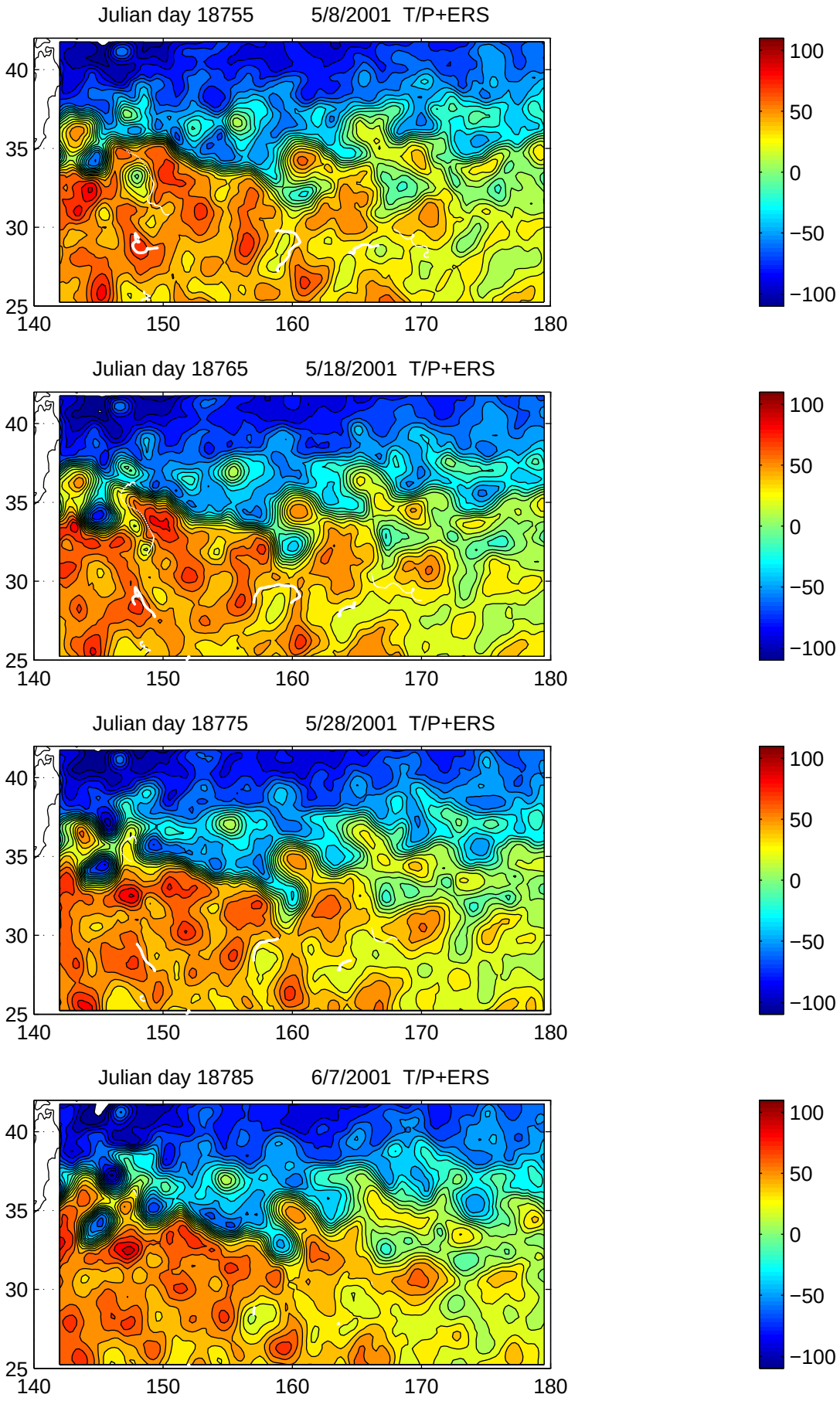

Julian day 18755 5/8/2001 T/P+ERS
Julian day 18765 5/18/2001 T/P+ERS
Julian day 18775 5/28/2001 T/P+ERS
Julian day 18785 6/7/2001 T/P+ERS
40
35
30
25
140
150
160
170
180
100
50
0
−50
−100

Fig.9−79

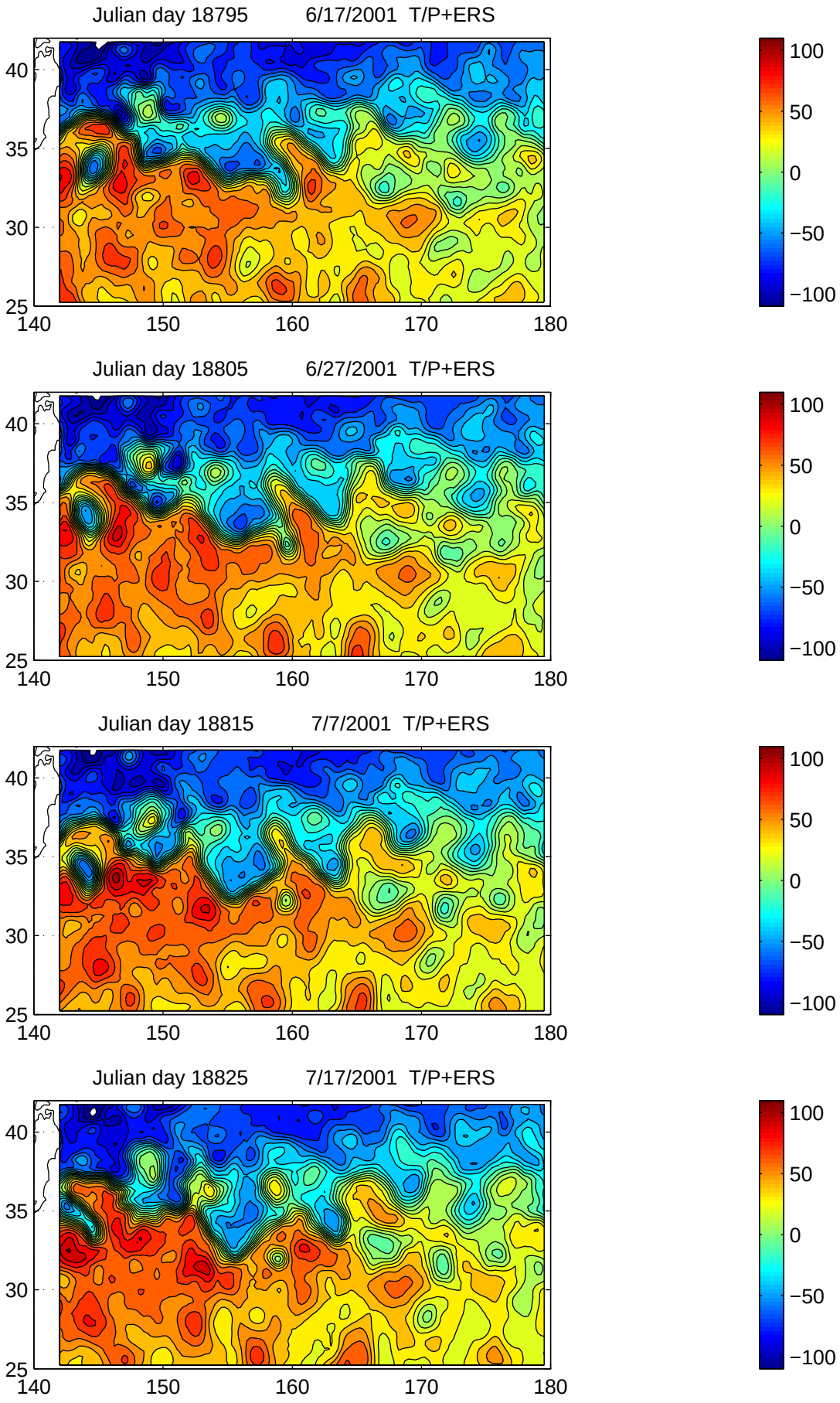

Julian day 18795 6/17/2001 T/P+ERS
Julian day 18805 6/27/2001 T/P+ERS
Julian day 18815 7/7/2001 T/P+ERS
Julian day 18825 7/17/2001 T/P+ERS
40
35
30
25
140
150
160
170
180
100
50
0
−50
−100

Fig.9−80

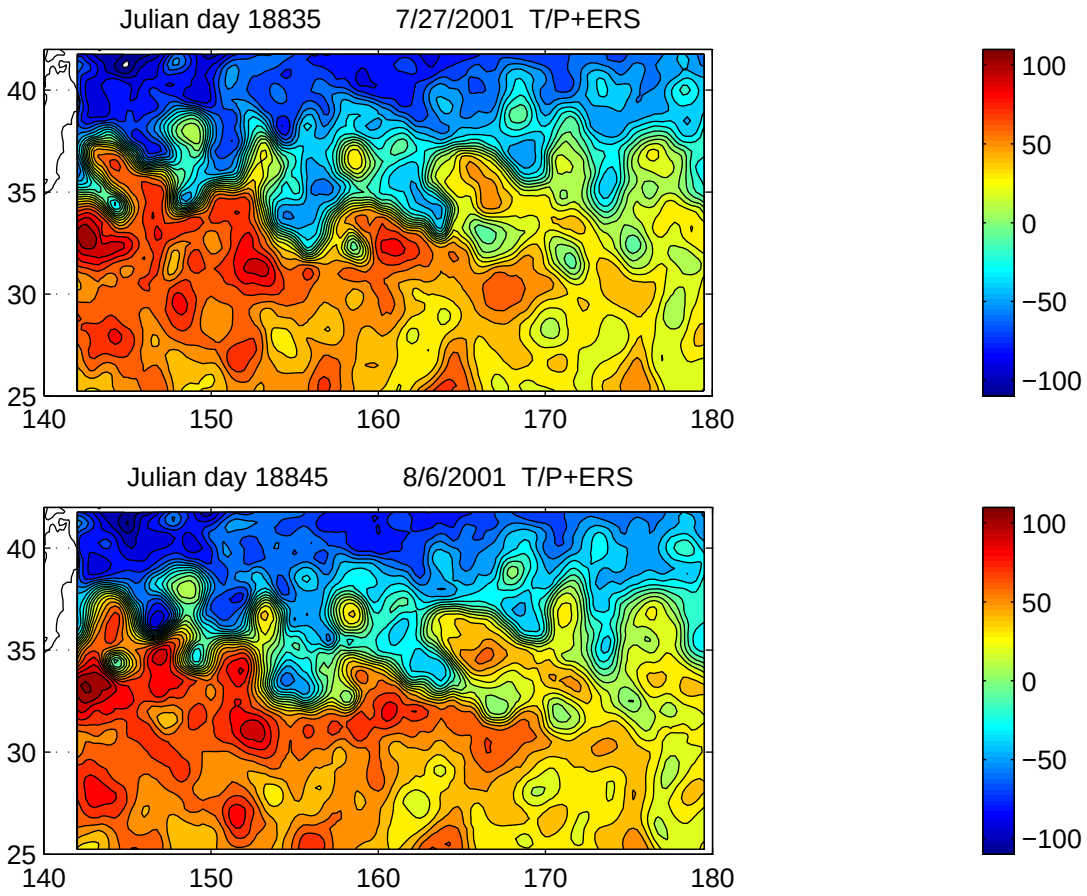

Julian day 18835 7/27/2001 T/P+ERS
40
35
30
25
140
150
160
170
180
100
50
0
−50
−100
Julian day 18845 8/6/2001 T/P+ERS
40
35
30
25
140
150
160
170
180
100
50
0
−50
−100

Fig.9−81